Synthesis and Characterisation of Nanocrystalline Titania Spheres: Application to Photocatalysis

A thesis presented to the University of London in partial fulfilment of the requirements for the degree of Doctor of Philosophy

Julio Agnelo DeSouza

Department Of chemistry

University College London

ProQuest LLC
789 East Eisenhower Parkway
P.O. Box 1346
Ann Arbor, MI 48106-1346

Abstract

This thesis describes the making of titania nanocrystalline particles (photonic crystals) and their use as photocatalysts. Chapter 1 describes the work that motivates this research – this includes a description of these structures as propagating a 'slow photon' effect that could make them excellent photocatalysts for decomposing organic compounds.

Chapter 2 describes the synthetic procedures that make these photonic crystals. The three-step procedure is detailed; involving the infiltration of voids of an opal structure, by either sol-gel or CVD with the characterisation of these structures revealed by several procedures.

Chapter 3 documents the photocatalysis studies performed on these structures, which involve the use of the stearic acid test. It was shown that stearic acid is decomposed with half-lives as low as ~20 minutes. This does compare very favourably with the other forms of titania tested. Actinometry was performed and quantum efficiency was calculated for quantification purposes which compares favourably with values reported elsewhere. The series of studies showed no correlation of activity with thickness of film. These new films were super hydrophilic but also displayed physical frailties. Chapter 4 details work correlating photocatalytic activity to particle sizes, work with controls, dye absorption experiments and BET area measurement.

Chapter 5 describes some studies of inverse opals as gas sensors.

Table of Contents

Table of Figures

List of Tables

Table of Abbreviations

nm = nanometres

μm = micrometres

μl = microlitres

CVD = Chemical Vapour Deposition

APCVD = Atmospheric Pressure Chemical Vapour Deposition

UV-vis = Ultraviolet-visible Spectroscopy

IR = Infrared Spectroscopy

PXRD = Powder X-ray Diffraction

SEM = Scanning Electron Microscopy

BET = Brunauer, Emmett and Teller (BET) surface area measurement

R= Reflectance

A = Absorbance

I = Intensity

Xe = Xenon lamp

N/NPA = Normalized photocatalysis data

T ½ = half-life

P25 = Titania powder standard (degussa)

Acknowledgements

First, I would like to thank Professor Ivan Parkin, Professor David Williams at UCL and Professor Geoff Ozin at the University of Toronto for their supervision, guidance and discussion throughout the course of this research. Additionally, I am grateful to Dr. Keith Pratt for discussion and advice concerning particular aspects of the work as well as carrying out some measurements.

I'd also like to thank people who have helped me in the analysis of the materials made. Dr Chris Blackman, who helped me with reflectance and PXRD measurements. Kevin Reeves for assistance with SEM imaging, Dr Firth, Mr Dave Knapp for assistance with the CVD rig, Dr Robin Clark's group for assistance in using the Raman, Dr Russell Pryce (Imperial college) for BET measurements and Professor Ozin's group, in particular Dr Vladimir Kitaev, Nicolas Tetreault and Dr Hernan Miguez for advice and help with measurements while I carried out work at UoT.

I am extremely grateful to the EPSRC for funding my work for the last three years. Thanks to everyone from the department who I have lunched, worked and conversed with over the last three years and who have made them more enjoyable.

Last but not least I'd like to thanks my Mum, Dad and Alex for their support and encouragement.

Chapter 1 Introduction

Photodestruction of organic molecules by semiconductors requires photons of greater energy than that corresponding to the band gap of the semiconductor. In the case of anatase titania, this means that less than 3% of the total solar radiation at the earth's surface can be harnessed for photodestruction purposes. Less energetic photons could in principle degrade some light sensitive organics. Colloidal titania has a tail to its absorption edge, extending into the visible region. This tail is associated with excitation into surface trap states. This thesis was undertaken on the premise that if the interaction time of light with the colloidal titanium could be increased sufficiently- for example by slowing the light within a photonic matrix - then the quantum efficiency for excitation into surface trap states could be increased and hence more of the solar spectrum could be effective for the oxidation of organics. The proposal was that the interaction time of light with the semiconductor could be increased by forming the titania as a photonic crystal.

The aim of this section is to introduce the concept of photocatalysis (**section 1.1 - 1.4**), to describe photonic crystals (**section 1.5 -1.7**) and to give details concerning the expected enhancement that will be investigated in the experimental chapters.

Templating and deposition routes were conceived for photonic crystal fabrication and these are reviewed in **sections 1.8 - 1.10**.

1.1 What is Photocatalysis?

The term photocatalysis implies that, in a reaction, light is acting as a catalyst. This would be incorrect as in reality it acts as a reactant that is consumed in the chemical

process. Photocatalysis is a term in widespread use but it should not mean catalysis by light but rather, the acceleration of a photoreaction by the presence of a catalyst.[1, 2]

This definition of photocatalysis includes the process of 'photosensitization', i.e. a process by which a photochemical reaction occurs in one chemical species as a result of the initial absorption of radiation by another chemical species (called the photosensitizer). Therefore heterogeneous photocatalysis (when referring to semiconductor photocatalysis) involves photoexcitations taking place in the catalyst substrate and this interacts with the ground state of the adsorbate molecule.

It is argued that heterogeneous catalysis is only demonstrated when the turnover (i.e. the number of product molecules per number of active sites) number for the process under investigation is bigger than unity.

Titanium dioxide features predominantly in any discussion of semiconductor photocatalysis. When TiO_2 is the semiconductor sensitizer, the assumption is made that the number of active sites is taken as the product of the surface density of hydroxide groups and of the specific surface area of TiO_2. The surface density is measured in the dry state whereas for photocatalysis these must be dispersed in solution and so the surface area depends on the degree of aggregation of the particles. Besides, not all hydroxide surfaces will be active. Therefore if turnover number is still greater than unity then it follows that the process under investigation is 'catalysed'.[1]

1.2 How does semiconductor photocatalysis work?

The process known as semiconductor photocatalysis can be summarised as follows:

$$A + D \xrightarrow[\text{Light} \geq E_{bg}]{\text{Semiconductor}} A^- + D^+ \qquad \textbf{(1.1)}$$

In **eqn. (1.1)** E_{bg} is the semiconductor bandgap (the gap between the highest occupied or 'valence' band and the lowest unoccupied band or conductance band). If $\Delta G°$ is negative for the reaction above then photocatalysis occurs.[1, 2]

So when this semiconductor is irradiated with energy greater or equal to this band gap an electron (e^-) is excited from the valence into the conduction band thus creating a hole in the valence band (h^+), an electron hole pair is the result (e^-- h^+). As **figure 1.1** shows, this process can result in 'activating' processes such that the photogenerated electrons can reduce an electron acceptor (A) or the photogenerated holes can oxidise an electron donor (D). The effectiveness of photocatalysis depends on whether these processes occur or whether an electron-hole recombination ('deactivating' process) occurs instead .[1] In titanium dioxide the band gaps for anatase and rutile forms of this semiconductor are 3.2 and 3.0 eV respectively (**Figure 1.2**). A disadvantage of using titania is that UV light is needed to generate the electron-hole pairs and UV of < 400 nm is required – only 3% of the solar spectrum has those wavelengths.[3]

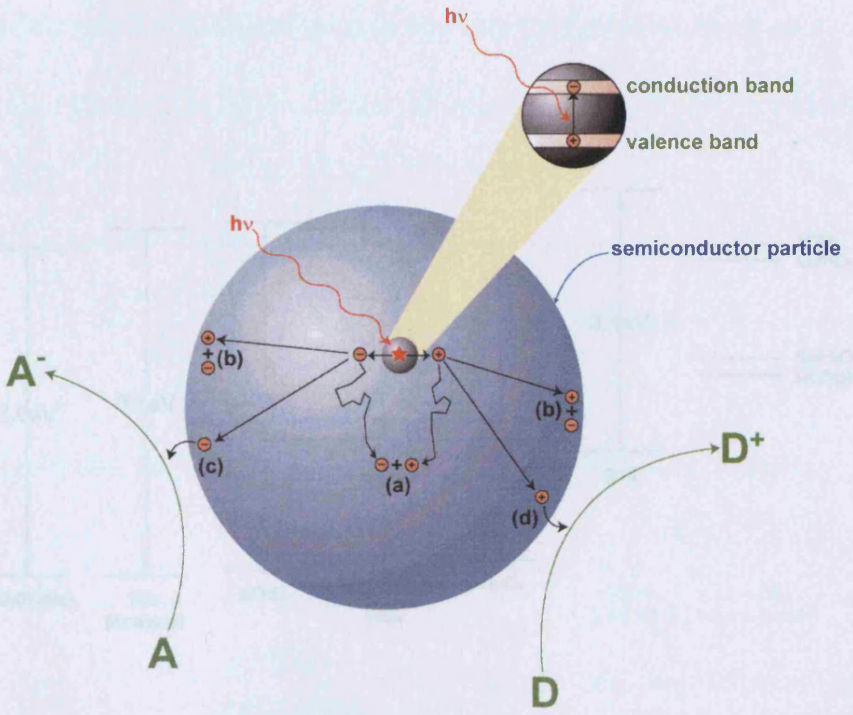

Figure 1.1 Illustration of the major processes occurring on semiconductor particle following electronic excitation. Electron-hole recombination can occur in the surface (a) or in the bulk (b) of the semiconductor. Also, at the surface, photogenerated electrons can reduce an electron acceptor A (c) and photogenerated holes can oxidise an electron donor (d). [1, 9]

Fujishima and Honda used the principles at work in semiconductor photochemistry, in 1972, to propose the first photoelectrochemical cell to be used for water splitting:

$$2H_2O \longrightarrow 2H_2 + O_2 \qquad \textbf{(1.2)}$$

The e^- - h^+ pair is produced by absorption of ultraband gap light, the photogenerated holes move, through an electrical circuit, toward the surface of the semiconductor and oxidise the redox species, and then move toward the counter electrode for the reduction process. For the photo-reduction to be efficient, the conductance band must be more negative than the hydrogen potential (H^+/H_2) and photo-oxidation will be feasible if the position of the valence band is more positive than the oxygen potential (O_2/H_2O) (**Figure 1.2**).[1, 8]

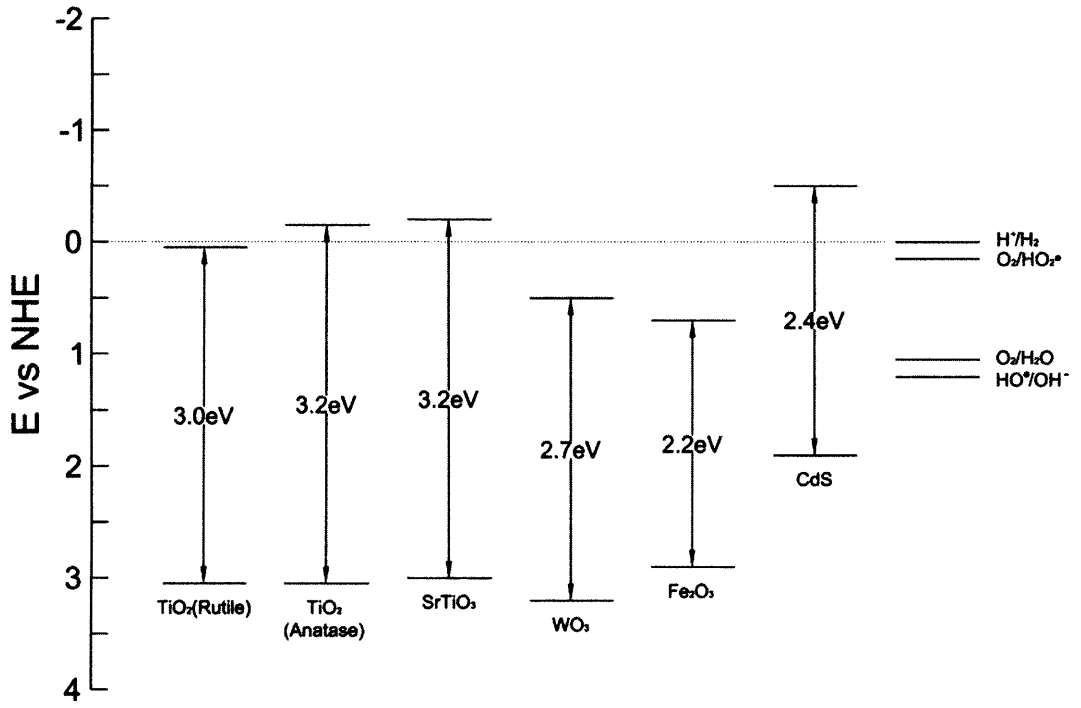

Figure 1.2 Valence and conductance band for various semiconductors with relevant redox couples. [1]

1.3 Why use TiO_2 as a photocatalyst?

Titanium dioxide is:

1) Photoactive

2) Able to use UV or near UV light

3) It is biologically and chemically inert

4) Photostable (not liable to corrosion for instance) and

5) Inexpensive

1.4 Semiconductors as photocatalysts for the removal of organics

The equation for this process follows from the equation for a typical photocatalysis process (**Eqn. 1.1**):

$$\text{Organic} + H_2O \xrightarrow[\text{Light} \geq E_{bg}]{\text{Semiconductor}} CO_2 + H_2O + \text{mineral acids} \qquad \textbf{(1.3)}$$

The energetic processes and intermediate details can be seen from this diagram:

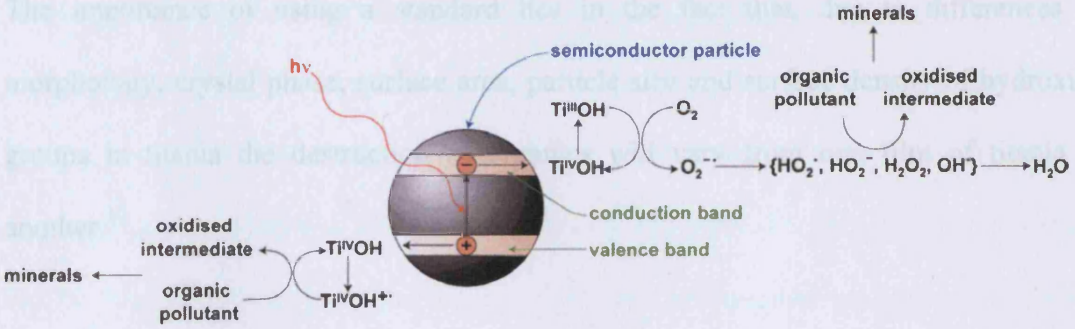

Figure 1.3 The photo-oxidative mineralization of organic pollutants using titania. [1,9]

In the major processes outlined above (**Figure 1.3**) - valence band holes of sufficient energy are created, generating surface-bound hydroxyl radicals by oxidation. Conduction band electrons reduce oxygen to form radicals. It has been speculated that oxygen radicals also form species such as $HO^{\bullet}_2$, H_2O_2, HO^{-}_2, as well as the hydroxyl radicals, and that these take part in the oxidation of the organic substrate. There have been doubts expressed as to the role of oxygen in this process when electron acceptors other than oxygen are involved although the extent of photocatalytic oxidation is changed. Investigations, both experimental and theoretical, by Gerischer and Heller indicate that electron transfer resulting in the reduction of oxygen is the driving force and the rate-limiting step behind the process. [1, 6-7]

Ollis *et al.* [4] was the first to try to implement semiconductor photocatalysts for this application for aromatic compounds with other groups doing the same for non-aromatic

compounds; other classes of organic compounds have also been photomineralized. Among them are alkanes, alcohols, carboxylic acids, polymers, dyes, surfactants, pesticides and herbicides.[1, 4] Titanium dioxide is used because, apart from the fact that it meets the criteria specified in **section 1.3**, it has an industrial standard – Degussa P25, a 70:30 mixture of anatase: rutile phase titania which could be used for comparative purposes between results of different groups.[1, 4-5]

The importance of using a standard lies in the fact that, due to differences in morphology, crystal phase, surface area, particle size and surface density of hydroxide groups in titania the destruction of organics will vary from one film of titania to another.[10]

1.5 Photonic Crystals

To have an understanding of what a photonic crystal is, comparison to a crystal is necessary. A crystal is a periodic arrangement of atoms or molecules. The crystal lattice is formed when a small, basic building block of atoms/molecules is repeated in space. The crystal geometry will determine most of its most important properties. If the crystal lattice presents a strong potential modulation an energy gap may be introduced into its band structure. If that is the case, the electrons with certain energies are forbidden to propagate in the crystal. A complete band gap will result if the gap can be extended to all directions. [11]

The photonic crystal is the optical analogy but with the difference being that the periodicity is not due to atoms but macroscopic dielectric media. If a photon propagating in the photonic crystal is subjected to a periodic modulation of the dielectric constant a highly directional photonic band gap (PBG) will open. In the PBG,

light can be prevented from propagating in certain directions with these specified energies. Photonic crystals can therefore be used for optical control and manipulation.[11]

There are different types of photonic crystals: 1-Dimensional, 2-D and 3-D. Even though these structures are different (**Figure 1.4**) they all have in common the periodicity of two media with different dielectric constants. By solving Maxwell's equations to obtain their band structure, different properties can be extracted for each of them. A one-dimensional photonic crystal will exhibit a photonic band gap but only in one direction (it is homogeneous in the other two). A three-dimensional crystal will have a complete photonic band gap, which means that no photons are allowed to propagate in any directions if their energy falls in the PBG. The gap width and position can be precisely tailored by choosing the right dielectric contrast and periodicity length scale to allow a higher amount of optical control.

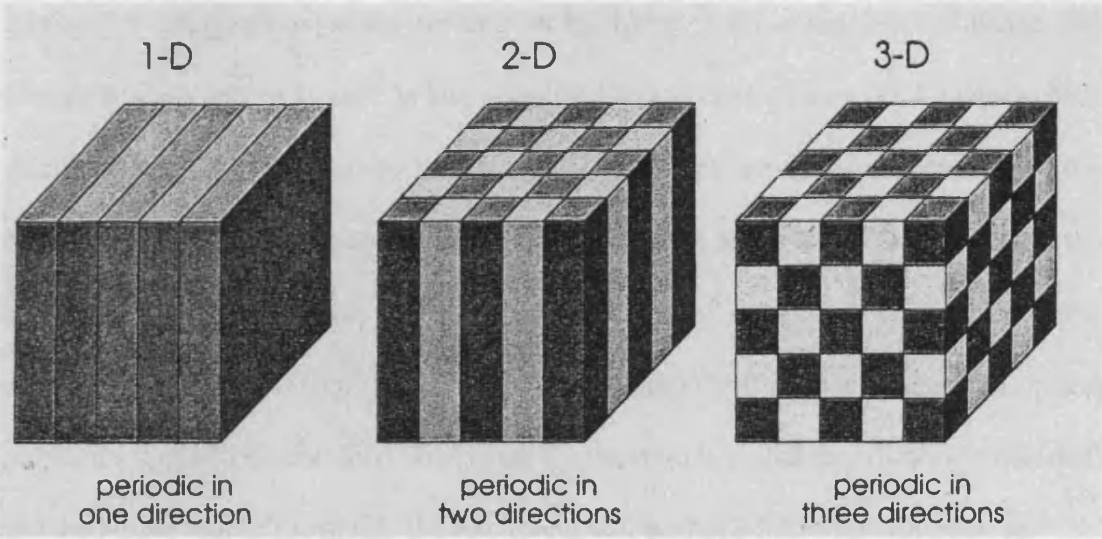

Figure 1.4 Simple examples of one-, two-, and three- dimensional photonic crystals. The different shadings represent materials with different dielectric constants. The defining feature of a photonic crystal is the periodicity of a dielectric material along one or more axis. [11]

1.6 Three-Dimensional Photonic Crystals

The photonic band gap is analogous to the electronic band structure of semiconductors, in which the 'conduction' and 'valence' band surround the gap. In a PBG we have an 'air' band above the gap and a 'dielectric' band below it. [11] A three-dimensional photonic crystal is usually made of two different materials that have a different dielectric constants. Certain geometries in a 3D photonic crystal promote the existence of PBGs. Only a few materials with a complete photonic band gap in three dimensions have been discovered. The first of these was *Yablonovite* (named after its discoverer E. Yablonotovich). PBGs can be was fabricated by drilling a high dielectric medium along the three axes of the diamond lattice. It produces a full photonic bandgap (**Figure 1.5**) and it can thought of as having two interpenetrating diamond lattices, one a connected region of dielectric and another of air.

Lately, the inverted opal structure has attracted attention because of its relative ease of fabrication using self-assembly techniques by taking a three-dimensional lattice and placing a silica sphere at each lattice point of the face centre cubic (FCC) lattice. This sacrificial template can then be infiltrated with high-dielectric material and then SiO_2 opal can be removed. You end up with a high-dielectric material with air bubbles at the initial FCC lattice position. The crystal is therefore composed of two dielectric constants and the ratio (not the value) is what is important in determining the optical properties that will be obtained. The value for the ratio is called the 'dielectric contrast' and the higher this is, the higher the likelihood will be that a full PBG will open up.

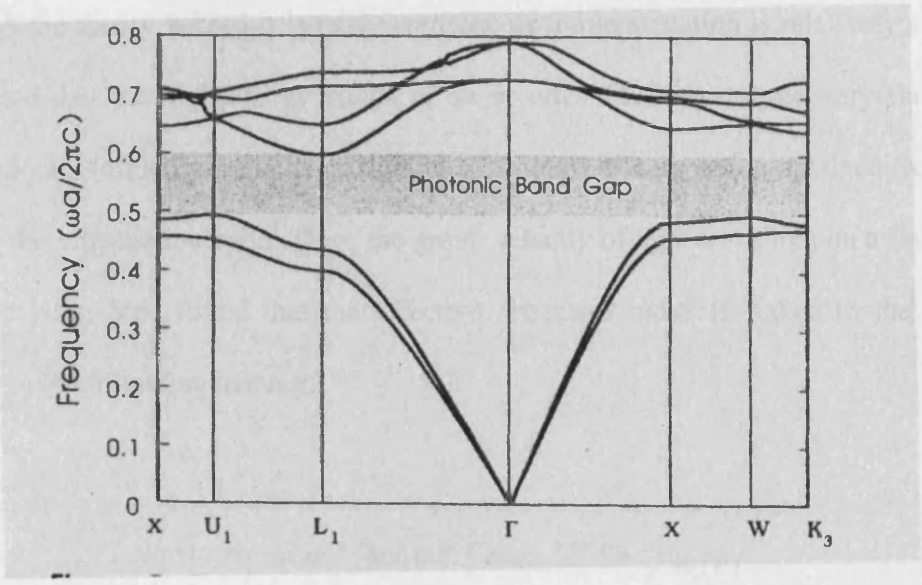

Figure 1.5 The photonic band structure of the Yablonovite. This shows the difference in dielectric ratios ('frequency') along the crystal directions (y-axis). The differences in ratio give rise to the PBG. [11]

It has also been found that, by introducing a defect, the lattice site is perturbed and therefore light can be trapped at a single point in the crystal. Light is trapped as a result of pulling a state from the continuum above or below the gap into the gap itself; a linear defect that extends in one direction. These can be introduced as air defects, for instance when a column of dielectric material is removed from the crystal, and a defect band with a frequency falling in the PBG can be thus created. Anything that changes the width or the frequency of the PBG can be very useful.

1.7 Photonic Crystals and Photocatalysis Enhancement

Recently, Sipe *et al.* found that photons propagating through a photonic crystal at certain frequencies or directions can effectively be slowed down by absorption when compared to a material that is not constructed in the form of a photonic crystal.[12] A way of testing this is to see whether photocatalytic enhancement can be obtained as this is a process that is based on photon absorption.[13]

Although the theory behind it is fairly complex its implementation is relatively simple. It is found that the high energy bands of an inverted FCC crystal are very flat. The group velocity (effective velocity of light in a medium) of a photon is obtained from the slope of the propagation band. Thus, the group velocity of light travelling on a flat band is almost zero. Sipe found that the effective refractive index is linked to the group velocity in the following manner:

$$\tilde{n}_{eff} = n_{eff,R} + n_{eff,i} \cdot i = \sigma \cdot \frac{c}{v_g(k)} \qquad \textbf{(1.4)}$$

$n_{eff,R}$ and n_{effI} are real and imaginary parts of the refractive index, i is the imaginary number, c is the velocity of light in a vacuum, $v_g(k)$ is the group velocity and σ is a function of the wavevector (the average of the dielectric constant of the photonic crystal weighted by the distribution of electromagnetic energy) that is given by:

$$\sigma = \frac{1}{2Vcell} \int \frac{\varepsilon c(\vec{r})}{\varepsilon 0} \left| \vec{E}\alpha, \vec{k}(\vec{r}) \right| d^3r \qquad \textbf{(1.5)}$$

V_{cell} is the volume of the unit cell of the lattice and $\varepsilon_C(r)$ is the dielectric constant of the system. This function may have an imaginary part that contains information about the losses of the materials of which the photonic crystal is made of. Therefore, as the group velocity of the photons decreases, the real part and absorption part of the refractive index increases rapidly. Absorption amplification then occurs for high energy flat bands. Titania made photonic crystals could be used since they have a high refractive index (2.5) and good oxidizing/reducing properties (as it has been discussed **sections 1.1- 1.3**). [13]

1.8 PBG structures and the Sol-gel process

1.8.1 Introduction

Sol-gel processing, because of its simplicity and low cost has been used to prepare PBG materials in all dimensions. Chemists began to be interested in this technique mid-1800s with simple observations on the hydrolysis of tetraethoxysilane (TEOS), where fibres could be pulled out from a "glass-like material"; nothing but descriptive studies were found until the 1950s and interest was only revived when Roy *et al* developed novel ceramic oxide compositions. Since then a fine-tuning and further (both theoretical and practical) understanding of the process has taken place. [14]

Three main approaches have been identified as being part of making a sol-gel monolith: 1) Gelation of a dispersion of colloidal powders; sols being defined as a dispersion of colloidal particles, and gels being defined as the interconnection formed by these particles to produce polymeric chains and 3 dimensional networks with an average length of a micrometer. 2) Hydrolysis and polycondensation of alkoxide precursors – followed by drying and 3) the same process as 2) but – followed by aging and drying under ambient atmospheres. *Mixing* in method 1) involves a suspension of colloidal powders with water at an appropriate pH to prevent precipitation; alkoxides precursors aren't mixed in 2) and 3) with water as it leads to hydrolysis. Sols are a low viscosity liquid that can be *cast* into a mold. In the next step, the viscosity subsequently increases and *gelation* occurs over time. The gel can be left to *age* (syneresis) where polycondensation increases inter particle connection and subsequently porosity decreases. This process is successful if it resists cracking under *drying*, where the liquid is removed from this network and capillary stresses develop. These can be reduced by adding surfactants that decrease the liquid surface energy or by hypercritical evaporation. In a sol-gel monolith derived from silica, *dehydration* (removal of Si-OH

bonds from the pore network) produces an ultraporous solid and these pores are eliminated by *densification* (heating at high temperatures).

Overall this process allows for control of the surfaces and interfaces of the material to produce more reliable materials. Researchers have discovered ways to integrate these methods to produce PBG materials chemically.[14]

1.8.2 1-Dimensional Photonic Crystals

The structures produced by sol-gel processing – either by dip or spin-coating, are called distributed Bragg reflectors (DBR). This is because their overall reflectivity, as well as being due to Bragg reflection, is also found to be very high; it consists of an alternating – high and low – stack of refractive index material. Consequently the refractive index can be changed by the use of different materials and also the number of layers that are produced. These terms are linked to produce a term for the optical thickness, the expression *nx*, of each layer, equals $\lambda/4$, where n = refractive index of the material, x = layer thickness and λ = wavelength for the Bragg reflection for the material. [15]

The differences in refractive indices have led researchers to try silica, titania and zirconium oxide as materials. Differences in contrast and number of layers that are achieved by using materials like these alter the reflectivities of the 'stop' band, which is where the forbidden range of light frequencies reflected by a dielectric mirror are located. Short densification heat treatments at higher temperatures have been used by researchers such as Rabaste *et al* to reduce the number of cracks that appear due to the higher number of layers. [15, 16]

Additionally, the controlled introduction of defects (the addition/suppression of a layer within an alternating refractive index stack) may increase the propagation of light within the stop band of - for example: doped semiconductors. Layer cracking can also be reduced, in a 1-D structure (**Figure 1.6**), and by using sol-gel processing, by introducing a Fabry-Perot microcavity; its quality can be calculated by using the full width at half maximum for a peak obtained from a reflectance spectrum.[17]

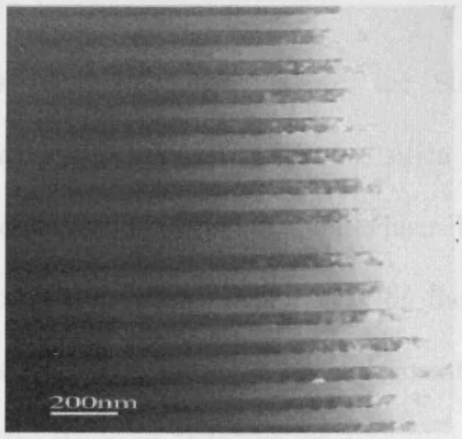

Figure 1.6 Examples of 1-dimensional structures (left), dark and bright regions correspond to SiO_2 and TiO_2 layers, respectively. [17]

1.8.3 2-D Photonic Crystals

Even though there aren't many examples of these structures in the literature they have been made by a molding procedure. Schuller *et al.*, used an organically modified silicate (a hybrid sol-gel material) to produce a photonic lattice. The material was pressed onto an elastomeric mold. [18] Shimada *et al.* dipped a patterned silicon wafer onto a titania solution of high concentration; once the gelation was completed, the titania gel PBGs were peeled off the silicon micromold, 2-D patterns such as rods and holes being extracted.[19] Line defects were also introduced. Bise *et al.* made fibres, composed of a silica core and a lower index triangular lattice of air holes running along the length of the fibre. [20]

1.8.4 3-D Photonic Crystals

The use of colloidal suspensions of opals has been the solution put forward to solve the problem of making highly ordered porous material with uniform sizes. Opals exist in natural forms – as precious gemstones (**Figure 1.7**) – that are made up of packed silica spheres surrounded by regions of disordered and amorphous silica. Artificial opals are the templates used to make PBG materials.

Colloidal suspensions have been prepared by the Stober and Stober-Fink-Bohn methods[13], where an arrangement of closed packed silica spheres are obtained by self-organization; obtained either by sedimentation, either by gravity, convective self-assembly, centrifugation and even combinations of these processes in steps. The processing time varies from days to weeks but its generally found that the longer it is then the more ordered the structure. [14, 21-23]

Inverse opals are made by infiltration with a high index sol and the subsequent removal of the template. This is a negative structure of the template, therein lies the importance of high quality of, say, a polystyrene template. This is called the template-assisted method as described by Colvin *et al.* [24]

Figure 1.7 Varieties of mineral opal (clockwise from top left): 'black', 'jelly' and 'precious fire' opals. [26]

Inverse opals may also be made by emulsion templating, as conceived by Imhof *et al.*, which use an emulsion of oil in formaldehyde as a template. The metal oxide sol is prepared in formamide, the solvent, with a little water (but not too much as the oxide vigorously reacts with this) that is added to the emulsion obtained. Samples with a high degree of order were obtained.[25]

Other synthetic approaches have been recently published on the making of 3-D crystals so that these could accommodate different conditions or substrates such as making these under quartz glass. Caruso *et al.* accomplish this by coating polystyrene spheres with polyelectrolyte multilayers (PEMs) of poly(allylamine hydrochloride) (PAH) or poly (sodium 4-styrenesulfonate) (PSS), which causes the silica opals to maintain their structural integrity in very dilute precursor solution, such as the ones used to make inverse opals from a lithium niobiate precursor. [27] Ozin *et al.* use micromolding in inverse silica opal (MISO), which involves creating a silica micromold by infiltrating a PS template with a silica precursor, and then infiltrating this with disilane by using

chemical vapour deposition (CVD, discussed in **section 1.9**), the thickness and structure controlled by the deposition conditions. The mold is removed by using a solution of hydrogen fluoride. This results in a structure with a full PBG. [28]

1.9 Chemical Vapour Deposition (CVD)

1.9.1 Introduction

This technique, which involves the dissociation/chemical reactions between gaseous reactants in a heated/light/plasma environment – forming a stable powder or film – was first used in 1893 by de Lodyguine to deposit tungsten onto carbon filaments. This was used industrially as a means to extract elements such as titanium and nickel to produce high purity refractory materials. Further understanding and refinement of the process (resulting in variants of CVD and lowering of chemical and safety hazards) for other applications - as coatings for production of semiconducting thin films or, more recently, nanostructured materials such as carbon nanotubes - has taken place in the last 40 years.[29]

Most CVD is performed in an 'open' system, whereby, after deposition, the reaction chemicals are removed from the reactor; recovery of the reactants depends on the cost efficiency of doing so. This is why a 'closed' system, where reactants and products are recovered, is rarely used.

The process has several advantages mainly to do with ability to produce dense, pure materials; in films this translates to high uniformity, coverage and overall high reproducibility of process with control of crystal structure and morphology of the material. This control extends to deposition rates (which are also made at, more often

than not, low temperatures) and thickness of films. The set up can be reasonable, which comes with a reasonable cost. CVD is flexible - a wide range of precursors can be used. CVD proceeds via the steps shown below (**Figure 1.8**): 1) Generation of gaseous reactants, 2) their transport to a reaction chamber and 3) their reaction to form intermediate species. If the chamber temperature is above the decomposition temperature for these species, then reaction occurs to form powder and by-products, the latter being transported away from the chamber. If the chamber temperature is below the decomposition temperature, then diffusion across the boundary layer – a layer close to the substrate – occurs. The subsequent steps are that these intermediate species undergo 4) absorption onto a heated substrate, 5) reaction on the surface and diffusion to growth centres onto the film, 6) by-product removal from the boundary layer by diffusion, 7) transport of unreacted precursors away from the reaction chamber. [29]

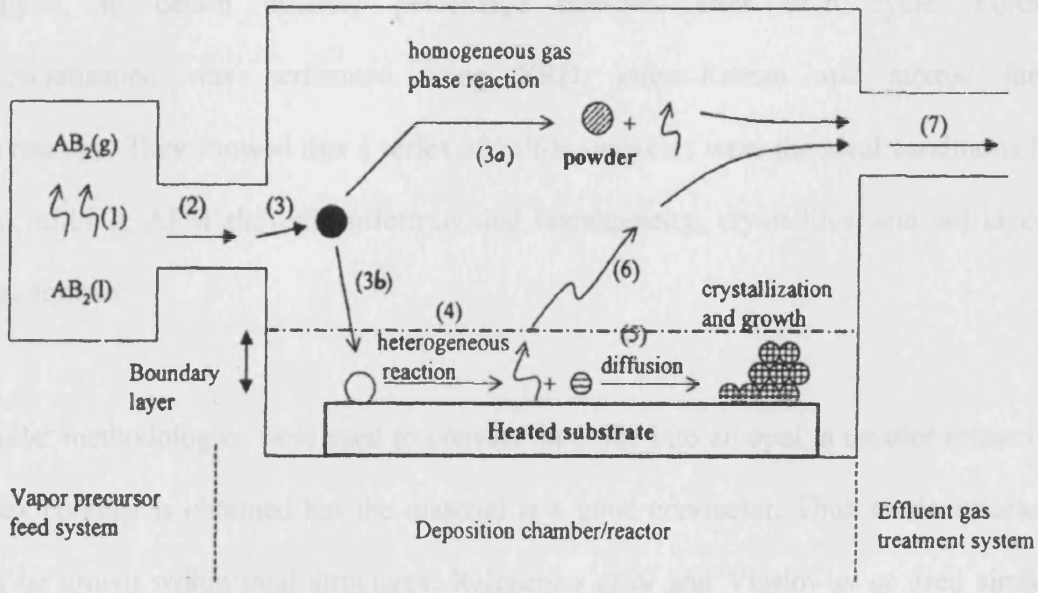

Figure 1.8 Scheme showing the steps for the CVD process. [29]

1.9.2 CVD and PBG materials

Chemical vapour deposition has been used as an alternative to void-infilling of latex templates. Yates *et al.* fabricated high quality synthetic indium phosphate from silica opals, these have a higher dielectric contrast than that found in a silica opal ($\varepsilon = 2.1$ as opposed to $\varepsilon = 3.5$-4 in a InP inverse opal), which is necessary so as to produce an enhancement of PBG behaviour if not an actual full photonic band gap.[30-32] By using silica opals the material could be sintered (950°C, 3 hours) to enhance the mechanical stability and metal-organic vapour CVD applied. This method consists of a pre-growth heat treatment under hydrogen (to remove any moisture) and subsequent application of the reactants (trimethylindium and phosphine; added separately, and at different temperatures, which has the effect of increasing diffusion into the sample as well as reducing the formation of side-reactants). The cycle is repeated several times. To optimise the experiment the authors used the shift in Bragg reflections, and the spectral analysis, to obtain infilling percentage numbers after each cycle. Further characterisation was performed using XRD, micro-Raman and atomic force microscopy. They showed that a series of half-hour cycles were the ideal conditions for best infilling. AFM showed uniformity and homogeneity; crystallites, and not layers, were formed.

Similar methodologies were used to convert tin oxide into an opal; a smaller refractive index contrast is obtained but the material is a good conductor. Thus semiconductors can be grown within opal structures. Ralchenko *et al* and Vlaslov *et al* used similar techniques to make inverse opals of carbon and silica respectively. [33-35]

Ozin *et al* have made further advances using CVD by making germanium inverse opals using digermane as a precursor. As before the conditions were varied until optimum

infilling conditions were achieved; different pressures resulted in different degrees of coating, and, ultimately, materials with different optical properties. The difference from previous work is that germanium has a very high dielectric constant ($\varepsilon = 16$) which allows for bandgaps of larger widths in the near infrared. [36]

Ozin's also used CVD, and reflectance/transmission spectroscopy, to map the infilling of a silica opal; they showed how the spectroscopic characteristics of the opal in the higher regions - its 'flat bands' - would gradually decompose into 'Fabry-Perot' fringes and finally into an absorption dip, as the silica-tungsten oxide composite is formed. By using reflectance spectroscopy to monitor the process, overfilling of the opal can thus be avoided and structural integrity of the inverse structure can be obtained. [37]

Finally, a variant of CVD - atomic layer deposition (ALD), which uses two or more precursors - was used by Tolbert *et al* to create inverse opals of tungsten nitride films, a non-oxide material, on flat substrates. [38]

1.10 Alternative Methods for preparing 3-dimensional Photonic Crystals

1.10.1 Polymerisation

Macroporous polymers are synthesised using organic precursors - liquid monomers crosslinked by thermal treatment - within silica or polymer colloidal templates. Compositions such as polydivinylbenzene (PDVB), polyurethane and poly (methyl acrylate), among others, have been prepared.[39-41] Inverse opals have also been made by filling opals – e.g. silica with preformed polymers – e.g poly (vindenylidene fluoride trifluoroethylene) copolymers in a cyclohexenone solution or a phenolic resin to make macroporous 'glassy' carbon.[39, 42-43] The silica was removed by using HF solution.

1.10.2 Salt Precipitation

Metal salt solutions can be used to prepare materials with increased order compared to polymerisation because, by using this route, complications arising due to atmospheric humidity are avoided. Immersion of these solutions in PMMA or PS with treatment in an oxalic acid solution to obtain a metal oxalate can be used to obtain a thermally stable metal oxalate. The framework can be calcined in an oxidising atmosphere to leave the 3 dimensional network of metal oxides/carbonates (e.g. MgO, $CaCO_3$). [44]

1.10.3 Nanocrystal Deposition

The removal of material has the disadvantage of causing shrinking and cracking. The effect can be avoided by codepositing small nanoparticles with colloidal spheres (**Figure 1.9**). Thin films of macroporous titania were prepared using this method by Ho *et al.* and Pine *et al.*; the degree of order would depend upon factors such as the drying rate/orientation of the glass substrate – horizontal or vertical, during deposition. Similar ideas were implemented to make inverse opals from CdSe and gold.[39, 45-47]

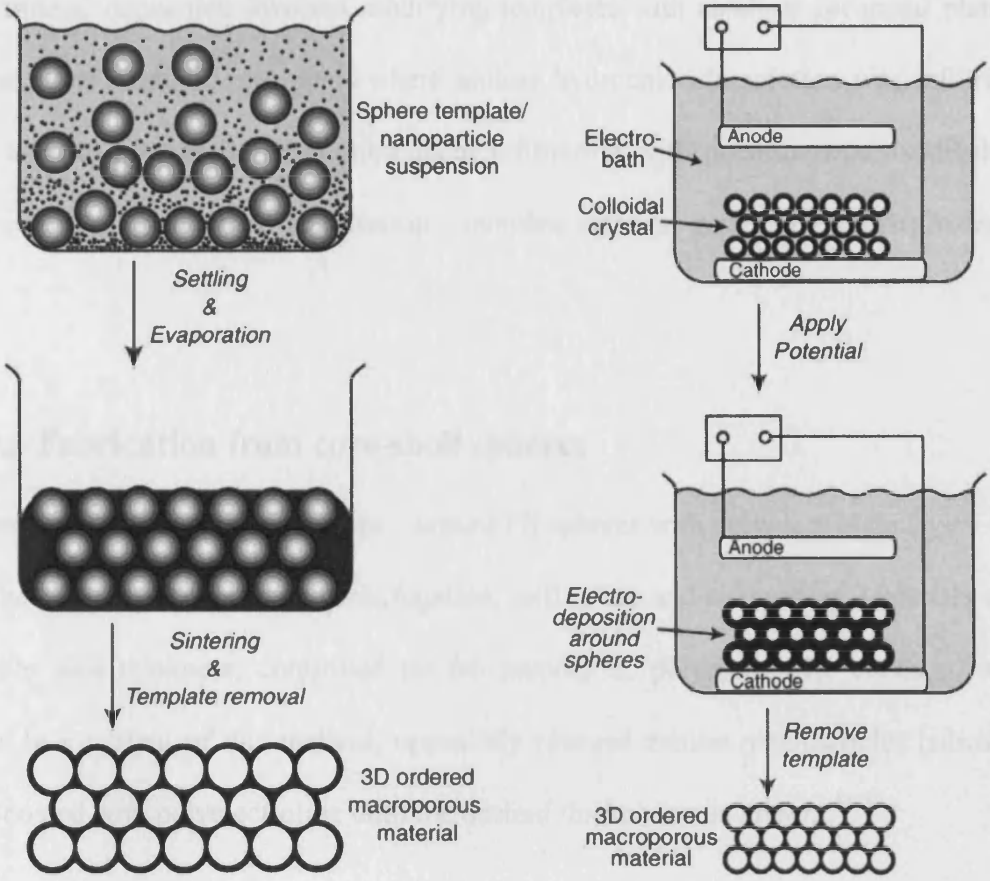

Figure 1.9 Schematic summarising two approaches for making inverse opals: the nanocrystal deposition is shown on the left and the electrodeposition approach on the right. [39]

1.10.4 Electrodeposition

An electrochemical method (**Figure 1.9**) for making inverse opals has been described. This involves placing ITO- colloidal crystal coated glass, which is formed by sedimentation, onto an electrode, placing a counter-electrode such as Pt above the sample and immersing it in an electrobath; once the potential is applied, the voids are filled by electrodeposition; metals are filled into the voids by reduction at the electrode from a salt solution and the template is removed; cadmium sulphide, selenide and zinc oxide have been prepared in this manner. [48,49]

'Electroless' deposition involves modifying templates with catalysts for metal plating. Caruso *et al* made inverse opals where aniline hydrochloride solution was infiltrated onto an opal by filtration and subsequent infiltration with potassium peroxodisulfate caused in situ oxidation polymerisation – template removal gave poly(aniline) material. [50]

1.10.5 Fabrication from core-shell spheres

Caruso *et al* used core-shell spheres – coated PS spheres with polyelectrolyte layers – as templates, with packing using centrifugation, infiltration and calcination. Materials with variable wall thickness, controlled by the number of polyelectrolyte coatings, were made. In a variant of this method, oppositely charged zeolite nanoparticles (silicates) were coated with polyelectrolyte until the desired thickness was grown. [51, 52]

1.10.6 Inverse opal Templating

Wiley *et al.*, used templates in a nanomolding approach, to form 'opal replicas', so that multi-composition shells could be manufactured. Non-polymeric templates such as nickel oxides inverse opals were made to electrochemically template gold spheres arrays. [53]

1.11 Conclusion

In this chapter a review of the work which forms the basis of this project has been carried out. **Sections 1.1 – 1.7** involved an introduction to photocatalysis and photonic crystals, respectively, and the theory that aims to combine the harvesting of light using titania photonic crystals (or inverse opals) has been elaborated upon. In sections 1.8 – 1.10 an introduction to chemical methods used to make inverse opals was given. Two of these, namely, sol-gel and CVD, are the methods to be applied here. These will be used

to make the titania photonic crystals for photocatalysis and the methodology used is outlined in **chapter 2**.

Chapter 2 Synthetic Preparation of Photonic Crystals

All experimental data reported in this chapter comes from a three-month secondment to Geff Ozin's lab at the University of Toronto. This chapter deals with making photonic crystals using the templating method. It also covers the infilling of synthetic opal structures by sol-gel and CVD methods. The purpose of this chapter is to present and discuss the experimental methods used to form ordered opal structures; to infill these opal structures with a titanium dioxide precursor and then to convert the precursor into a titanium dioxide matrix of tightly controlled microstructure.

2.1 Colvin Films of Latex Microspheres

Films were prepared with the method first described by Colvin *et al.* [54-55] This uses a vertical, self-assembly type deposition technique, relying on capillary forces to lay down colloidal crystal multilayers onto a substrate. The 'Colvin' method described in the **experimental** section. This way of laying the template originated from papers published by Nagayama *et al.* [56-57] except that the capillary forces were used to drive the assembly of larger polystyrene spheres (~ 1 μm diameter) to form well ordered monolayer films on a vertical surface. Later work from Nagayama showed how a precise control of thickness can be achieved. **Figure 2.1** shows a polystyrene sample. Colvin noted that the polystyrene spheres are oriented with the (111) axis of the colloidal crystal parallel to the substrate; this alignment, over millimetres of film, is given as the reason for the uniform colour displayed when viewed from a variety of angles. These films demonstrate close packing and long range order on the top surface. Colvin *et al.*, discuss the problem of establishing the exact nature of this arrangement as a product of the difficulty of establishing the angle of the cross-sectional view. Even if the top surface displays hexagonal close packing, calculations show that the face-

centred cubic arrangement is favoured.[54] Both ordered and partially ordered microstructures are obtained, as seen in **Figure 2.2**.

Two glass slides were secured face-to-face so as to make double the number of coatings from one liquid sample in the same vial (see **experimental chapter 6.2**). The film is thus only laid on one side of the substrate. UV and spectroscopic transmission-reflection analysis can thus easily be accomplished on the film. The substrate is marked to make sure that it can always be positioned in the same place in the spectrometer when carrying out UV measurements. This refinement is necessary to follow the infilling of the opal sample and examples of this process are given in **section 2.2**.

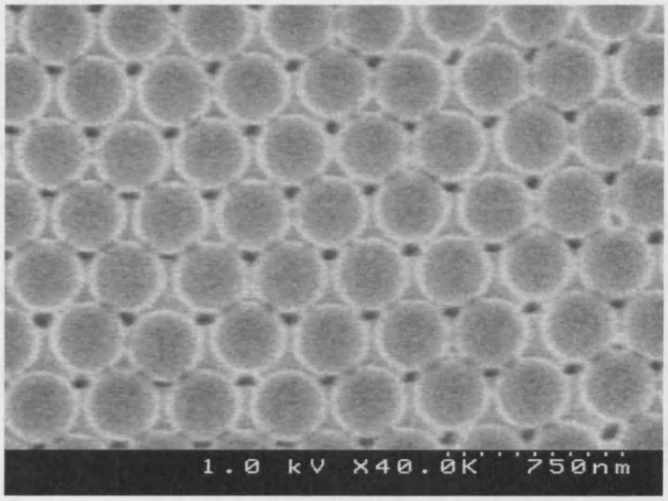

Figure 2.1 SEM picture showing Colvin film of ~250 nm diameter Latex microspheres made from a latex suspension in ethanol, made at GAO lab.

As the SEM in **figure 2.1** shows, the thin film has voids in-between the spheres. The latex spheres act as a template for the formation of titania 'inverse' opals. This colloid has no grain boundaries and was deemed to be a single crystal but not a perfect crystal as the dislocations seen in **figure 2.2** attest to. This is seen by Colvin as well as Lopez *et al.* in their studies involving silica opals. [58-59] However, any cracks and point defects can also be attributed to these films being exposed to high vacuum conditions when using

SEM and some slight structural changes engendered by using a thin gold coating required to avoid charging of the polystyrene sample.[54] The samples did not peel away easily upon scratching thus have good mechanical stability.

A film such as that shown in **figure 2.1** has peaks in two regions of the UV spectrum as seen in **Figure 2.3**. The other band, at ~ 700 nm for a 300 nm sphere size is called a 'stop band' and is where the propagation of light is inhibited over a narrow set of frequencies, producing a strong absorbance in the optical spectrum. The bands at 300-400 nm (the 'flat bands') are the absorption corresponding to low photon velocity in the crystal. Both bands are the result of an ordered periodic arrangement of particles - in this case latex spheres - where the optical properties are dominated by strong diffraction effects.

As explained in **chapter 1**, a photonic band gap can open up between photonic bands, and these gaps are the source of one of the optical features as seen in the UV-vis spectrum: the 'stop' band. This can be related to **figure 1.5** in **chapter 1**. In a study published by Miguez *et al.* that looks at the photonic band structure for silica/PS opals the stop band (formed at spectral range $(\phi/\lambda) < 0.7$ plotted at the y-axis) is shown to be formed by an absence of photon states along the L- Γ in the Brillouin zone except between the 2nd and 3rd bands (ϕ/λ = 0.4-0.45), where a maximum and minimum in the reflectance are observed. This is the origin of the pseudogap. The 'stop' band can be described as having both a 'blue' and a 'red' edge. On the former, light waves are localized on the low dielectric part of an opal or inverse opal. On the latter, light waves are localized in the high dielectric part of an opal/inverse opal. This situation is akin to that of an electronic semiconductor where electrons are localized just below or above the band bang gap (the top of the valence band and the bottom of the conduction band, respectively).[11] The 'flat' bands are cause by a pattern of transmittance dips that are

observed at a higher set of energies ($\phi/\lambda > 0.7$) in the photonic band structure for these opals), whose slope is very flat, hence the name, and its nature was explained further in **section 1.7**. [13]

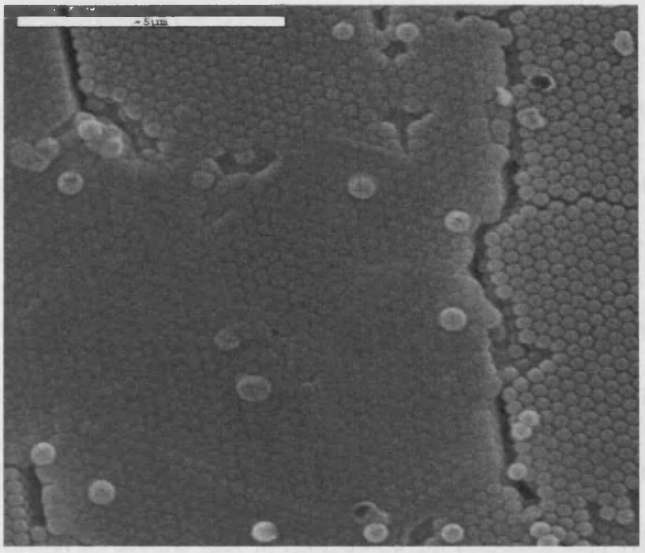

Figure 2.2 A less than ordered opal sample (cf to opal in figure 2.1) prepared using 'Colvin' method.

Colvin stated that the concentration of the spheres has a strong effect upon the number of layers that are placed on the glass substrate. Indeed, if the wrong concentration of latex solution is used there may not be enough layers present to display optical properties such as the 'stop' band. **Figure 2.3** illustrates this for two films made up of ~300 nm latex. The first film (black) displays a 'stop' band at ~700 nm and has a defined structure within the 300-400 nm region of the UV-visible spectrum. The other (green line) does not have enough material, evidenced by a smaller absorption in the 'flat' band region and a weaker 'stop' band. Additionally, this film's side-on SEM could not be observed – as it was too thin (effectively a single layer of spheres), unlike the kind of film shown in **figure 2.1**, which is about 10-15 layers thick.

Similar effects were observed by using reflectance measurements, which show a change in peak width with different thickness. [60] Also, a decrease in the total area covered on the substrate was observed and the film did not show birefringence when looked at

certain angles, which indicates a high degree of disorder. Therefore the film was not used for infiltration experiments.

2.2 Infiltration of voids in a latex film

The method used here to infiltrate the host latex-sphere structures involved either a sol-gel or CVD approach. The template used in each case being the well ordered\latex microspheres on a glass slide substrate (prominent flat and stop bands were seen). There are three problems to be overcome when using this method: 1) the preparation of a high-quality template must be ensured; 2) the voids must be infiltrated without damage to the template itself when completed; 3) when removing the template and making the 'inverse' opal, shrinkage must be as minimal as possible because this will influence the quality of the porous structure that is fabricated by this method, which impacts upon the optical quality and the definition of the 'flat' bands, as measured by UV-visible spectroscopy. Of the many approaches (as detailed in **section 1.8-1.10**) that have been described for infilling the voids in a template, three were evaluated for the present work:

1) Dip-coating in a sol-gel precursor.
2) Chemical Vapour Deposition
3) Self-assembly

2.2.1 Dip-coating of Latex Microspheres

Figure 2.4 shows the UV-visible spectra resulting from repeated dipping of a latex film into a titania precursor solution followed by hydrolysis and drying. See **experimental chapter 6.3**. Two things happen as the voids are filled by nanocrystalline titania: 1) the intensity of the UV peaks decreases and 2) the position of the stop band shifts to the red part of the spectrum. The shift of the 'stop' band is due to an increase in the refractive index contrast, which in turn is due to an increase in the filling fraction (i.e. the void

between the spheres being filled by a higher refractive index contrast material such as titania). Once the stop band does not shift position then it means that the voids have been completely filled and that calcination can be done to remove the latex microsphere template, leaving an inverse opal titania structure. Spectroscopy is necessary to follow the reaction as overfilling leads to unwanted coverage that may have consequences for the photoactivity displayed by the material. **Figure 2.5** illustrates the process for a different titania precursor.

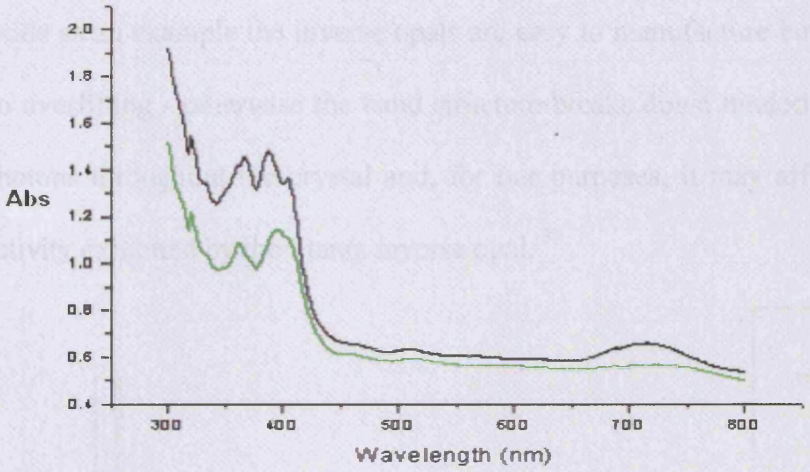

Figure 2.3 Optical absorption spectra for two ordered latex films made from ~300 nm spheres. One (black) has enough material to show a 'stop' band at ~700 nm. The other (green) is thinner and therefore does not show a pronounced 'stop' band.

The UV spectrum of the resultant inverse opal is shown in both **figures 2.4 and 2.5**. There is a shift in the 'stop' band to 450-500 nm. The 'blue' shift indicates removal of latex and that a different substance has taken its place as well as indication that shrinkage occurs. In the UV spectrum for the opal, Fabry-Perot fringes (or resonances) are seen after the stop band at ~500 nm, which result from the finite crystal size of the sample.[13] The organic material (and excess solvent) are removed by calcination, as is excess water. One consequence of this is some cracking of the structure as evidenced by SEM images in **Figure 2.6**.

The infiltration of the opal affects the flat band in the following manner: as the sample is filled with titania the higher energy bands are reduced in absorbance and the definition is decreased, smearing into "Fabry-Perot"- like fringes. In the last few spectra, the whole range is covered with them until these fringes disappear. What we have left with is an absorption dip. After calcination the 'flat' band of the resulting titania inverse opal is just observable – there is a slight 'bump', the line curves slightly, at ~350 nm as seen in **figure 2.4 and 2.5**. As von Freymann *et al* shows using tungsten oxide as an example the inverse opals are easy to manufacture but care must be taken - no overfilling - otherwise the band structure breaks down hindering the propagation of photons throughout the crystal and, for our purposes, it may affect the photocatalytic activity exhibited by the titania inverse opal.[37]

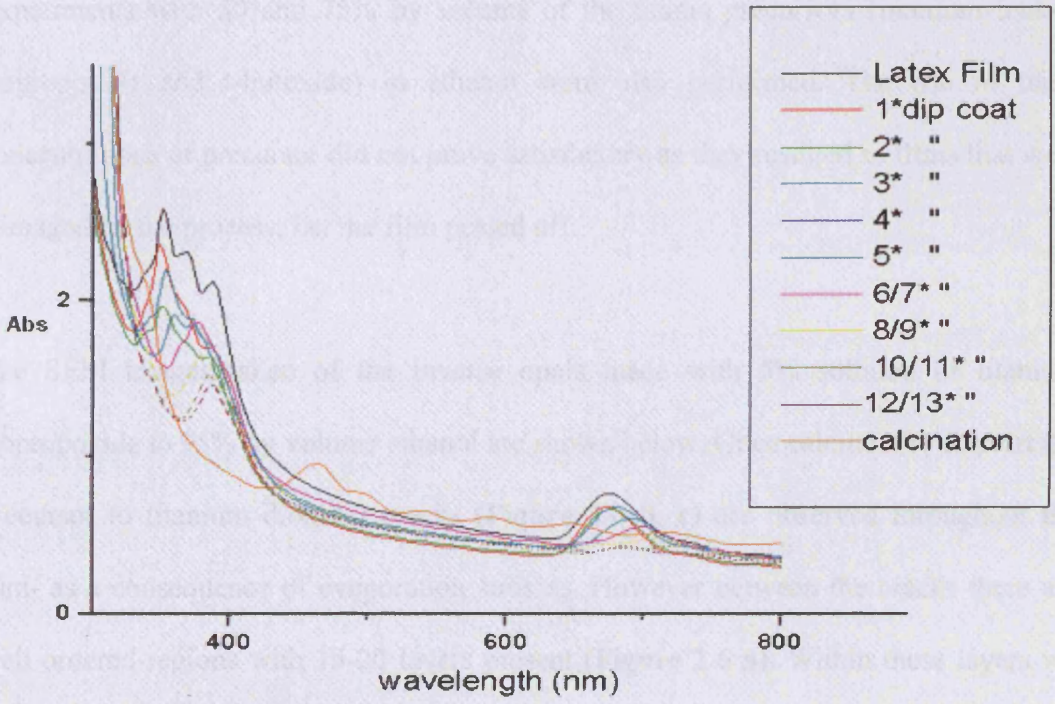

Figure 2.4 UV spectrum of latex film (PS, ~300 nm) that has been dip coated with a solution of 5% titanium butoxide.

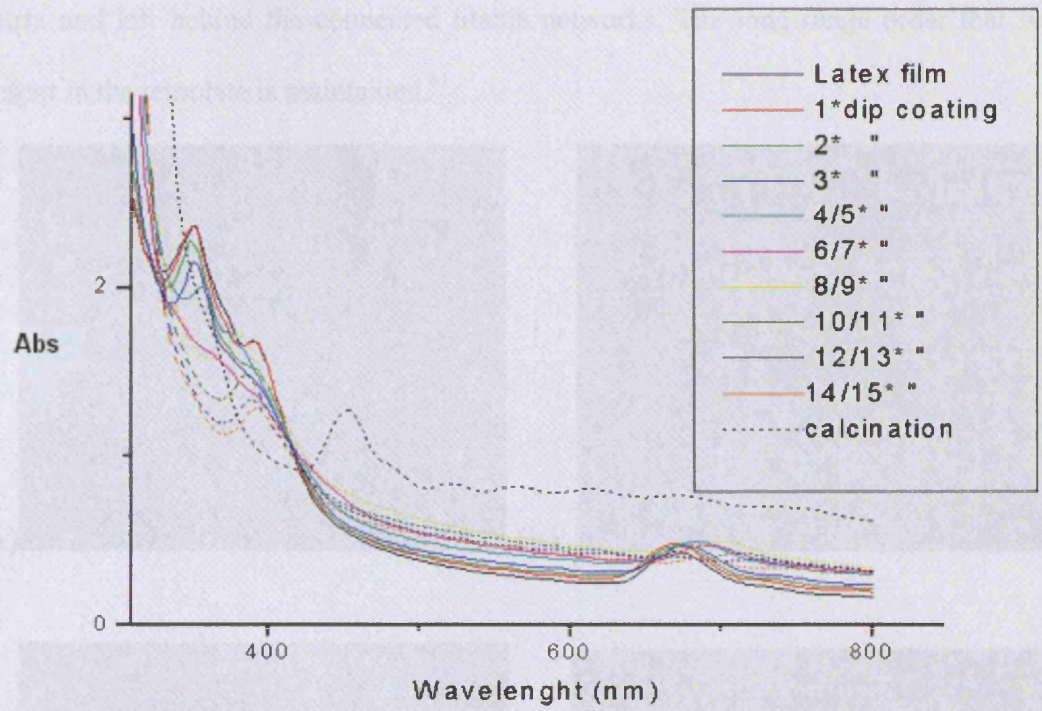

Figure 2.5 UV spectrum of a latex film (PS, ~300 nm) that has been dip coated with a solution of 5% titanium isopropoxide.

Experiments with 50 and 75% by volume of the titania precursors (titanium tetra-is isopropoxide and t-butoxide) in ethanol were also performed. The use of these concentrations of precursor did not prove satisfactory as they resulted in films that were damaged by the process; i.e. the film peeled off.

The SEM images taken of the inverse opals made with 5% solution of titanium isopropoxide to 95% by volume ethanol are shown below. Once calcined (to convert the precursor to titanium dioxide) cracks (**Figure 2.6 b, c**) are observed throughout the film- as a consequence of evaporation stresses. However between the cracks there are well ordered regions with 15-20 layers present (**Figure 2.6 a**). Within these layers we can see a mixture of material (titania) and little black holes- these holes are the air voids that are present. This is a highly porous structure - water/stearic acid can go through these air voids in a photocatalysis experiment (**Figure 2.6 a, d**) and, furthermore, cracks are present throughout the film (**figure 2.6 b, c**). It should be noted that the residual structures are that of inverse opals. The calcination procedure has burnt away the latex-

matrix and left behind the connected titania networks. The long-range order that was present in the template is maintained.[61]

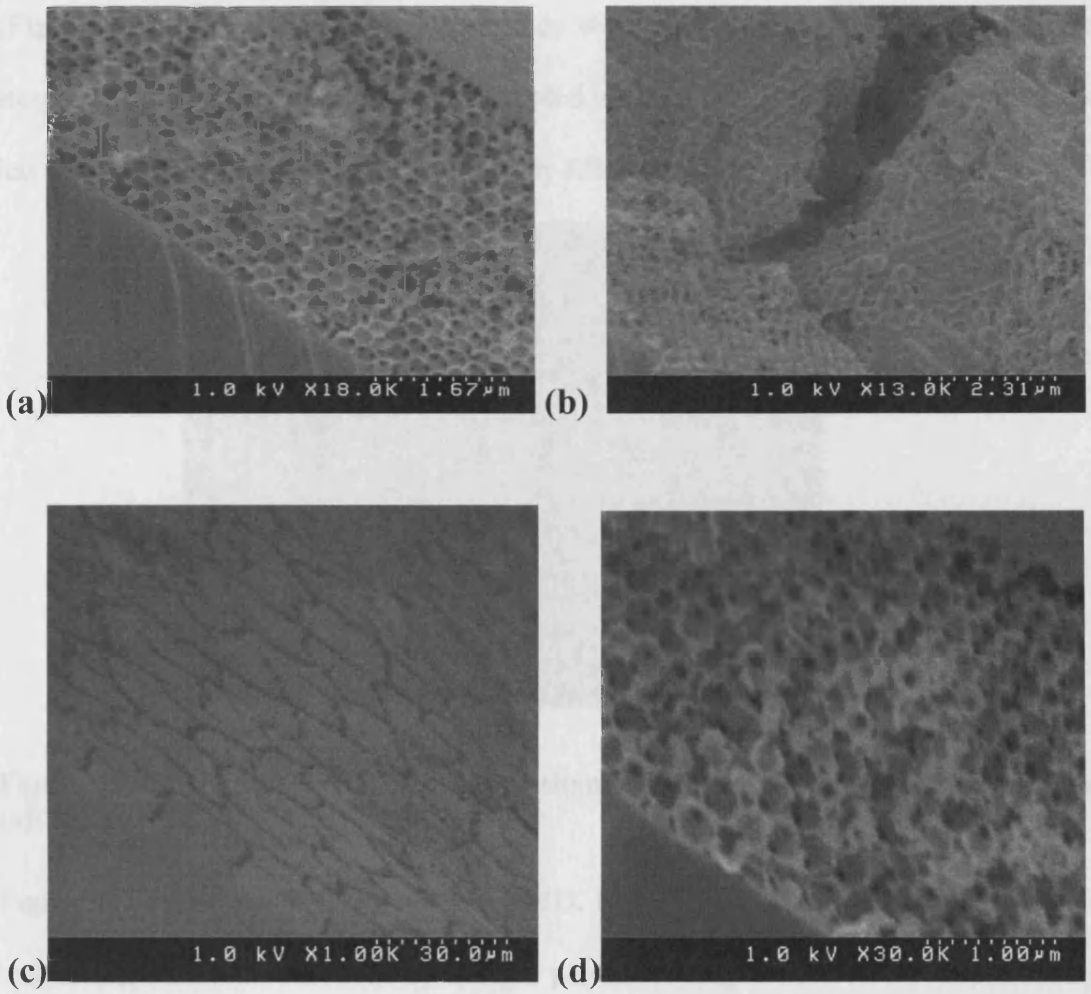

Figure 2.6 SEM images of one Titania inverse opal film produced by infiltration with a sol-gel precursor and removal of template by calcination.

2.2.2 Infiltration of the porous latex network by CVD

The Latex films were also infiltrated via CVD. This approach was reviewed in **chapter 1**. The opal film was placed in a small chamber in an upright position in a CVD rig, which consists of, among other things, a titania precursor bubbler. For full details of the rig and operation see **experimental chapter 6.5**. The reaction that occurs is shown in **eqn. (2.1)**. Note this CVD reaction is conducted at room temperature.

$$TiCl_4 + 2H_2O \longrightarrow TiO_2 + 4HCl \qquad \textbf{(2.1)}$$

Figure 2.7 shows that a honeycomb-like structure is obtained by doing low temperature CVD infiltration of the latex self-assembled structure. As the UV spectrum shows (**Figure 2.8**), after a couple of CVD cycles with titanium tetrachloride precursor the stop band has stopped shifting, which, coupled with the observation that the iridescence has ceased, means that the film is completely filled with titania.

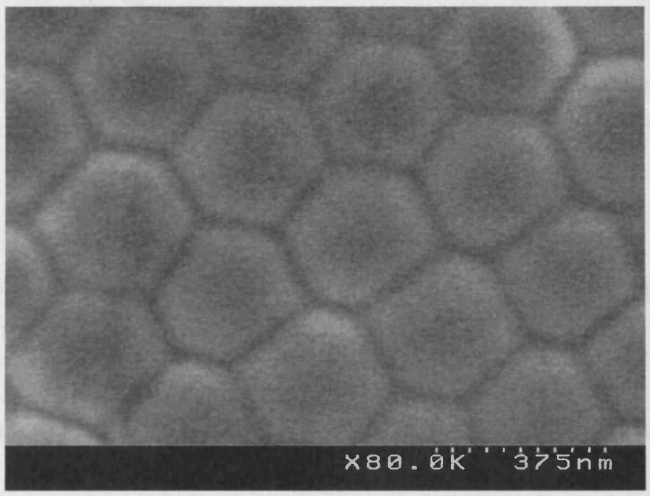

Figure 2.7 Latex film (PS, ~300 nm) - titania composite whose voids have been infiltrated by CVD.

Figure 2.7 shows a film filled by using CVD. Half of this was calcined, the other half had its latex template removed by using a plasma-etching device. A shift in the stop band position was observed when the latex was removed by using a plasma etching device, with concomitant loss of the definition of the 'flat' band – some of the optical property was lost. For the other half of this film, calcination caused loss of the stop band as well as the 'flat' band. This is illustrated in **figure 2.8** showing the spectrum of the film, which shows no optical features at all.

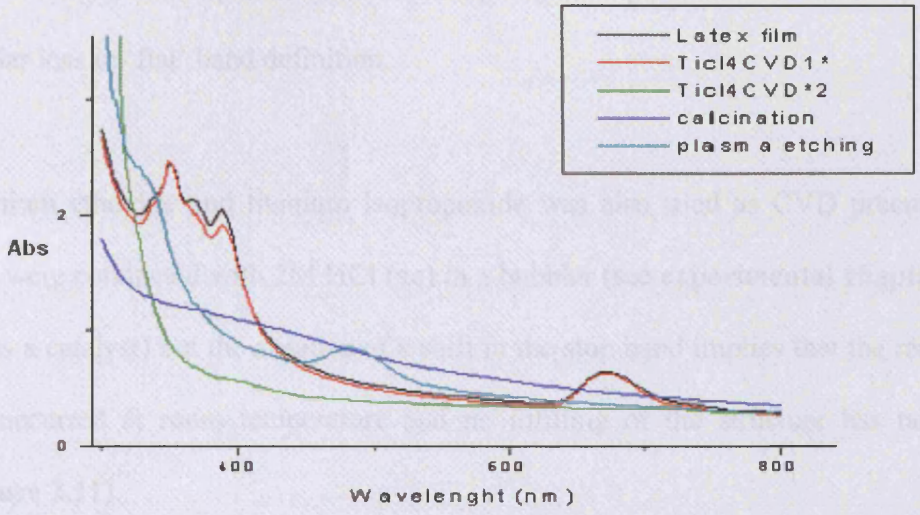

Figure 2.8 UV spectrum taken after each infiltration by using CVD: Latex film = PS, 300 nm, Ticl4CVD*1 = 1st run with CVD apparatus with titanium tetrachloride, Ticl4CVD*1 = 2nd run with CVD apparatus with titanium tetrachloride, calcination = UV spectrum taken after the composite film was calcined, plasma etching = UV spectrum taken after the composite film was plasma etched.

SEM comparison of the effects of plasma etching and calcination of the film is made in **figures 2.9 and 2.10**.

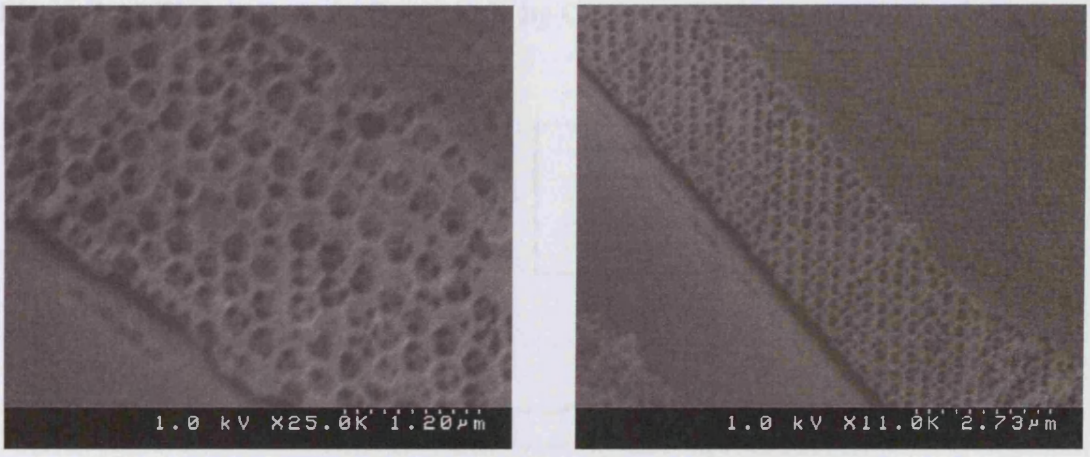

Figure 2.9 Titania inverse opal made by CVD ('edge' shots, left image) and plasma etched (about 12 layers are shown, right image).

As a comparison of **figure 2.9 and 2.10** shows, plasma etching seems to be more effective than calcination in forming well ordered inverse opal structures with more regularity and not as much cracking. However, the quality of optical properties has not been improved on the sol-gel method. Films prepared by CVD/plasma etching show a

similar shift in the stop band. The loss of optical quality is similar and is evidenced by a similar loss in 'flat' band definition.

Titanium ethoxide and titanium isopropoxide was also tried as CVD precursors, and runs were conducted with 2M HCl (aq) in a bubbler (see **experimental chapter 6.5**) (to act as a catalyst) but the absence of a shift in the stop band implies that the reaction has not occurred at room temperature and no infilling of the structure has taken place (**Figure 2.11**).

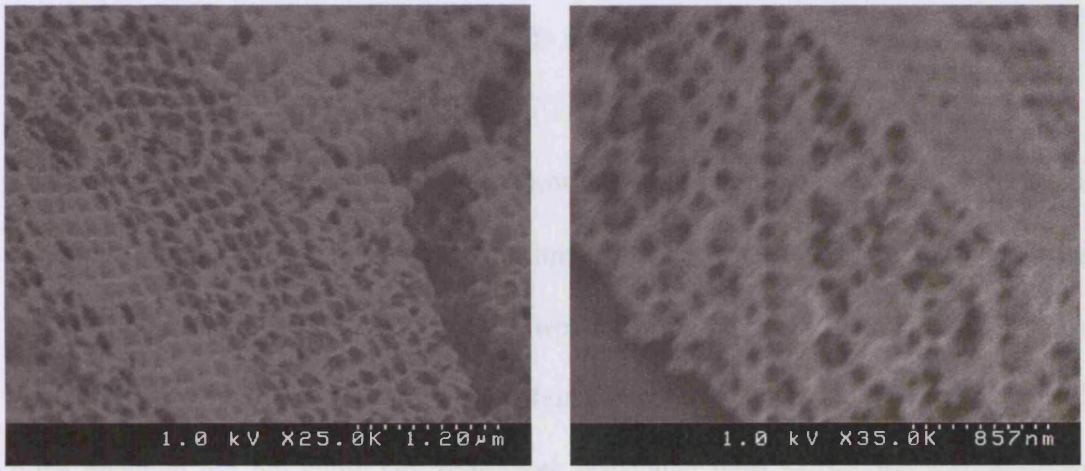

Figure 2.10 Titania Inverse Opal made by CVD; template removed by calcination.

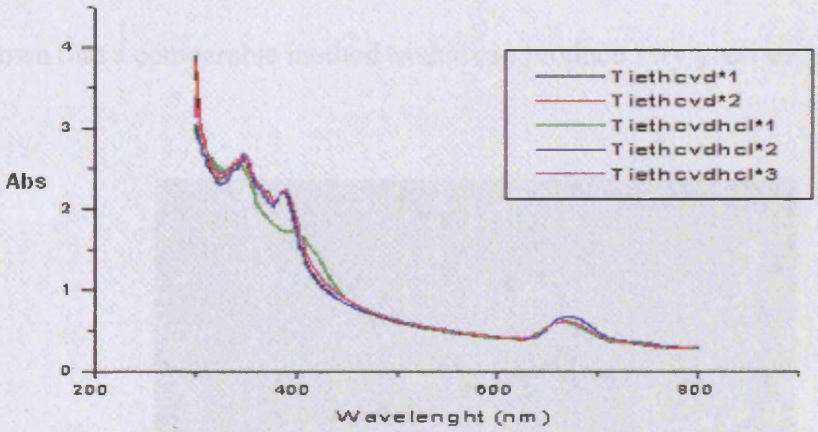

Figure 2.11 UV spectrum with Titanium ethoxide as precursor. Tiethcvd*1 = first CVD run with ethoxide precursor, tiethcvdhcl*1 = one CVD run with titanium ethoxide precursor with HCl in bubbler, tiethcvdhcl*2 and 3 = 2nd and 3rd runs with titanium ethoxide and HCl in bubbler.

2.2.3 Preparation of Inverse Opals by a Self-Assembly Method

This experiment involved co-assembly of titania particles along with the polystyrene. The slide is dipped into a solution containing both prepared colloidal titania particles (10-100 nm) (see experimental section for details) and polystyrene particles (a few hundred nm). The titanium dioxide particles are then dispersed in the liquid layer as the ordered template (polystyrene latex) is assembled. It was anticipated that the nanosized titania particles will fill the voids of the template when the liquid evaporates as a result of a convective water flux that carries the particles towards the voids. In another words, steps one and two (**section 1.10.3**) are made in one step.[62-63]

The UV spectrum of the resulting film showed no stop band and viewing by SEM did not show the anticipated microstructure, implying that titania covered the polystyrene latex structure (**Figure 2.12**). In this work using the preformed titania particles disrupted the formation of an ordered Colvin network of latex-spheres. This meant the films obtained did not show any properties associated with an ordered film (stop and flat bands). It should be noted however that during this work Sato and co-workers have shown that a comparable method to this can produce very good structures.[62-63]

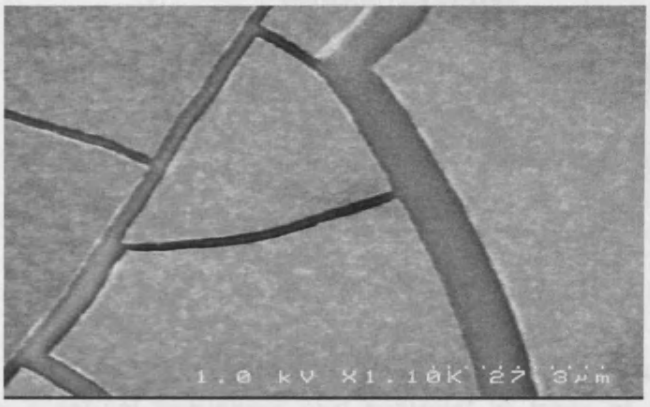

Figure 2.12 SEM image from self-assembly experiment.

The sol-gel and CVD methods for infiltrating opals worked easily and quickly and therefore were chosen to make the inverse opals of titania that were useful for photocatalysis experiments.

2.3 X-ray Diffraction of Titania Inverse Opals

Powder XRD was performed on films prepared using these techniques. A typical diffraction pattern is shown below. Both traces have poor resolution but despite that the first, sample **a**, (**Figure 2.13**) has a strong peak at $2\theta = 25°$, which has been matched to the anatase phase of titania. When calcined to 500 ^{0}C this peak disappears which might indicate conversion to the rutile phase. PXRD of an inverse opal made by CVD, which is then plasma etched, does not show a strong peak (**Figure 2.14**). Sample **a28**, when calcined at 500 ^{0}C showed a broad band at $2\theta = 25°$, which shows that it has not changed phase – PXRDs samples that have been used for photocatalysis will be shown **chapter 3** together with Raman data.[64]

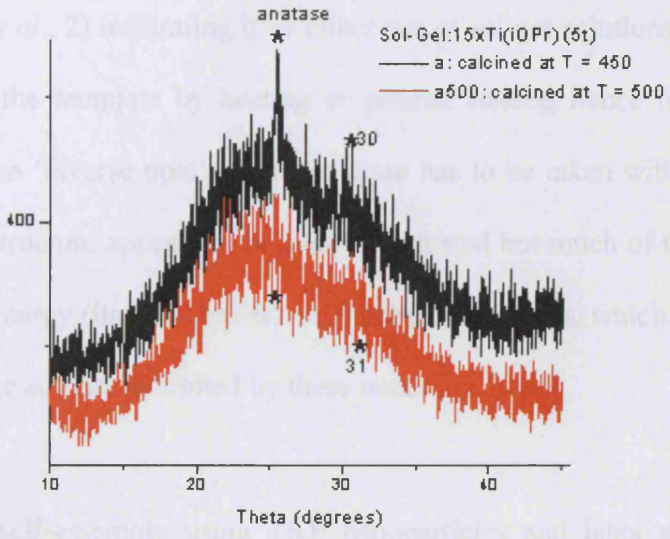

Figure 2.13 Powder X-ray diffraction of Titania Inverse opal made from infiltration by a sol-gel precursor and removal of latex at 450 °C (black) and further calcination at 500 °C (red). The numbers (*) show the matching peaks.

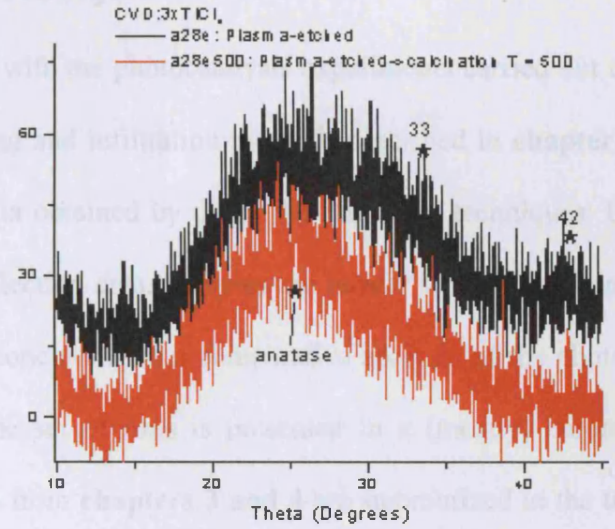

Figure 2.14 Powder X-ray diffraction of an inverse opal made by CVD (removal of template by plasma etching, black line) and calcination at 500 °C (red line).

2.4 Conclusions

In this chapter inverse opals of titanium dioxide were made using methods devised for other metal oxides as seen in **chapter 1** by following a 3-step method that consisted of: 1) constructing an opal template of polystyrene by laying it on glass using methods developed by Colvin *et al.*, 2) infiltrating it by either use of sol-gel solutions or by CVD and 3) getting rid of the template by heating or plasma etching hence inverting the structure and leaving an 'inverse opal' of titania. Care has to be taken with overfilling the opal; overall, the structure appears to be easily fabricated but much of the photonic structure at its higher energy (its 'flat' bands) are lost by this process, which in turn may affect the photocatalytic activity exhibited by these materials.

The method of dual self-assembly using TiO_2 nanoparticles and latex spheres was attempted and did not work. One attempt at this was, however, documented here.

Chapter 3 Photocatalysis

This chapter deals with the photocatalysis experiments carried out on samples made by using the templating and infiltration methods described in **chapter 2** together with the characterisation data obtained by using the following techniques: UV, Raman, PXRD, SEM and some reflection data. Samples are mostly written about individually, with the particular section concluding in a comparative analysis of the photocatalytic properties of all samples. The set of runs is presented in a (mostly) chronological order. The photocatalytic data from **chapters 3 and 4** are summarized in the table in the appendix section of this thesis.

3.1 Photocatalysis on samples made via CVD/sol-gel infiltration methods

These were the first attempts at making titania samples for photocatalysis using 365 nm light. The PS template, 300 nm, was laid on glass following the Colvin method, as described in **chapter 2**. The voids were infilled and the film was annealed at ~ 500 $^{\circ}$C (see **experimental chapter 6** for details). The opal sample, '5B', whose infiltration is shown in **figure 3.1**, had its voids filled by CVD, using UV spectroscopy as detailed in **section 2.2.2** to follow the infiltration cycle. In this case, the sample was treated in a metallic chamber and the reaction by-products were let out onto the open air. The first attempt at making an opal sample by CVD yielded a 'flat' band with poor definition, but the shift of this band to ~500 nm upon the first CVD cycle showed that the reaction in **eqn 2.1** had taken place. By the 3rd impregnation cycle the sample had been fully covered with titania, as there was no structure in the spectrum. Notably the 'stop' band had been nearly flattened indicating that the refractive index contrast present at the beginning of the sample had now gone and that the band had stopped shifting its position.[37] The sample was calcined at (a slightly higher) 500 °C (5 hrs), its spectrum

measured and the absorption obtained was compared to other samples as shown below in a 'normalised' plot.

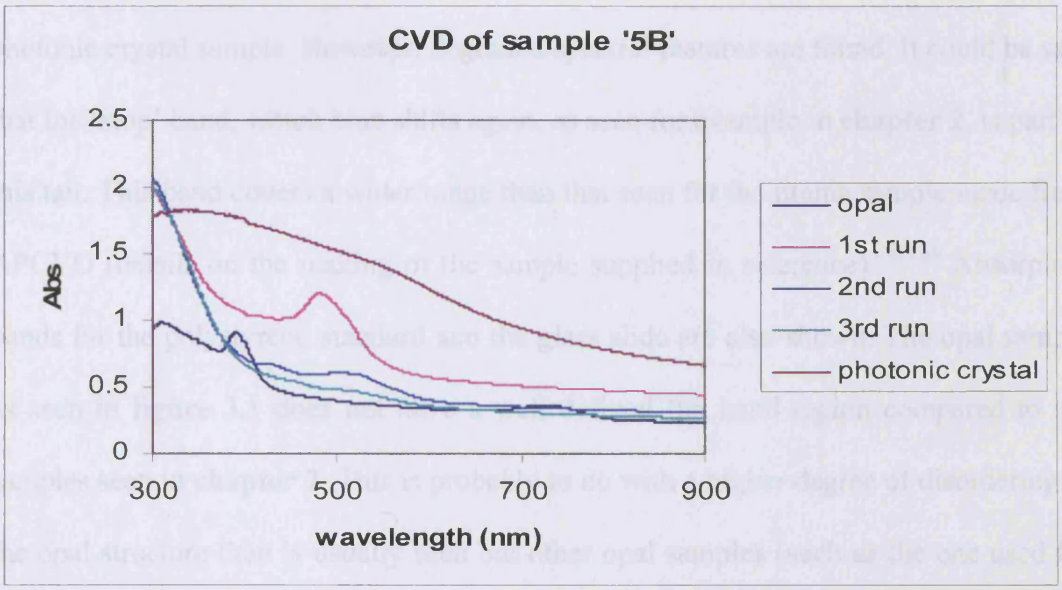

Figure 3.1 Infiltration of sample 5B using CVD, UV follows the opal (PS, 300 nm) infiltration; this consists of three runs; photonic crystal = UV after calcination of film at 500 °C (5 h).

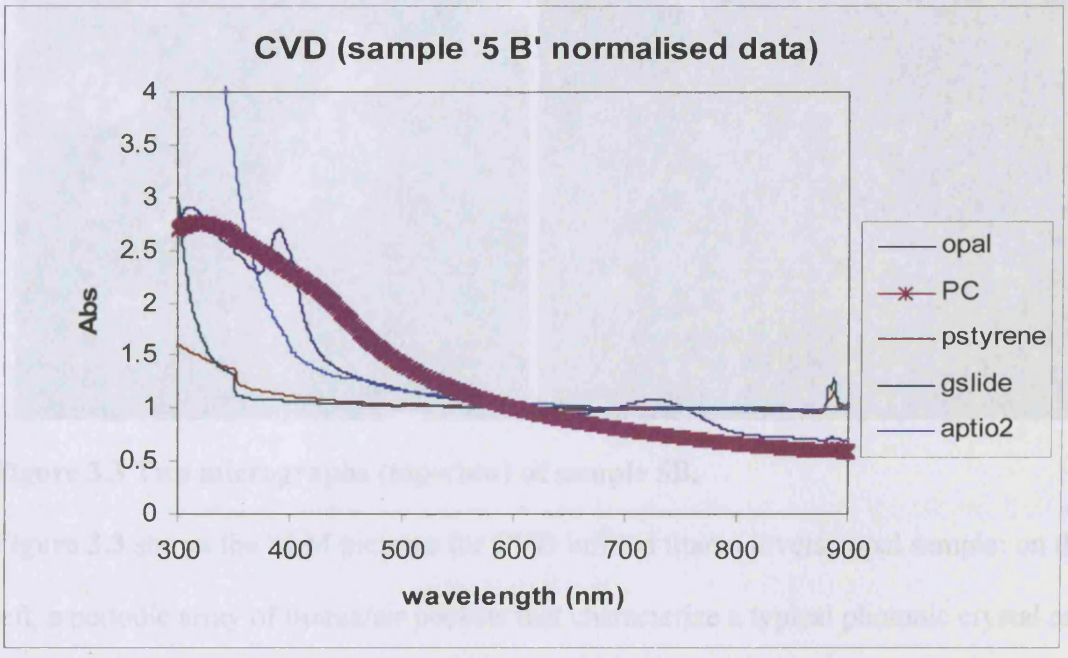

Figure 3.2 Comparison of absorptions of PC = Photonic crystal sample '5B' with pstyrene = polystyrene standard (film of polystyrene, 0.05 mm, supplied by Perkin-Elmer), gslide = glass slide and aptio2 = titania – no template - deposited on glass by using APCVD (one coat, supplied by S.O'Neill), opal = PS, 300 nm.

Figure 3.2 shows data that has been normalised, i.e. where the absorption for each sample has been made to equal 1 at 600 nm, so that the differences in the 'flat' band region (350-450 nm) are more apparent. By doing this, the spectra are slightly distorted,

though the variation of optical characteristics can be discerned more clearly between the samples. From this diagram a tail, which extends into the visible region, is seen for the photonic crystal sample. However, degraded spectral features are found. It could be said that the 'stop' band, which blue shifts again, as seen for example in **chapter 2**, is part of this tail. This band covers a wider range than that seen for the titania sample made from APCVD (details on the making of the sample supplied in reference). [65, 66] Absorption bands for the polystyrene standard and the glass slide are also shown. The opal sample as seen in **figure 3.1** does not have a well defined flat band region compared to the samples seen in **chapter 2**. This is probably to do with a higher degree of disordering in the opal structure than is usually seen but other opal samples (such as the one used for infilling via sol-gel, see **figure 3.3**) are of better quality.

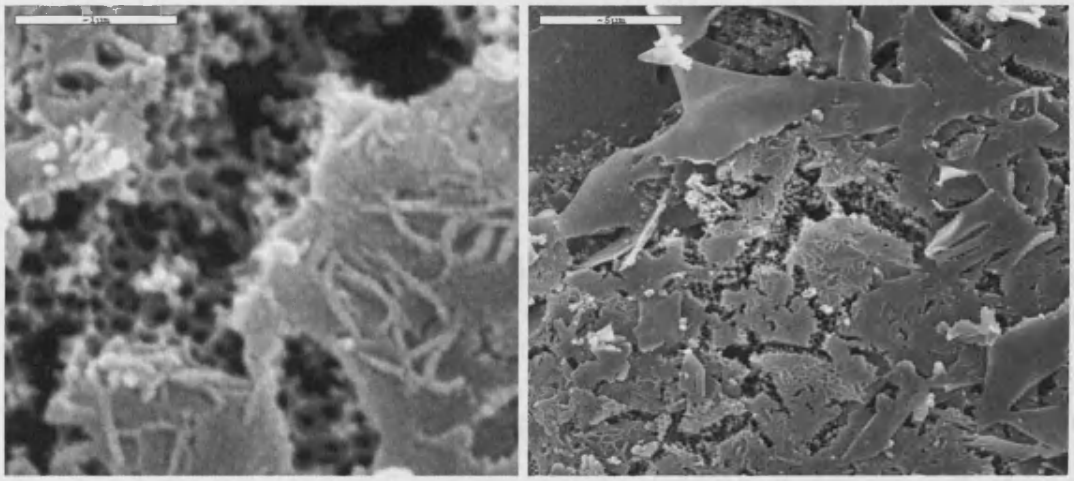

Figure 3.3 Two micrographs (top-view) of sample 5B.

Figure 3.3 shows the SEM pictures for CVD infilled titania inverse opal sample: on the left, a periodic array of titania/air pockets that characterize a typical photonic crystal can be seen, but the periodicity is broken by cracking and is seen underneath a layer of material not observed for samples reported in **chapter 2**. By using CVD an extra covering was made by overfilling the air-voids of the opal sample. Also, straw-like strands can be seen on this layer. On the right hand picture, extensive cracking can be seen across 15-20 microns of this film with regions of air/titania pockets seen among

the amorphous layer at the surface. The 'edge' of this particular sample could not be viewed using microscopy but similar samples show that 10-15 layers were obtained at similar concentrations. Void infilling was also performed on a similar PS opal structure, '21' using a sol-gel solution made from titanium isopropoxide and ethanol in a 90/10 ratio (v/v); as with the CVD sample, the infilling was followed by UV spectroscopy.

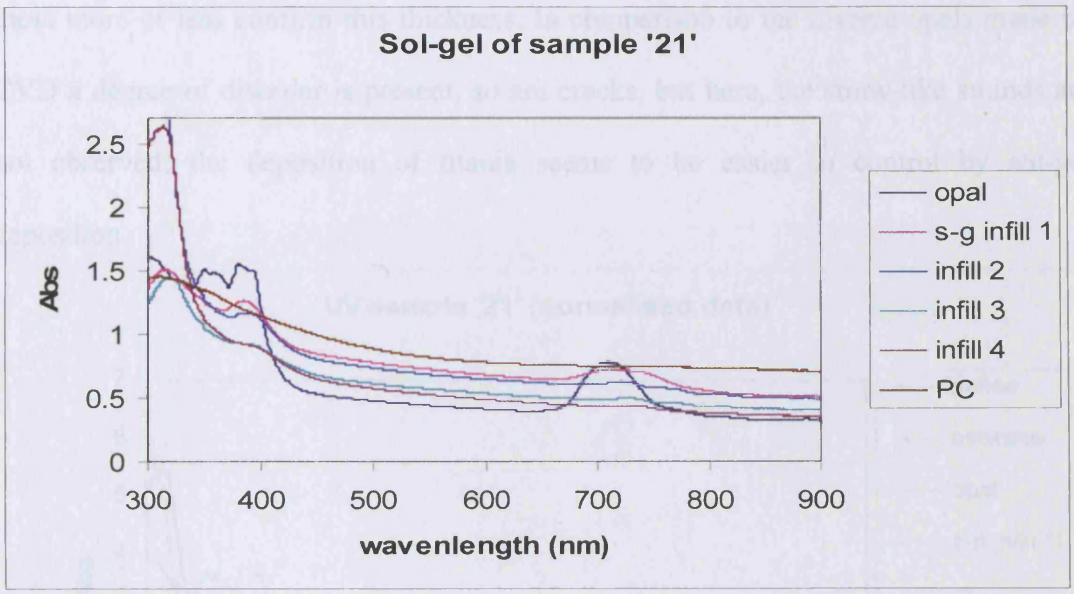

Figure 3.4 Sample '21', infiltrated via sol-gel procedure, using titania tetraisopropoxide/ethanol solution, and the experiment followed by using UV spectroscopy. Infill 1-4, UV taken after each dip-coating at 5-6 cm/min. PC = UV profile of photonic crystal after calcination at 500 °C (5 h).

The same spectroscopic characteristics are seen: the stop band is red shifted upon infiltration and the flat band is resolved into "Fabry-Perot" like fringes, signifying a breakdown in band structure. Once the sample is inverted under the same heating conditions (500 °C, 5 hrs), a weak band extending to the visible region is seen; a band that is not seen for any other sample, for instance (**figure 3.5**). The bands for the inverted photonic crystal sample are also compared to the opal/titania composite in **section 3.2** and a more pronounced peak is seen before heating. This unambiguously demonstrates a loss in optical quality.

Figure 3.6 shows regions of titania/air pockets that are obtained (top left) and that these are grouped as islands (top right). When the cracks are viewed closely, some of the 'edges', show layers of inverse opals, that can be readily seen (bottom picture). The 'edge of the structure could not be obtained but ~2-3 μm thickness could be estimated from that picture. The edge was obtained for other structures (seen in later sections) and these more or less confirm this thickness. In comparison to the inverse opals made by CVD a degree of disorder is present, so are cracks, but here, the straw-like strands are not observed; the deposition of titania seems to be easier to control by sol-gel deposition.

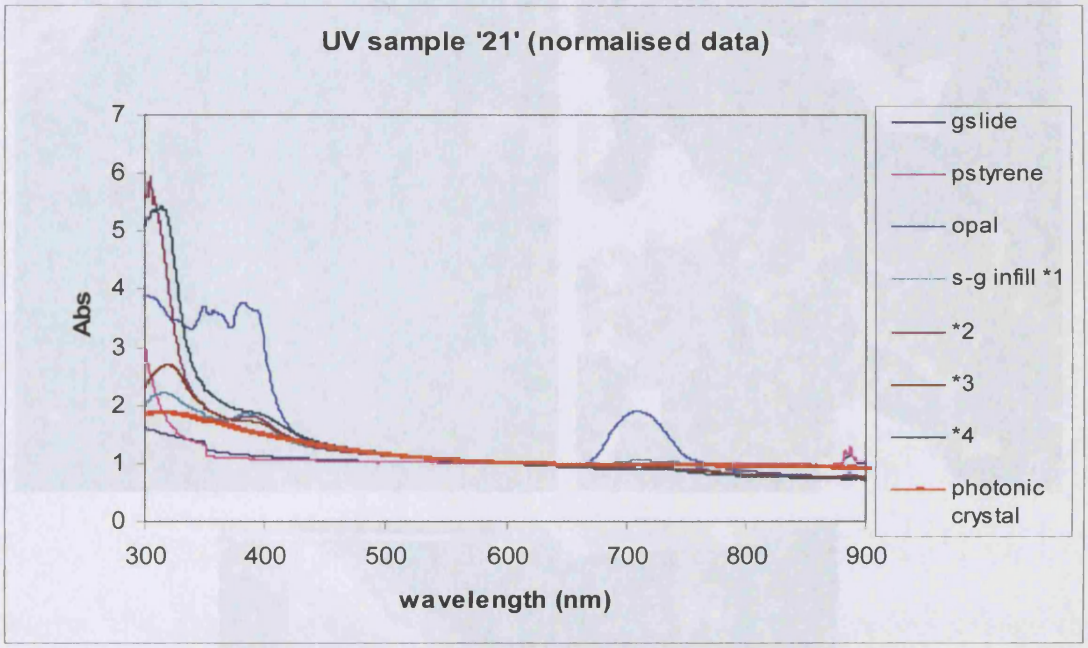

Figure 3.5 Comparison of absorptions of Photonic crystal sample '21' with pstyrene = polystyrene standard (film, as in figure 3.2), opal = latex template used, and *1 - *4 = latex/titania composites are also shown, gslide = glass slide and aptio2 = titania - no template - deposited on glass by using APCVD.

Raman spectra (**figure 3.7**) carried out on these samples shows that they display the same peaks as that seen for an anatase titania powder: 143 (vs), 396 (w), 516 (m) and 639 (ms) cm^{-1}, which differ from the values given for the rutile structure. [67] For the photocatalysis experiments as described in **experimental chapter 6.7**, a film of latex opal was placed alongside these inverse opal structures for comparison purposes. The

Raman pattern is given in **figure 3.7**. There is no Raman structure seen for the latex opal.

The XRD patterns for photonic crystal samples also match to the anatase phase of titanium dioxide. The most intense peak, at around $2\theta = 25°$ is assigned to the (1 0 1) plane of anatase (**figure 3.8**). [64] The powder XRD was performed in the range: $10<2\theta>70$.

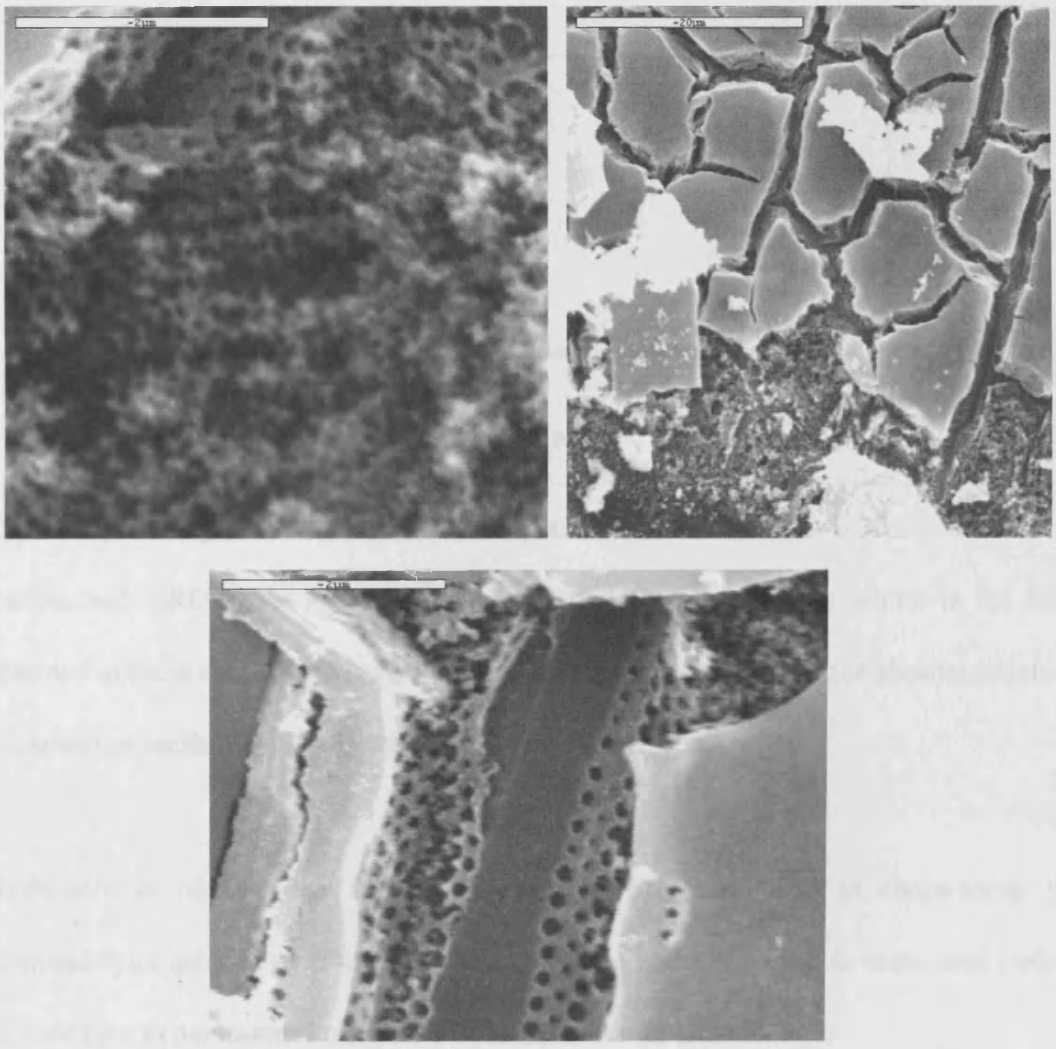

Figure 3.6 SEM micrographs of sample '21': top view (top pictures) and one of the cracks, showing inverse opals edge (bottom picture).

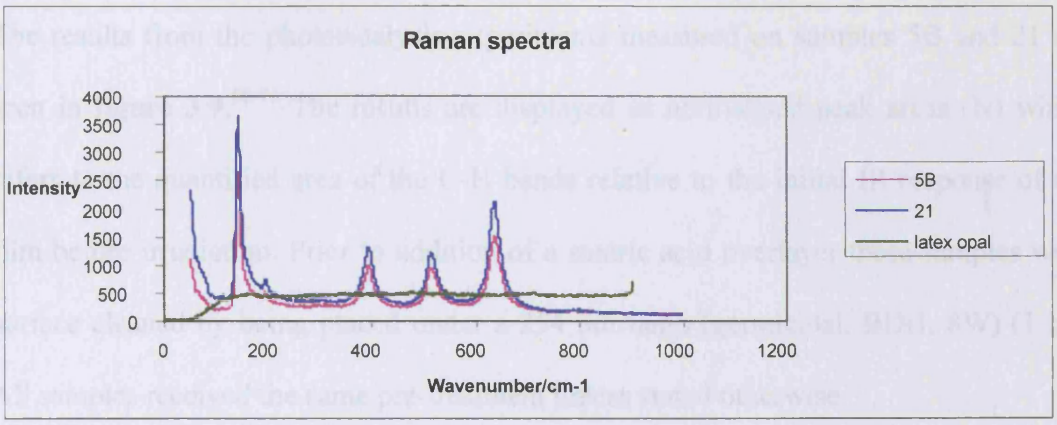

Figure 3.7 Raman pattern for photonic crystal film of titania and latex opal prepared by Colvin method.

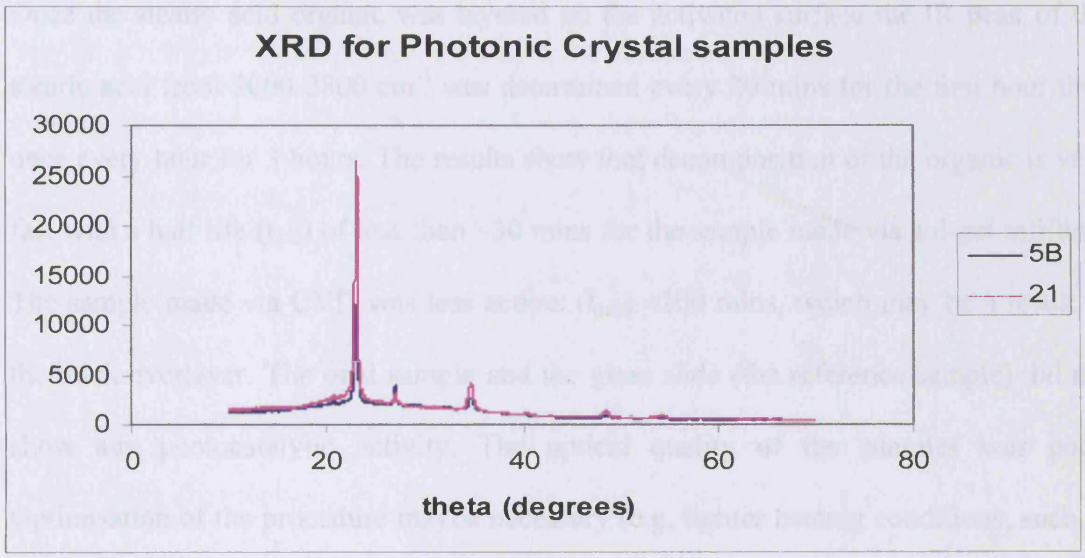

Figure 3.8 XRD patterns for photonic crystal films.

Raman and XRD show spectra that match to the anatase phase, which is the form obtained at these calcination temperatures. This is the desired form for photocatalysis as discussed in **section 1** and elsewhere in the literature.[1]

Hashimoto *et al.* was the first to use a layer of stearic acid to characterize the photocatalytic activity of films, where this organic is decomposed to water and carbon dioxide (see **experimental chapter 6.7**) as seen in **eqn (3.1)**, below:

$$C_{17}H_{35}COOH + 26O_2 \xrightarrow[\text{Light} \geq E_{bg}]{\text{Semiconductor}} 18CO_2 + 18H_2O \qquad \textbf{(3.1)}$$

The results from the photocatalysis experiments measured on samples 5B and 21 are seen in **figure 3.9**.[68-70] The results are displayed as normalised peak areas (N) which refers to the quantified area of the C-H bands relative to the initial IR response of the film before irradiation. Prior to addition of a stearic acid overlayer these samples were surface cleaned by being placed under a 254 nm lamp (germicidal, BDH, 8W) (1 hr). All samples received the same pre-treatment unless stated otherwise.

Once the stearic acid organic was layered on the activated surface the IR peak of the stearic acid from 3000-2800 cm^{-1} was determined every 20 mins for the first hour then once every hour for 3 hours. The results show that decomposition of the organic is very fast with a half life ($t_{1/2}$) of less than ~30 mins for the sample made via sol-gel infilling. The sample made via CVD was less active: ($t_{1/2}$) ~100 mins, which may be a result of the thick overlayer. The opal sample and the glass slide (the reference sample) did not show any photocatalytic activity. The optical quality of the samples was poor. Optimisation of the procedure maybe necessary (e.g. lighter heating conditions, such as a decrease in temperature, and heating for a shorter period of time, further care with infilling, especially when using CVD) if an improvement in optical quality is to be achieved. But overall; a very strong photocatalytic activity was observed despite the poor inverse opal optical quality. It should be noted that although the results were normalized care was taken to ensure that samples had an initial IR absorption for stearic acid that was within 10% of each other.

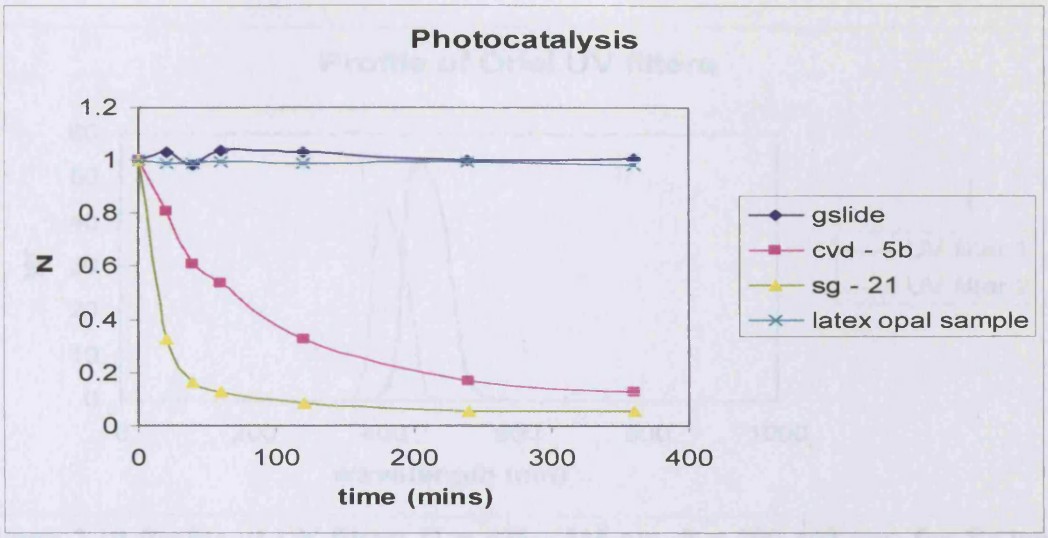

Figure 3.9 Photocatalysis run for the destruction of stearic acid overlayer using 365 nm irradiation for PC samples (5b, 21) and latex opal sample (300 nm) with gslide (glass slide, no coatings except with stearic acid) being used as a standard.

3.2 Photocatalysis run with Xenon Lamp

The slow-photon effect should be manifested in an increase of absorption at sub-bandgap wavelengths. The question is whether the increased light absorption results in photocatalysis at sub-bandgap wavelengths. This was evaluated by using a filtered Xenon lamp (Bentham IL1). Filters selected light in the following ranges: 435-515 nm and 390-460 nm – see details in the **experimental chapter**. The transmission spectra for these filters are shown in **figure 3.10**. Milder processing conditions (calcination at 450 °C, 2-3 hrs) yielded variable quality of inverse opal. The spectra are shown in **figure 3.11**. Inverse opals were prepared from opal sample '25' (via CVD) and sample '28' (via sol-gel). Both were used in runs with the 435-515 nm filter. Sample '25' shows a more defined band resulting from a blue shift in the 'stop' band, as shown in **figure 3.11** but sample '28' and '2' show a lack of definition. Both samples were assessed for photocatalytic activity using stearic acid on glass using Xe lamp with filter attached. However no photoactivity was observed even after prolonged radiation (72 h). This experiment indicates that these samples require sub 435 nm light for photoactivity.

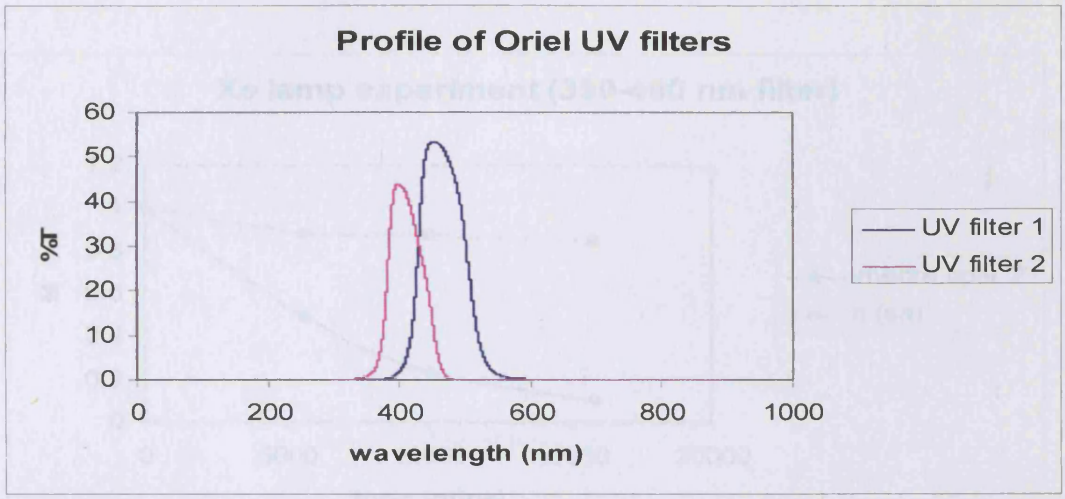

Figure 3.10 Profile of UV filters (1 = 435 - 515 nm, 2 = 390-460 nm) for Xe lamp experiments.

Sample '2' was prepared via sol-gel and was assessed for photocatalysis using a 390-460 nm filter. It did manage to decompose stearic acid with this filter as seen in **figure 3.12**. However, if the filter transmission spectrum is closely examined, some light is passed through at 365 nm. Indeed, it could be the light at this frequency that leaks through (sub-390 nm) that is responsible for the slow photocatalytic turn over. As before, a glass slide (layered with sa = stearic acid) was used as a reference.

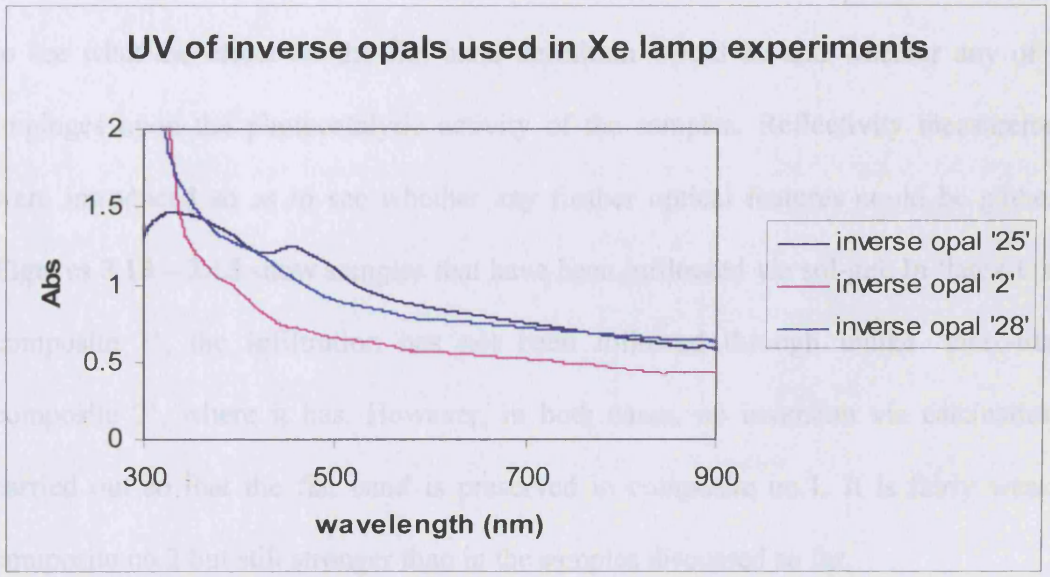

Figure 3.11 Band comparisons between photonic crystal samples made from PS, 300 nm, from dip-coatings with titania sol-gel precursor, and calcined at 450 °C. To be used for photocatalysis run with Xe lamp as a source. Sample '25' is the only one which seems to show any optical features and the 'flat' band at ~350-400 nm has lost its definition compared to the opal, the 'stop' band moves toward ~500 nm.

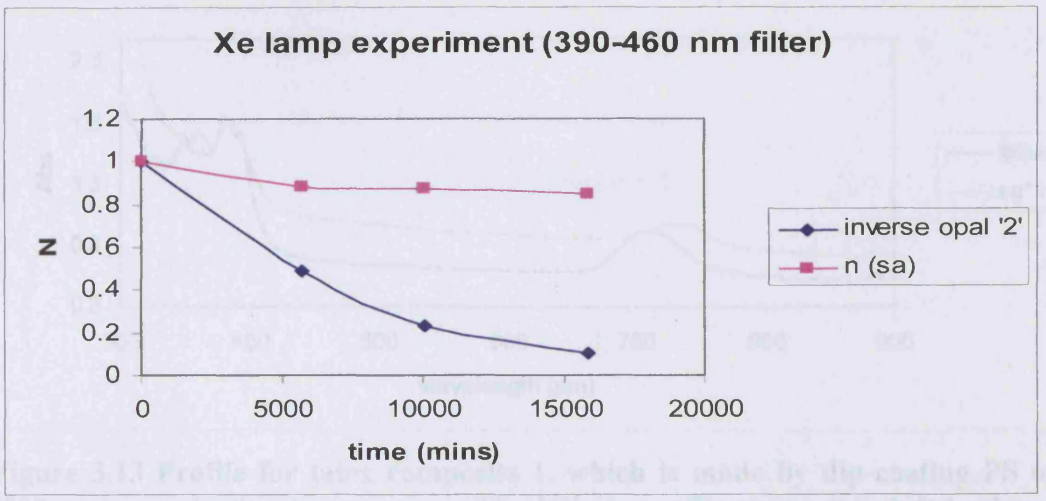

Figure 3.12 Photocatalysis run show degradation of stearic acid overlayer using Xe lamp with attached filter (390-460 nm) as source.

3.3 Further infiltration/Photocatalysis studies

In **section 3.1** it was seen that full infiltration and calcination leads to samples whose optical quality is quite poor – i.e. the 'flat' band definition has been reduced by the inversion process when compared to that of the latex opal template. In this section, latex-titania composites were made by varying the amount of titania deposited onto samples so that the opal voids were filled to varying degrees. This was carried out so as to see what the effect on the flat band definition would be and whether any of this impinges upon the photocatalytic activity of the samples. Reflectivity measurements were introduced so as to see whether any further optical features could be gathered. **Figures 3.13 – 3.15** show samples that have been infiltrated via sol-gel. In 'latex-titania composite 1', the infiltration has not been followed through unlike 'latex-titania composite 2', where it has. However, in both cases, no inversion via calcination is carried out so that the flat band is preserved in composite no.1. It is fairly weak in composite no.2 but still stronger than in the samples discussed so far.

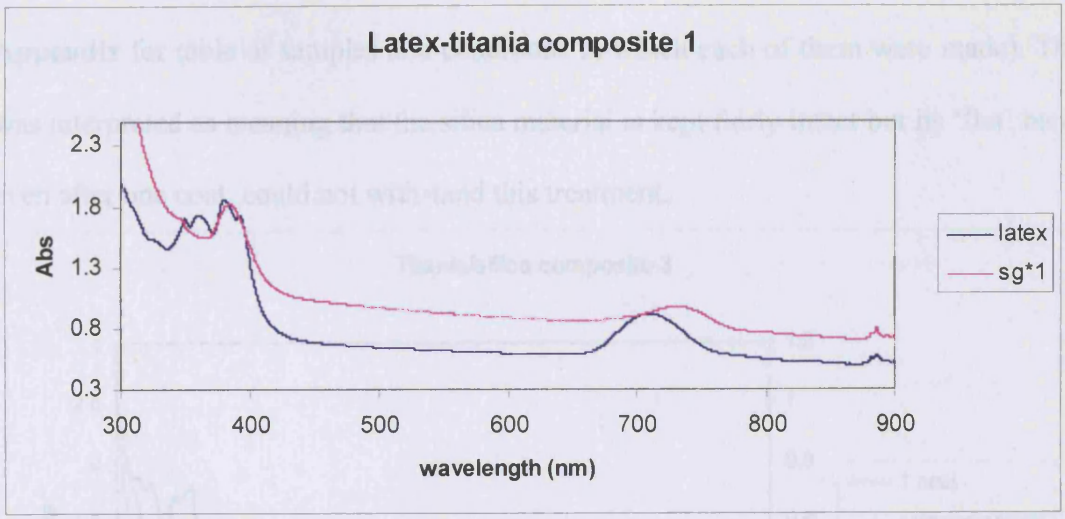

Figure 3.13 Profile for latex composite 1, which is made by dip-coating PS opal (300 nm) once in titania precursor. The UV-vis profile shows the shift in the stop band signifying a change in refractive index contrast. This sample was not calcined.

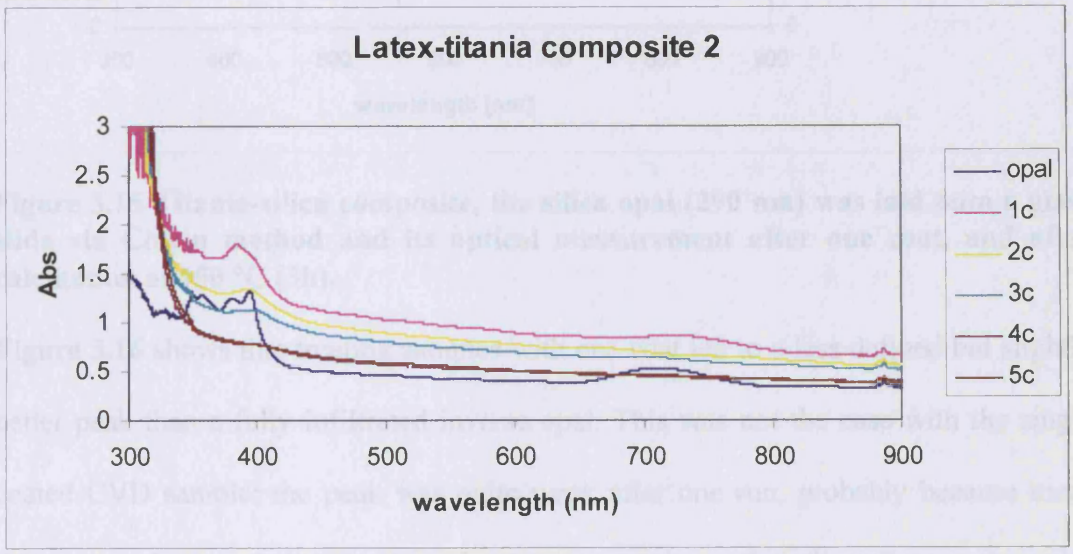

Figure 3.14 Profile for latex-titania composite 2: complete infiltration of latex (300 nm) sample with each UV taken after each coating, the structure is said to be fully infiltrated after 5 coatings (5 c) as the stop band has disappeared and there are no shifts in the 'flat' band. This sample was not calcined.

Finally, a composite was made from a silica, not polystyrene, opal. This is because silica can withstand higher temperatures – i.e. it is not calcined at 450 °C hence the photocatalytically active form of titania could be made as well as keeping the composite structure. 'Silica opal 4' was coated once and calcined at 450 °C for 3 hrs, a temperature that will effect a conversion to anatase titania (as confirmed by Raman measurement). The UV (**figure 3.15**) measured shows the 'stop' band has been blue shifted, but only slightly when compared to that of the fully inverted photonic crystal '6 A' (see

Appendix for table of samples and conditions in which each of them were made). This was interpreted as meaning that the silica material is kept fairly intact but its 'flat' band, even after one coat, could not withstand this treatment.

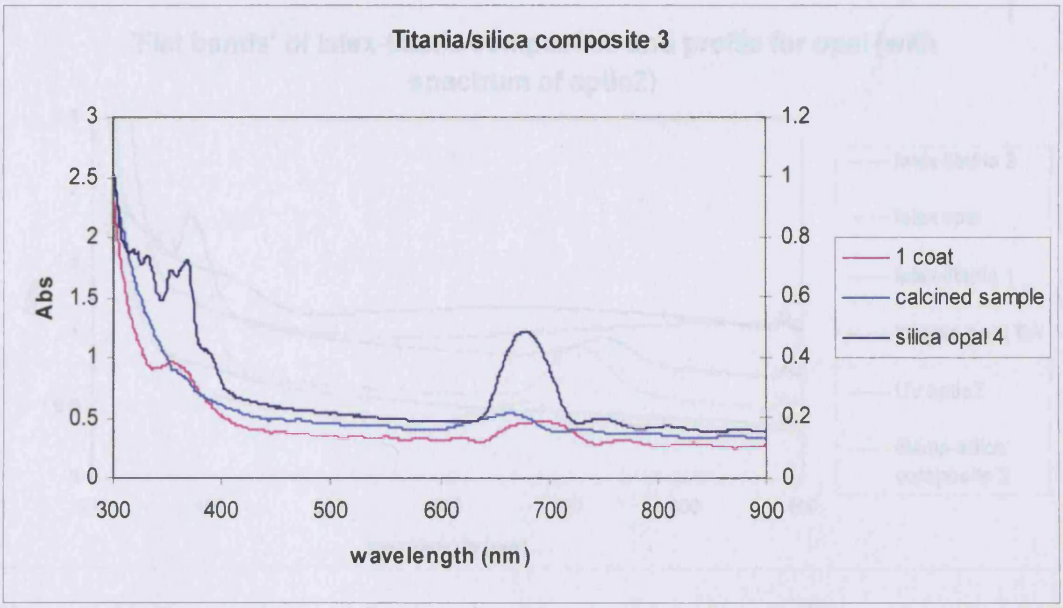

Figure 3.15 Titania-silica composite, the silica opal (290 nm) was laid onto a glass slide via Colvin method and its optical measurement after one coat, and after calcination at 450 °C (3h).

Figure 3.16 shows that treating samples with one coat led to a less defined but slightly better peak than a fully infiltrated inverse opal. This was not the case with the single coated CVD sample: the peak was quite weak after one run, probably because more titania was deposited than in the sol-gel treatment, even though surface coverage of titania was partial (see figure 3.13 for UV-vis of one coated sample).

A new photonic crystal sample ('6 A') was prepared for comparison. It differs from sample '21' (also made via sol-gel, see **section 3.1** for details) because of the heating conditions employed (450 °C, 1.5 h as opposed to 500 °C, 5 h). **Figure 3.16** compares the spectrum of that material with those of composites 1-3 described in the preceding paragraphs. The spectrum for a typical latex opal and for a titania film formed by APCVD are also shown ('aptio2'). As seen before, the spectrum for titania made from APCVD shows no extension into the visible, which resembles that for latex composites

2 and 3 but not 1 and '6 A'. The Raman spectra for both inverse opals are compared in **figure 3.17 (a)**. Although the signal for '21' is somewhat less intense than for '6 A' it still corresponds to anatase.

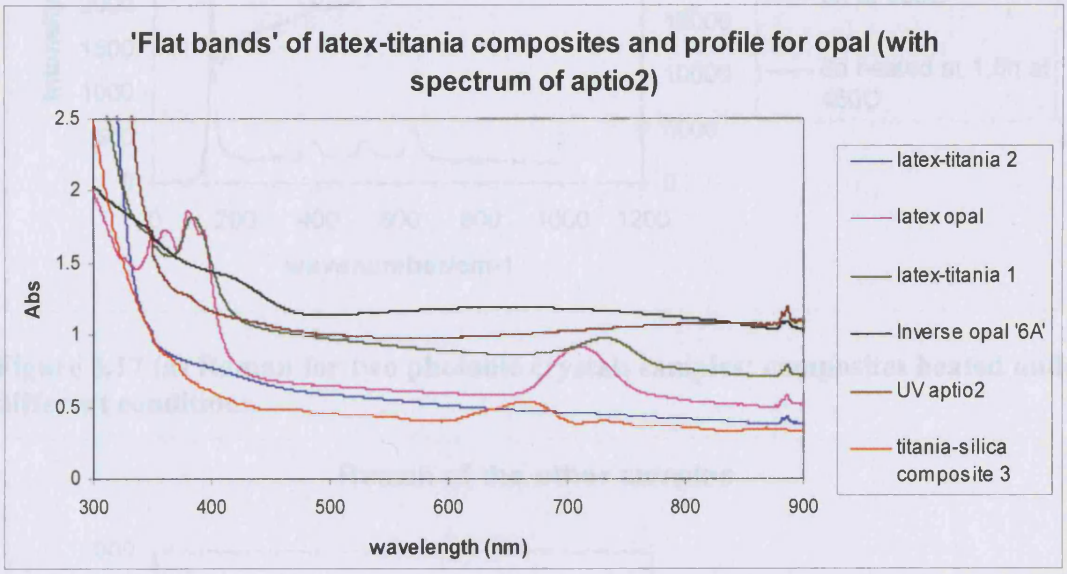

Figure 3.16 Comparison of flat bands of latex-titania composites and opal sample: it can be seen that none of the composites, whether silica or polystyrene based, exhibit the level of definition of the opal (PS, 300 nm) or the weak bands (~350 nm 'flat' band with 'stop' band at 450 nm) exhibited for inverse opal '6 A'.

Figure 3.17 (b) looks at the composite samples: both '1'and '2' have a similar pattern, which does not correspond to anatase titania therefore they should not be very active and will serve as further control like samples, in the way that the purely opal sample did in the previous photocatalytic 'run'. Composite 3, however, was heated at the temperature at which conversion to anatase is affected: the primary signal at ~145 cm^{-1} is quite weak. Nevertheless, all the numbers for the 4 peaks match. The pattern for the sample made from APCVD also corresponds to titania as measured and published elsewhere.[66]

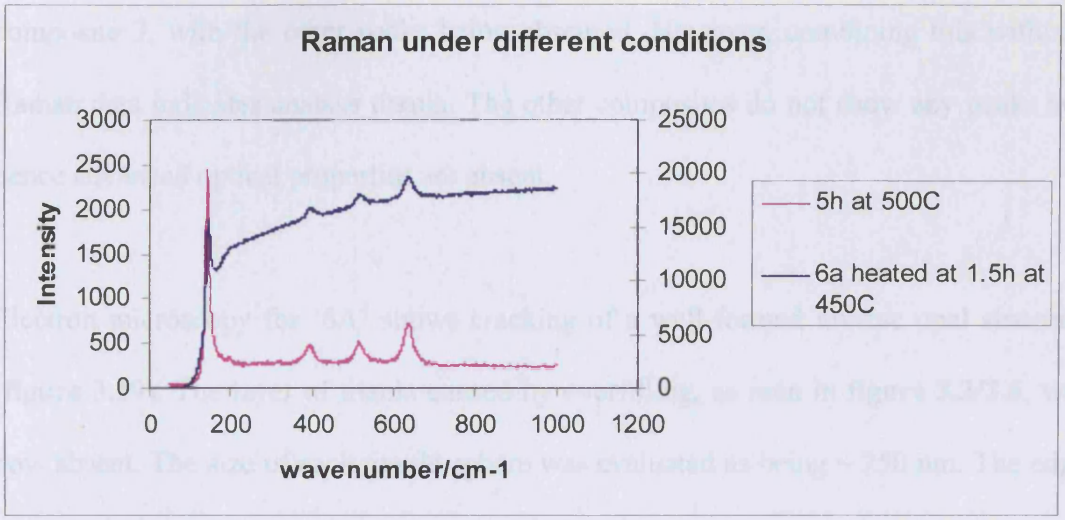

Figure 3.17 (a) Raman for two photonic crystals samples; composites heated under different conditions.

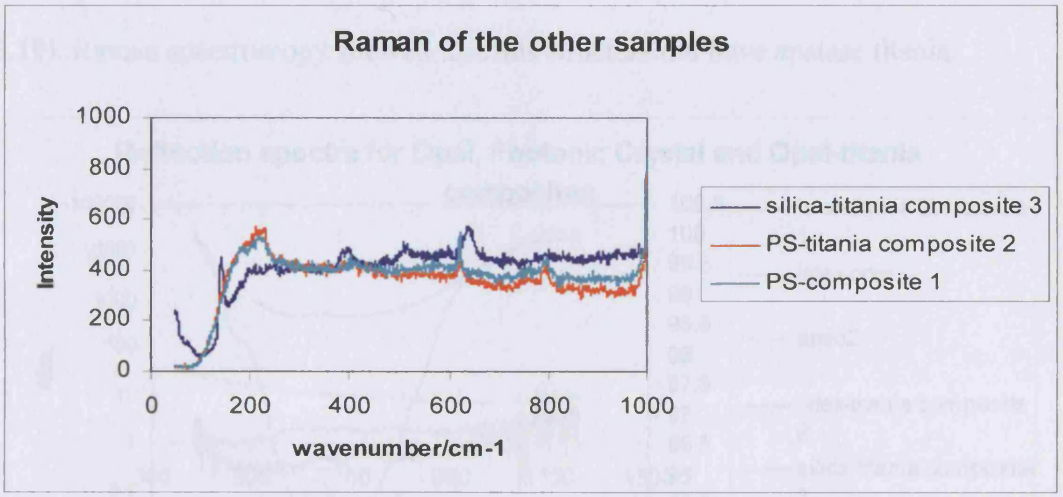

Figure 3.17 (b) Raman of other samples to be placed together with '6A' for photocatalytic run – see figure 3.20.

Figure 3.18 shows the reflection spectra measured for the samples that underwent the photocatalysis run. A stop band is seen at ~700 nm for the latex and latex/titania composite 1 (one coat of titania). There is also a reflectance pattern for composite '3' at ~600 nm; the 'stop' band is blue shifted just as when an inverse opal made of anatase titania has its stop band blue shifted in the UV, but here the shift is not so large; the structure is not fully inverted, the silica is still present. Inverse opal '6 A' barely shows any optical properties upon reflection, the intensity is so small and increased here by placing a secondary axis for clarification. The PXRD (not shown) for the composites show a pattern that does not correspond to anatase for 1 and 2 but a peak at $2\theta = 25°$ for

composite 3, with the other peaks being obscured. However, combining this with the Raman data indicates anatase titania. The other composites do not show any peaks and hence advanced optical properties are absent.

Electron microscopy for '6A' shows cracking of a well-formed inverse opal structure (**figure 3.19**). The layer of titania caused by overfilling, as seen in **figure 3.3/3.6**, was now absent. The size of each titania sphere was evaluated as being ~ 250 nm. The edge view was successfully taken and shows a 1.8 μm thick film. The SEM for the silica-titania composite shows well-formed opal structure with a thickness of ~2.5 μm (**figure 3.19**). Raman spectroscopy showed that this structure did have anatase titania.

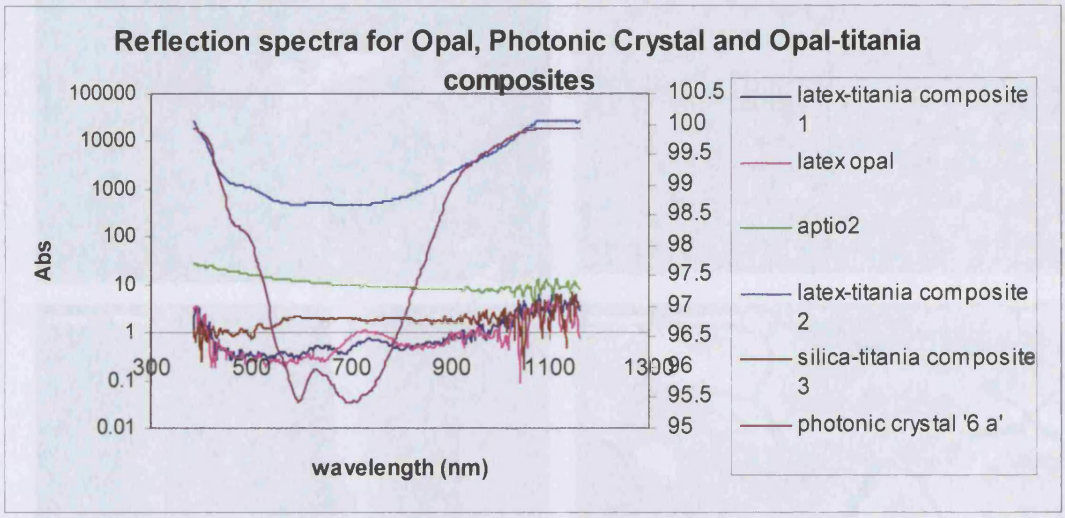

Figure 3.18 Reflectance measurements of samples that underwent photocatalysis: samples do not display any extra optical features apart from the 'stop' band displayed by latex opal and latex-titania composite 1 at ~700 nm. The secondary axis (95-100) is used to enlarge the very weak peak for photonic crystal '6 A'.

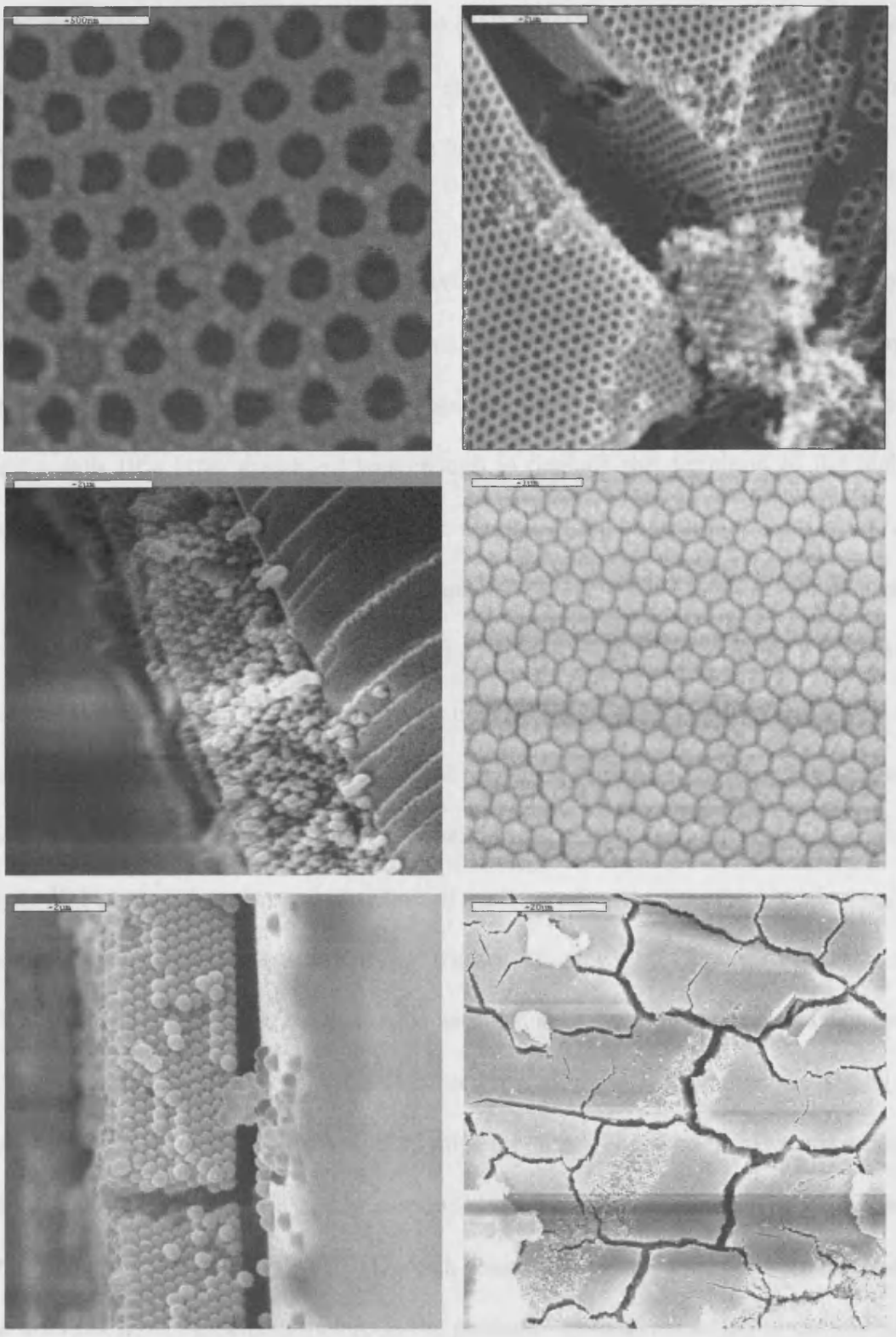

Figure 3.19 SEM: top of photonic crystal 6 A (top left and right), edge of 6 A (middle left), silica-titania composite 3 (middle right), edge of silica-titania composite 3 (bottom left), top view of silica-titania composite 3 (bottom right).

The photocatalysis results are shown in **figure 3.20**. This experiment was conducted for up to 660 minutes and shows no photoactivity for the un-fired latex-titania composite samples '1' and '2'. Opals need to be fully infilled and heated at the appropriate

temperature for conversion to anatase titania (450 °C). Calcination has been shown (in titania powders) to improve crystallinity, and to reduce crystal defects, leading to reduced e^- - h^+ recombination and increasing the ability to mineralize organics. [71]

Composite 3, however, did have good activity with a comparable half-life to that of sample '6 A'. A thin coating of titania, converted to anatase, as shown by Raman/PXRD, does effect the photocatalysis of stearic acid despite the fact that one coating with 10% (v/v) titania sol was enough to degrade the definition of the high energy optical band structure of this opal. It seems that the structure – composed of a periodic arrangement of air voids for the organic to get through – is sufficient enough for good photocatalysis, as shown by the (t½) values. **Figure 3.20** shows that these (t½) values are also seen to be insensitive to underfilling of the PS opal as composite 3 has a smaller (t½) than a fully infiltrated opal such as '6 A' but still decomposes stearic acid at a comparable rate. The lower calcination temperature (as used for '6 A – see **Appendix**) produced an inverse structure of better quality than previously observed. Comparison of the optical structure of '21' (**figure 3.4**) and '6 A' (**figure 3.16**) shows a difference in that two weak bands can be seen for the latter. However, this does not necessarily translate to the photocatalytic activity. Sample '21' shows the slightly shorter half-life: 16 mins as opposed to 25 mins for '6 A'. The band that extends to the visible does not seem to be solely responsible for photocatalysis with stearic acid although the sample made by APCVD, which does not have any optical absorption (but also does not have the same structure as the photonic crystals) extending to the visible did not show any activity. It can be deduced from this that the unique inverse opal structure could be the cause of higher photocatalytic activity. To test this hypothesis required different types of controls to be made and an experiment to check whether a 'flat' band was present. These details are discussed in **chapter 4**.

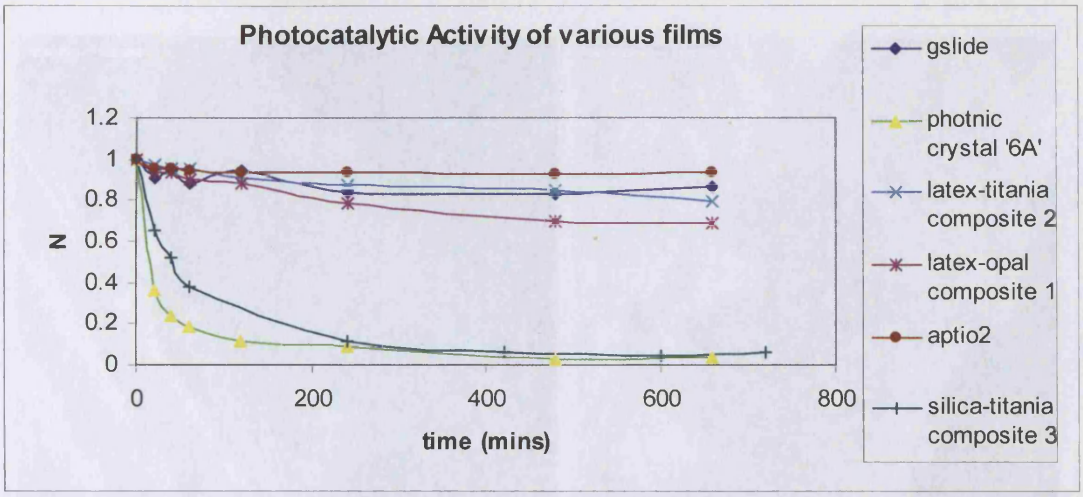

Figure 3.20 Photocatalysis run for the destruction of stearic acid overlayer using 365 nm irradiation for latex/silica-titania composites, photonic crystal sample '6 A' and aptio2 = sample made from one coating using APCVD. Gslide = glass slide coated with an overlayer of stearic acid to be used as control.

3.4 Thickness and photocatalytic activity

Trends have been noted in the literature in relation to photoactivity and to the thickness of films.[66, 72-76] The objective of the following experiments was to examine the effect of how film thickness influenced the photocatalytic activity. Several latex (300 nm)/ethanol solutions (see **experimental chapter 6**) were made up by mixing different amounts of latex solution (290 nm) (9 wt %) (400 and 700 μl as opposed to 900 μl) with ethanol (18 ml). Films were deposited on the glass by the Colvin method. Microscopy, shown in **figure 3.21** was taken from these opal samples and the thickness measured (3.5 – 4.0 μm). These same latex opals were converted to inverse titania as before (see **Appendix** for conditions).

The photocatalytic activity of the different inverse opal samples made from PS (~250 nm) of different thickness are compared to that for sample '6A' (**figure 3.22 (a)**). These samples are labelled by the value of the thickness measured. The sample made from ~ 4 μm thick PS sample, double the thickness from '6 A', has a similar t ½ ~25 mins whereas the inverse opal sample made from a ~ 3.5 μm thick PS opal has a far smaller t ½ ~ 135 mins. These films were infiltrated and calcined under similar conditions.

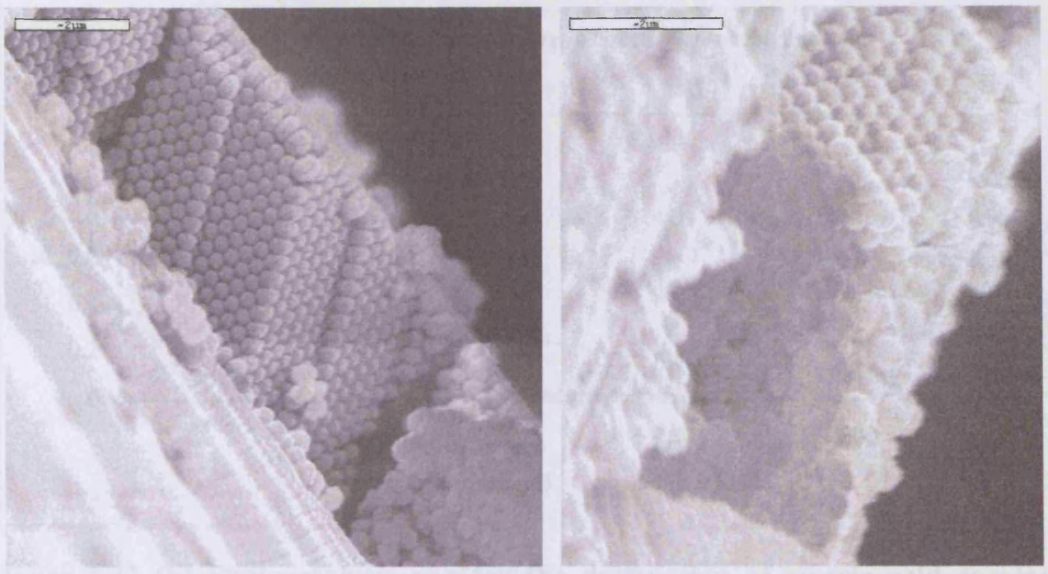

Figure 3.21 SEM of films with different thickness (in brackets) from concentrations in latex (in μl): from left-right: 400 μl (4.08 μm), 700 μl (3.5 μm).

Figure 3.22 (b) shows the samples from **3.22 (a)** and another two samples that have similar thickness of 3-4 μm (again, samples are labelled by thickness measured). Overall, there was no correlation of thickness with photocatalytic activity as measured by t ½ for the destruction of the stearic acid overlayer. The variability of t ½ across different samples of similar thickness was greater than any effect due to the variation of thickness (such as doubling it) as seen when comparisons with sample '6 A' are made.

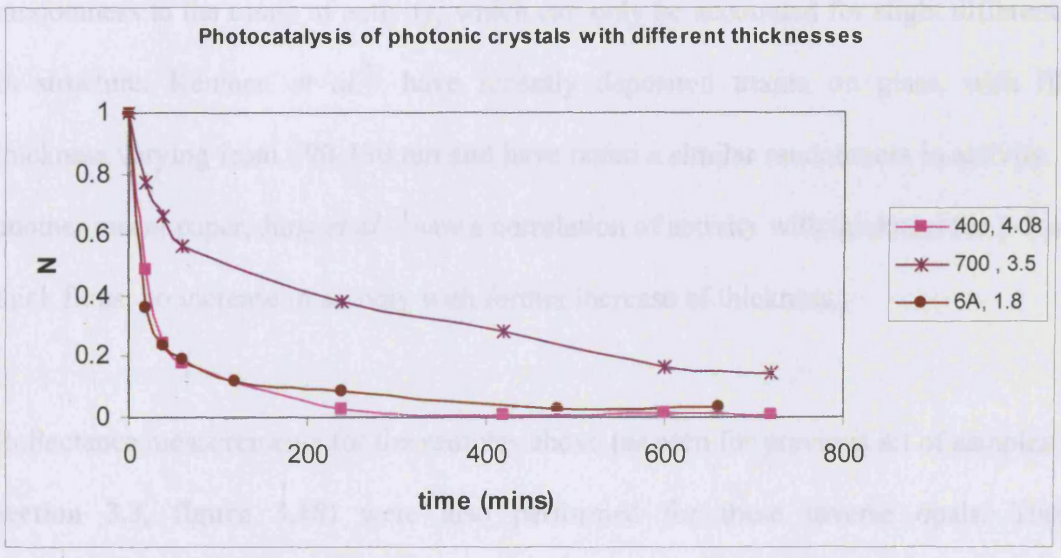

Figure 3.22 (a) Photocatalysis run for the destruction of stearic acid overlayer using 365 nm irradiation - inverse opals are of different thickness

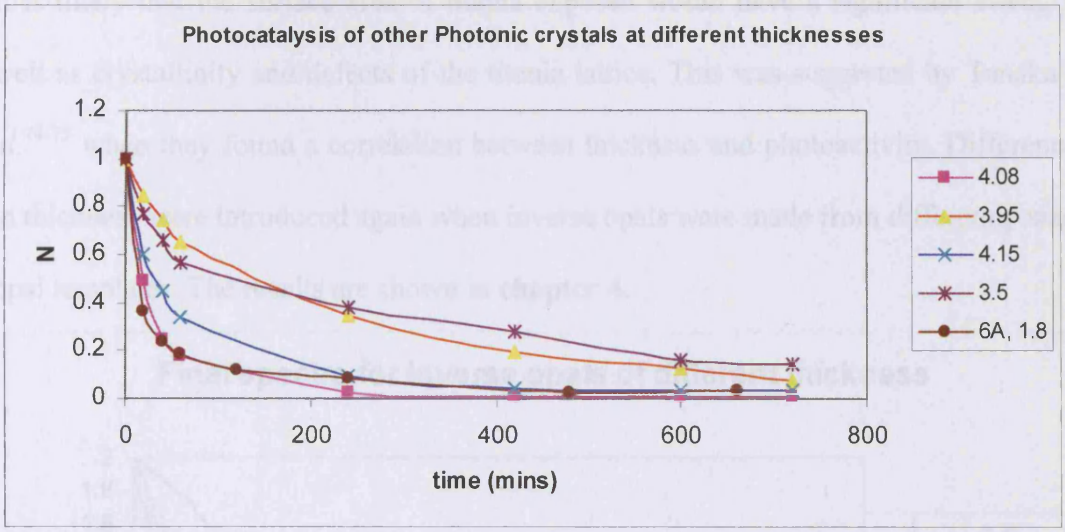

Figure 3.22 (b) Photocatalysis run for the destruction of stearic acid overlayer using 365 nm irradiation for inverse opals of different thickness with results from figure 3.22 (a) laid on for comparative purposes – all samples were run together.

The spectra for the inverted opals, together with '6 A' are compiled in **figure 3.23**. '6 A' displays a stronger stop band at ~400 nm but again its $t_{½}$ is similar to that of a ~4 μm sample. There are no differences in the 4 samples used in this set of experiments, as far as the UV spectra, beyond minor differences in absorption and slight curved "Fabry-Perot" like fringes, most notably for the 4.15 μm thick sample (400-600 nm range). So if we can be sure of anything, it is that minor differences in thickness seem to introduce randomness to the range of activity, which can only be accounted for slight differences in structure. Keinoen *et al.*[72] have recently deposited titania on glass, with film thickness varying from ~90-130 nm and have noted a similar randomness in activity. In another recent paper, Jung *et al.*[73] saw a correlation of activity with thickness for 3-5 μm thick films, no increase in activity with further increase of thickness.

Reflectance measurements for the samples above (as seen for previous set of samples in **section 3.3, figure 3.18**) were also performed for these inverse opals. These measurements showed no major optical features across the range 200-1100 nm.

It is likely that the surface area of titania exposed would have a significant effect, as well as crystallinity and defects of the titania lattice. This was suggested by Tanaka *et al.*[74-75] when they found a correlation between thickness and photoactivity. Differences in thickness were introduced again when inverse opals were made from differently sized opal templates. The results are shown in **chapter 4**.

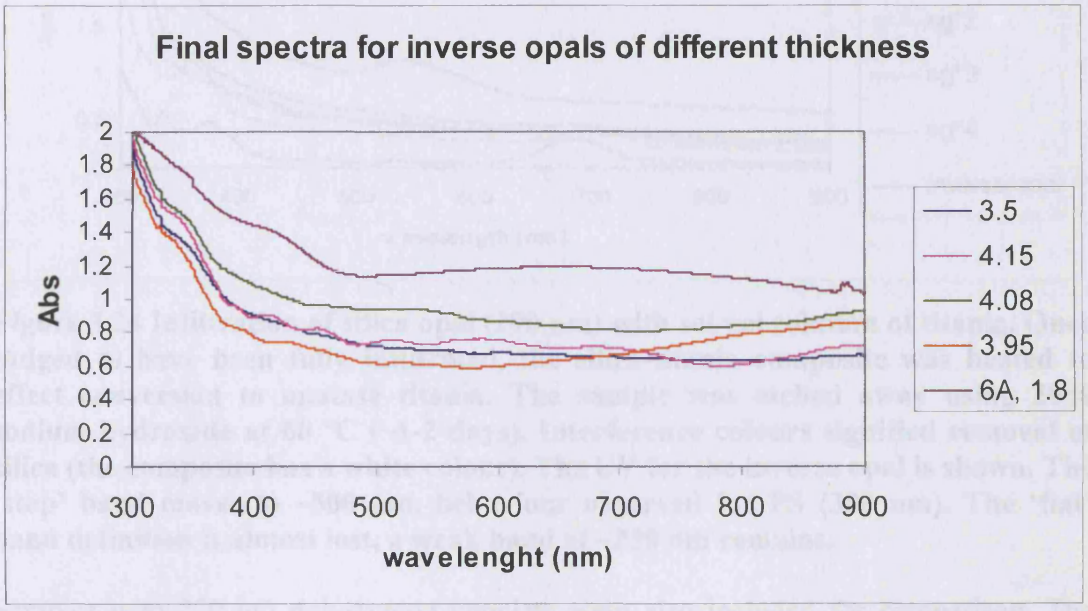

Figure 3.23 UV-vis profiles for inverse opals on glass. The numbers above correspond to the inverse opal sample's thickness. These all show a similar profile (a weak band at ~450 nm corresponding to the 'flat' band but no peak corresponding to the 'stop' band) that differ from inverse opal 6 A, whose details are given in section 3.3, which has a 'stop band at ~450 nm.

3.5 Other Titania Samples

Titania, as made and deposited by a variety of methods, such as spray pyrolysis, or whether tested against a variety of organics, has its ability to photo-decompose measured against a standard: Degussa P25. [76-78, 81] Elsewhere, for example, Char *et al.* have compared different forms of titania made by different assembly methods, and their respective abilities to photo-decompose.[79] A titania P25 standard film was made (which has been used for comparison by many researchers in the past) by screen printing onto glass. This run also included opals made of silica that were also laid on glass slides. An opal was infiltrated with the same solution as before, heated at 450 °C for 3 hrs and then

the template was etched away by using a 20% solution of sodium hydroxide leaving an inverse opal titania.[80] **Figure 3.24** shows the UV taken following these steps.

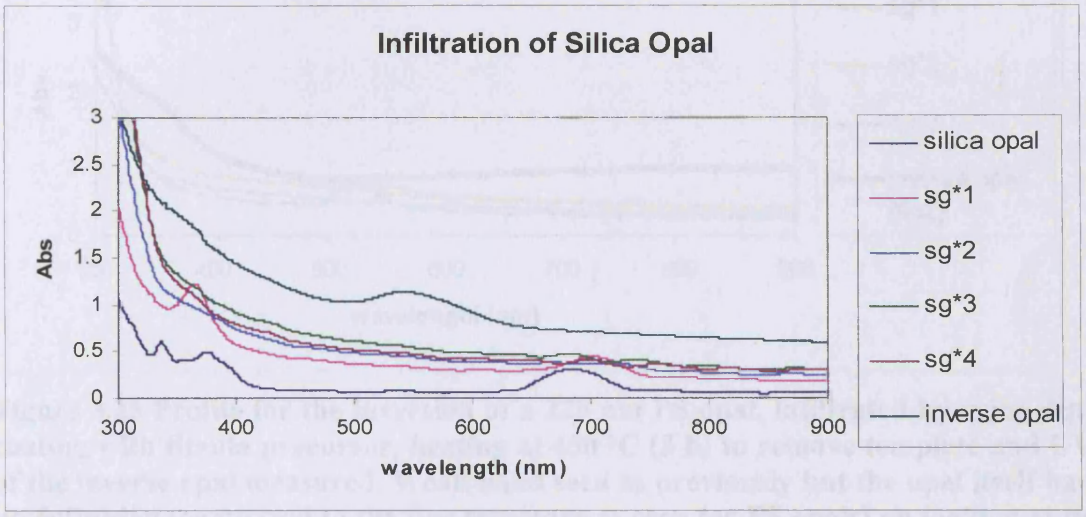

Figure 3.24 Infiltration of silica opal (290 nm) with sol-gel solution of titania. Once judged to have been fully infiltrated, the silica-titania composite was heated to effect conversion to anatase titania. The sample was etched away using 20% sodium hydroxide at 60 °C (~1-2 days). Interference colours signified removal of silica (the composite has a white colour). The UV for the inverse opal is shown. The 'stop' band moves to ~500 nm, behaviour observed for PS (300 nm). The 'flat' band definition is almost lost, a weak band at ~230 nm remains.

Samples with 220 nm polystyrene template were also included for comparison. The change in size of opal template has the effect of shifting the position of the weak band of the inverse opal. The opal band 'stop' band is itself shifted to ~500 nm because of the smaller sphere size (**figure 3.25**). **Figure 3.26** shows the absorption for titania P25 [81] that was screen printed onto glass as well as titania laid onto glass via a sol-gel procedure (2 coatings for each), with no template.

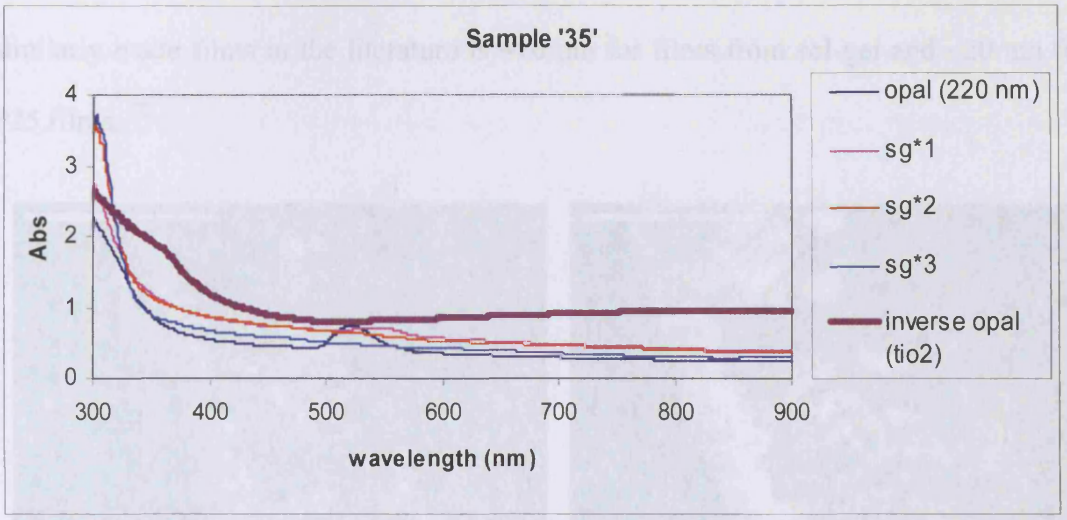

Figure 3.25 Profile for the inversion of a 220 nm PS opal, infiltrated by using dip-coating with titania precursor, heating at 450 °C (3 h) to remove template and UV of the inverse opal measured. Weak band seen as previously but the opal itself had no definition (compared to the fine structure as seen for PS opals) on looking at its 'flat' band.

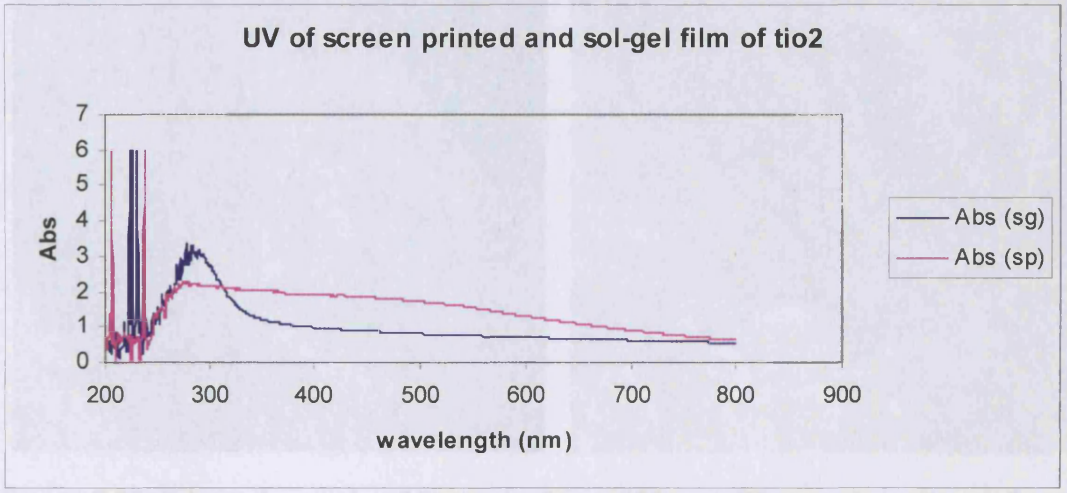

Figure 3.26 Profile for titania (P 25) screen-printed (= sp) or dip-coated from titania precursor onto glass (= sg) and annealed at 450 °C (3 h) to produce anatase phase titania. UV for each of these structures measured.

The SEM images for the latter, template-less titania on glass, are displayed in **figure 3.27**. Both sol-gel and screen printed samples display a 'rough' surface; from the micrographs and the angles shown, there was a difficulty in ascertaining the thickness; it was judged to be ~ 1 μm for screen printed sample. The edge for sample '35' (inverse opal made from a 220 nm PS template) was obtained and a 2 μm thick film is seen, whose sphere size is reduced to ~180 nm as shrinkage takes place. The particle size for

similarly made films in the literature is ~10 nm for films from sol-gel and ~20 nm for P25 films. [79]

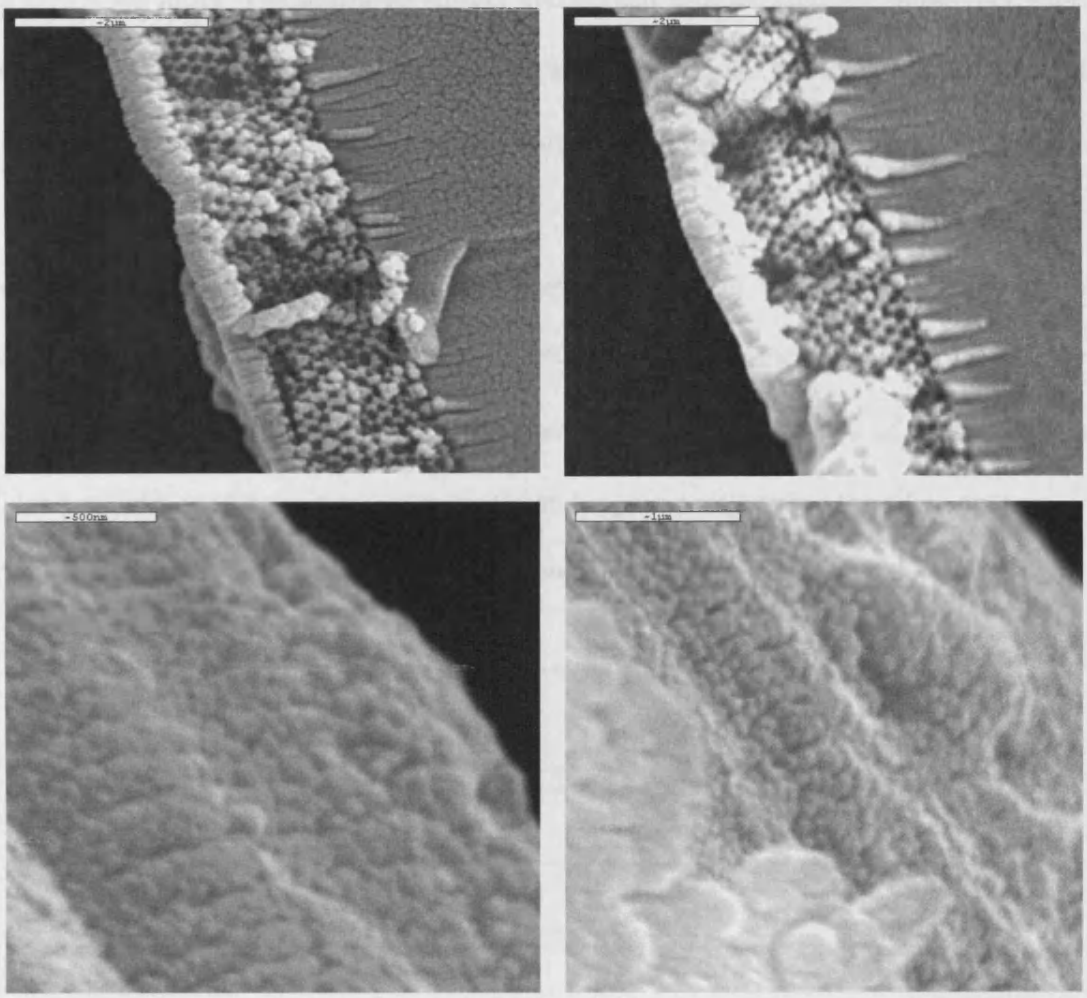

Figure 3.27 Edge of sample '35' made from 220 nm PS template (top left and right). Top view of screen printed film of titania P25 (bottom, left) and sol-gel titania (bottom, right).

The differences between these structures of titania can be seen above. How the optical spectroscopy differ from photonic crystals can be seen by comparing **figures 3.25** and **3.26**: the bands are much broader. In '35' a band – weak but present – extends from ~350-400 nm.

The photocatalysis measurements for these samples are shown in **figure 3.28**. The titania photonic crystal made from a silica opal template did not show any improvement in photocatalysis when compared to inverse opals made by the previous methods

discussed in this chapter. This is not surprising since the band definition does not appear to have been significantly improved. Sample '35' shows a similar performance to '6 A', its t ½ ~ 40 mins. The annealed sol-gel and screen printed samples show very little activity over this time period. These results also reflect upon the structural differences between the photonic crystal and non-photonic crystal samples.

Annealed titania inverse opals made from silica opals were also tested for in photocatalysis using the xenon lamp at 435-515 nm. These samples did not display favourable photocatalytic activity in this wavelength range. The UV of these samples did not exhibit good definition at the 'flat' band region compared to the silica opal.

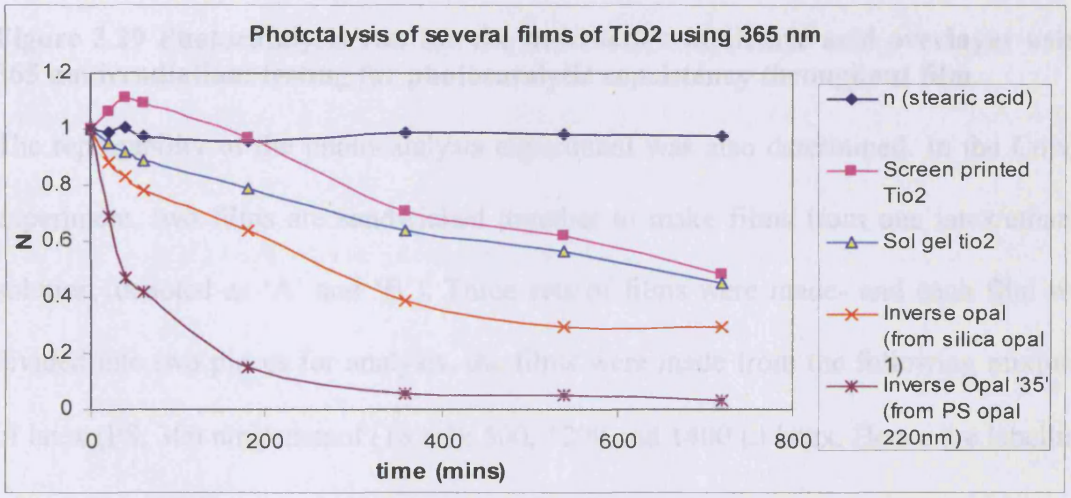

Figure 3.28 Photocatalysis run for the destruction of stearic acid overlayer using 365 nm irradiation for differently structured titania samples such as screen-printed and titania made from dip-coated precursor, as well as from inverse opals of different templates; one is PS but of a different size (220 nm), the other from a silica opal (290 nm).

3.6 Consistency, Repeatability, Hydrophilicity and other tests for films

A photonic crystal was made by the method described in **chapter 2** and tested for photocatalytic efficiency. Sample '28400' was broken in half, and labelled part 'A' and part 'B' and the photocatalytic efficacy of each section determined. **Figure 3.29** shows that the photocatalytic efficiency is consistent throughout the photonic crystal film. This is expected for a film formed by using a dip-coating device- with both halves of the

sample reaching a half-life for the destruction of stearic acid at the same time. The photonic bands for each half were measured (not shown) but this reveals the same definition in the 'flat' band region.

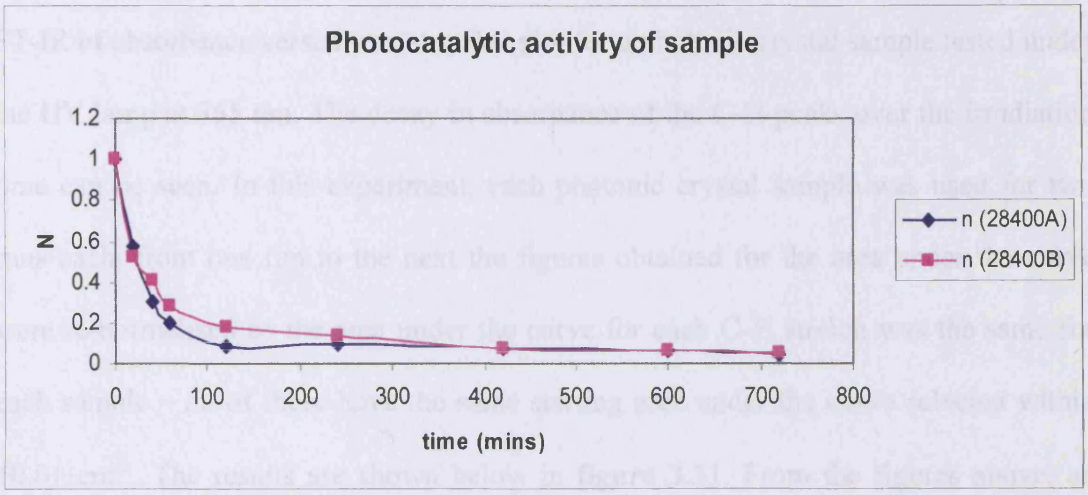

Figure 3.29 Photocatalysis run for the destruction of stearic acid overlayer using 365 nm irradiation: testing for photocatalytic consistency throughout film.

The repeatability of the photocatalysis experiment was also determined. In the Colvin experiment, two films are sandwiched together to make films from one latex/ethanol solution (denoted as 'A' and 'B'). Three sets of films were made- and each film was divided into two pieces for analysis, the films were made from the following mixtures of latex (PS, 300 nm)/ethanol (18 ml): 500, 1200 and 1400 µl latex. Hence the labelling of samples as: 500 A/B, 1200 A/B and 1400 A/B.

These were coated the same number of times (7) (with titania tetraisopropoxide/ethanol in a 10/90 (v/v) ratio, sol-gel infilling as shown in **chapter 2**) and were calcined together at 450 °C for 3 hrs. The photocatalysis was carried out, and, once the first run was completed, any remaining stearic acid was destroyed by irradiation with a 254 nm lamp (checked by IR to ensure that no residual stearic acid was present) and more stearic acid was laid on these films. The photocatalytic efficiency of each film was examined at exactly the same place. That is, the plate on which the film was laid has its position marked so that the IR is measured at exactly the same location as before. When

processing the results, the peak under the area for the C-H stretching peaks in the IR spectrum is taken and normalized, where the area under the curve is taken to be equal to 1 for the sample which is to be irradiated under the UV lamp. **Figure 3.30** shows the FT-IR of absorbance versus wavenumber plot for a photonic crystal sample tested under the UV lamp at 365 nm. The decay in absorbance of the C-H peaks over the irradiation time can be seen. In this experiment, each photonic crystal sample was used for two runs each: from one run to the next the figures obtained for the area under the curve were re-normalised so the area under the curve for each C-H stretch was the same for each sample – all of these have the same starting area under the curve selected within ± 0.01 cm^{-1}. The results are shown below in **figure 3.31**. From the figures above, an order of activity can be seen: 14 a/b, 5a/b and 12 a/b, the latter being the most active films. Firstly, the three sets of samples (a/b) are grouped together in terms of how active they are, and second, the exact order is repeated from the 1^{st} to 2^{nd} run.

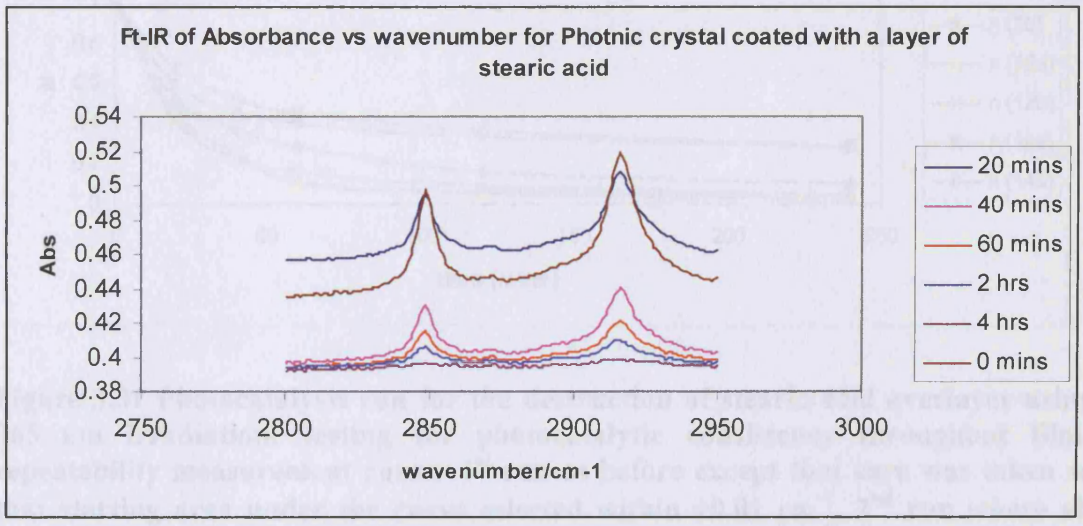

Figure 3.30 IR spectra showing film laid with stearic acid (and its two C-H peaks) for a photonic crystal sample.

The question as to why this order exists in the first place could be to do with how well structured the films are; the periodicity of 14 a/b seems to be most damaged by heating the sample as shown in **figure 3.32**. The top-down surface photographs are shown above and indicate that samples 5 and 12 have are not so damaged by the heating process, unlike that of 14. These samples were all heated together (450 °C) – this still

does not answer why there is more cracking on one sample and not in another, but the randomness of activity seen for samples of slightly different thickness as seen in **section 3.4** is repeated here. The photocatalytic activity for each sample is repeatable - that is the A/B samples made from the same films showed essentially similar photoactivity.

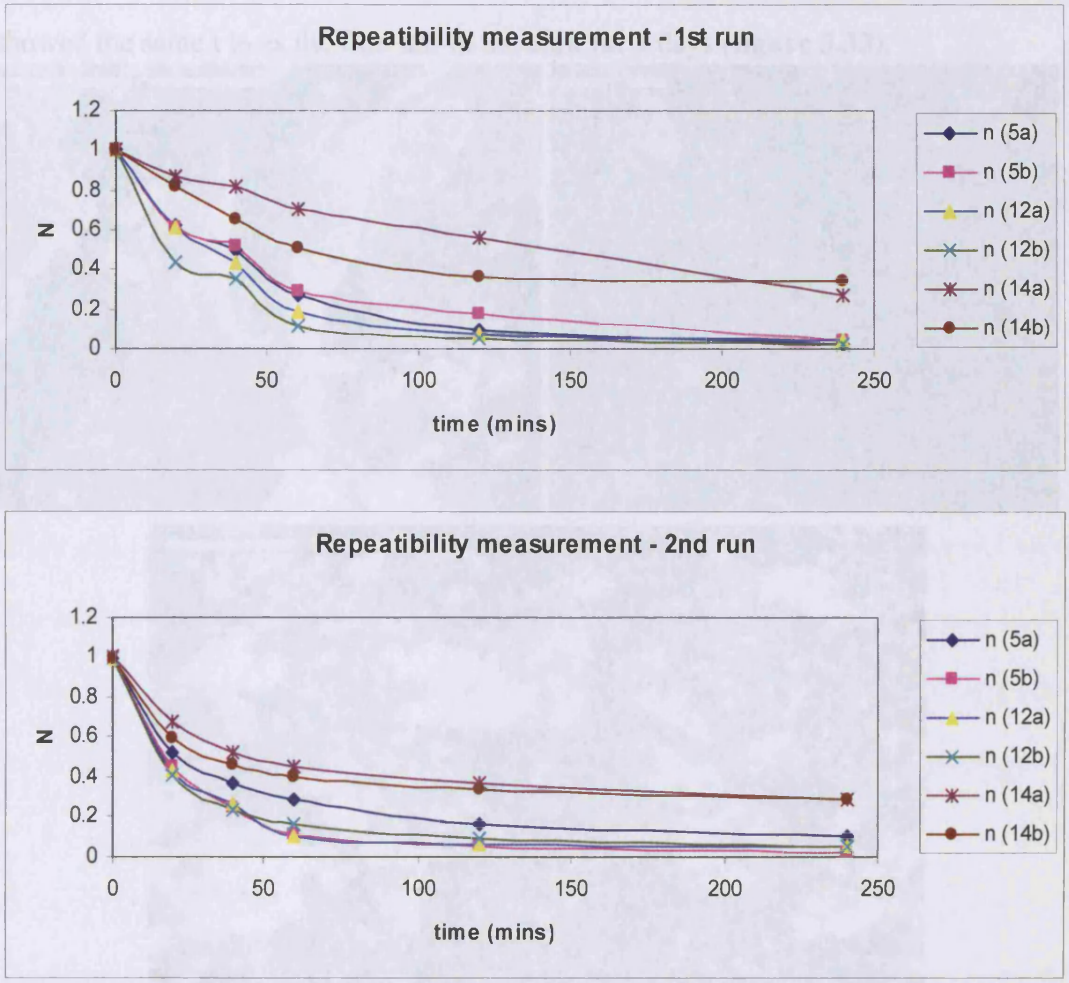

Figure 3.31 Photocatalysis run for the destruction of stearic acid overlayer using 365 nm irradiation: testing for photocatalytic consistency throughout film: repeatability measurement runs – 1st run as before except that care was taken so that starting area under the curve selected within ±0.01 cm^{-1}, 2nd run where all samples were repeated after any remaining stearic was cleaned with 254 nm irradiation (checked by IR).

The ability to photocatalyse without activating the surface of the film was also looked at. In all results shown thus far, the films, prior to layering with stearic acid, were activated by surface cleaning with 254 nm light for approximately 30 minutes. This is a procedure that has been used in all films undergoing photocatalysis thus far but here a sample was made and stored in the dark for 3 days, layered with the organic and tested.

This shows the same amount of photocatalysis as for many of the best surface cleaned samples: t ½ ~20 mins. The stearic acid film was cleaned off with 254 nm radiation (correlated by IR) and was stored for a week in the dark, and then the sample was layered with stearic acid once more and irradiated with 365 nm light. The second run showed the same t ½ as the film left in the dark for 3 days (**figure 3.33**).

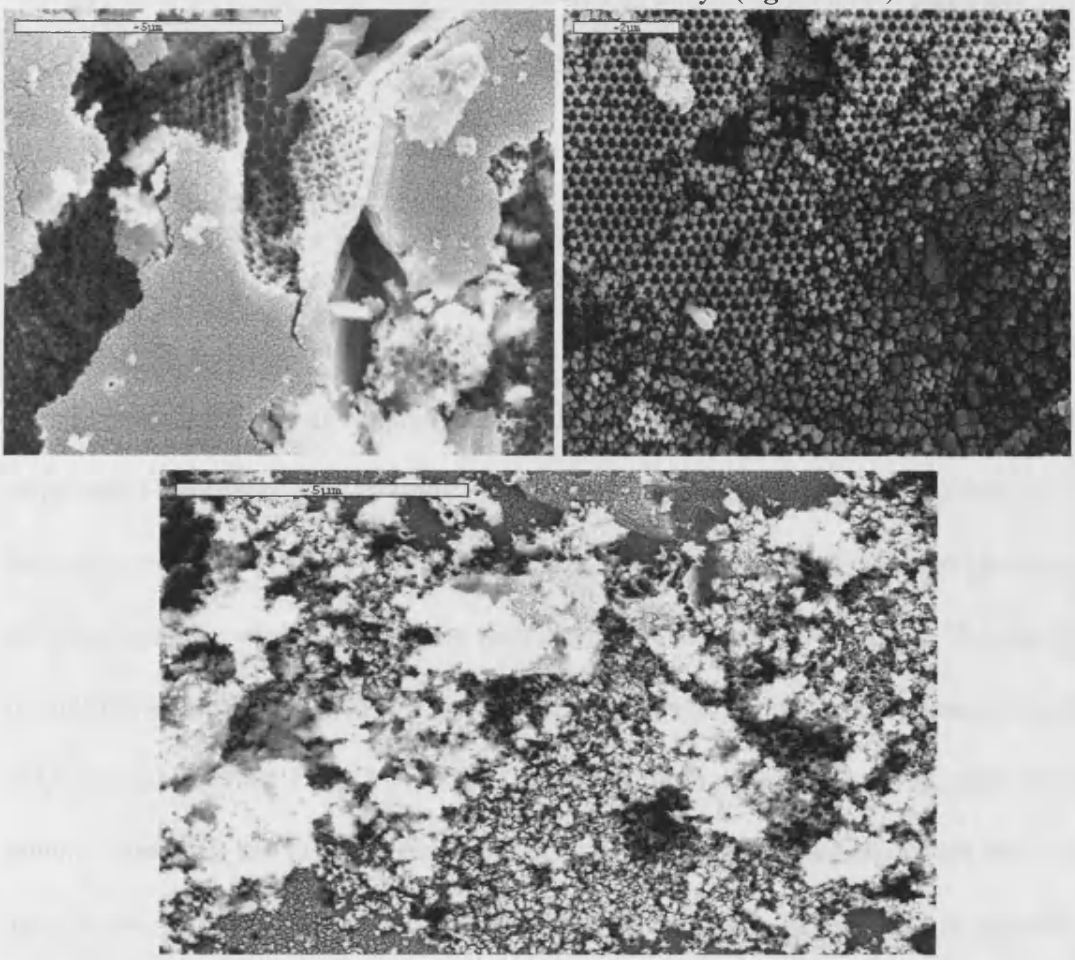

Figure 3.32 SEMs, top view of (clockwise, from top left) 5, 12 and 14: labelling explained in figure 3.30.

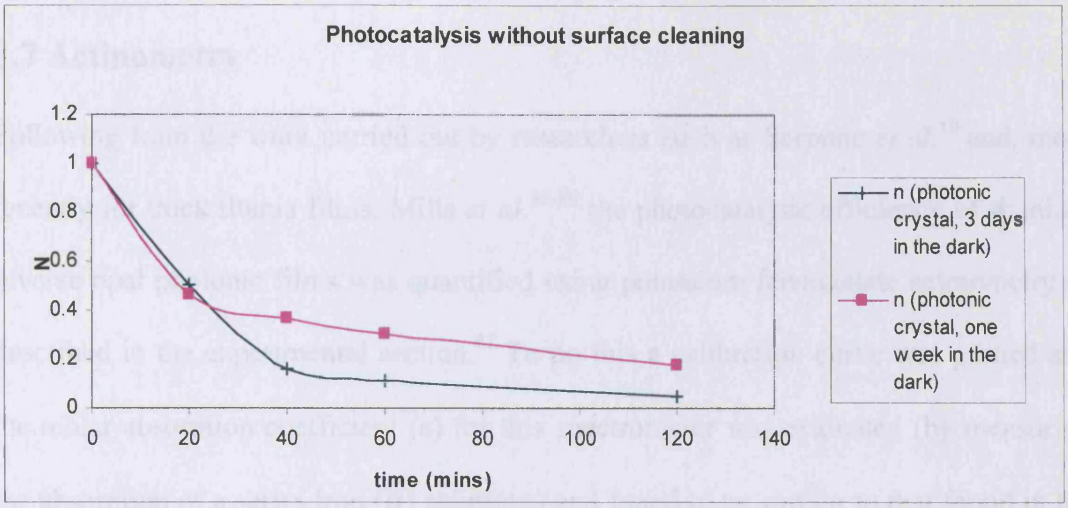

Figure 3.33 Photocatalysis run showing the destruction of stearic acid overlayer (365 nm irradiation) for photonic crystal sample without surface cleaning.

Photocatalysis involves, as seen in the review in **chapter 1**, the photogeneration of electrons which can combine with oxygen, producing superoxide anions that combine with photogenerated hydroxyl radicals to photomineralise organic compounds.[1] Parkin *et al.* and Hashimoto *et al.* found [82-84] that a photoinduced hydrophilic effect follows because generation of hydroxylated titania surfaces leads to water contact angle changes in titania samples as well as samples doped with metals such as tungsten. The photonic crystal films tested were found to be superhydrophilic as formed (measurements carried out every 20 mins for 1 hr). The droplet spread through the cracks very quickly and the contact angle was too low to measure. The very low initial contact angles are due to the very porous nature of the films, and, as these were so low it was difficult to quantify if any photoinduced hydrophilicity actually occurs.

Finally, a "Scotch tape" test was carried out. A piece of "Scotch" tape was attached to a photonic crystal sample and pulled off. This tests how strongly the material adheres to the film. Some photonic crystal was taken off from the substrate hence the film was not very strong: this therefore would prohibit use in applications such as window coatings.

3.7 Actinometry

Following from the work carried out by researchers such as Serpone *et al.*[10] and, more recently for thick titania films, Mills *et al.*[85-86] the photocatalytic efficiency of titanium inverse opal photonic films was quantified using potassium ferrioxalate actinometry as described in the experimental section.[87] To do this a calibration curve was plotted and the molar absorption coefficient (ε) for this spectrometer was evaluated (by measuring the absorption of a series iron (II) solutions) and found to be similar to that found in the literature. Indeed, this proved to be the case (ε = 9908 mol^{-1} dm^3 cm^{-1}, expected to be ~10000, **figure 3.34**).

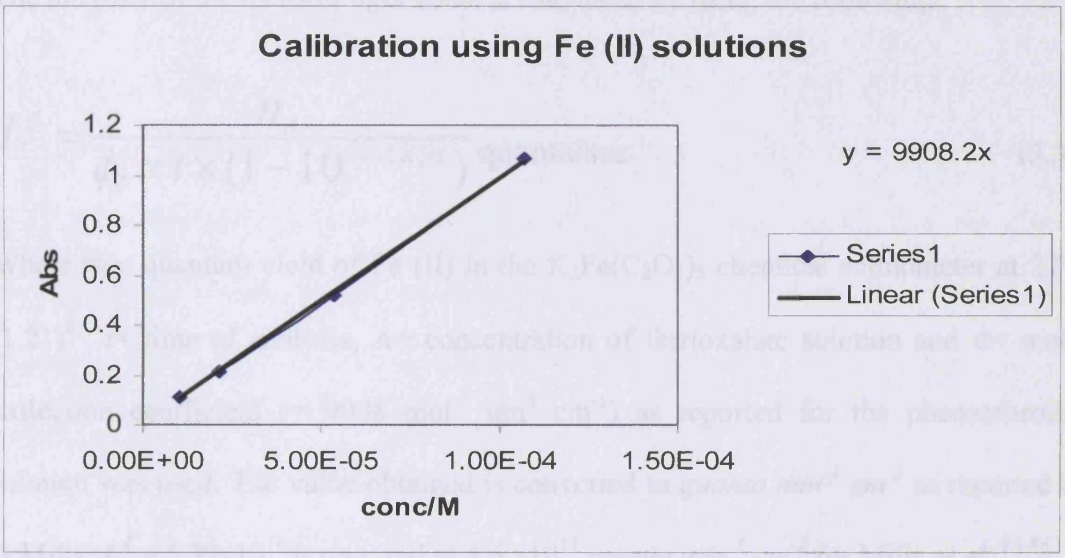

Figure 3.34 Calibration curve for Actinometry measurement using iron (II) phenanthroline solution.

Once calibrated a potassium ferrioxalate solution was made (0.006 M). The solution was then exposed to the UV light for an appropriate period of time (30 s) so that $6.12*10^{-7}$ (close to the recommended $5*10^{-8}$) mole Fe (II) could be generated. An aliquot was taken and a solution was prepared by mixing it with phenanthroline, acetate buffer and finally making up the solution (25 ml). A 'blank' solution (no exposure of solution to UV light) was similarly made. All manipulations were carried out in the dark. These solutions were left idle for one hour before absorption measurement. The experiment was repeated a number of times to produce a consistent response (the

absorption values are ± 0.05 of each other). The next step was to calculate number of Fe (II) ions from experiment by using the formula shown below:

$$N_{fe(II)} = \frac{6.023\times10^{23}\times V_1\times V_3\times \log10(I_o/I)}{V_2\times l\times \varepsilon} \quad \textbf{(3.2)}$$

Where l= path length, V_1, V_2 and V_3 are, respectively, the volume of actinometer solution irradiated, volume of aliquot taken for analysis and final volume of aliquot diluted. Log_{10} (I_o/I) =measured optical density at 510 nm and ϵ= molar extinction coefficient (= 9908 mol^{-1} dm^3 cm^{-1}).

The intensity of the incident light beam is calculated by using the following:

$$I_o^I = \frac{n_B}{\phi_B \times t \times (1-10^{-\varepsilon\times[A]\times l})} \text{ quanta/sec} \quad \textbf{(3.3)}$$

Where Φ_B= quantum yield of Fe (II) in the $K_2Fe(C_2O_4)_3$ chemical actinometer at 22°C (1.21)[87], t= time of analysis, A= concentration of ferrioxalate solution and ϵ= molar extinction coefficient (= 9908 mol^{-1} dm^3 cm^{-1}) as reported for the phenanthroline solution was used. The value obtained is converted to *quanta* min^{-1} cm^{-2} as reported by A.Mills. I_0^I = 5.39x10^{16}as opposed to 4.6 x10^{17} *quanta* min^{-1} cm^{-2} for Mills *et al.* [85-86]

Once the output was calculated the efficiency of the photocatalyst and its quantum yield, were obtained and compared to that of other titania films elsewhere in the literature. To do this the formal quantum yield (FQE) is first calculated by the following:

$$\text{FQE} = \frac{\text{rate of stearic acid destruction}}{\text{incident light intensity}} \quad \textbf{(3.4)}$$

To obtain the rate of destruction the integrated absorbance of the organic is extracted from the IR data (2850-2950 cm^{-1}) and then converted to its appropriate units ($mol/cm^2/min$) by using the concentration reported for the organic: $3.17x10^{15}$ molecules of stearic acid cm^{-2}.[88]

For comparative purposes the kinetics is assumed to be zero-order in relation to the stearic acid concentration, in line with other work published on titania films. Kinetic data can be extracted from FT-IR experiments because no major intermediates are generated. This can be assumed to be the case because removal of stearic acid by semiconductor photocatalysis produces no other film component that can be detected by FT-IR, no gas phase products other than CO_2 and H_2O are generated during the reaction and the ratio of the number moles of reactant to carbon dioxide is as expected from **eqn (3.1)** (**experimental chapter 6.7**). Zero-order kinetics does mean that the rate of decomposition is independent of stearic acid concentration. Stearic acid molecules occupy all the photocatalytically active sites, so that once the molecules are mineralized, others immediately above will take their place. [76, 84-87]

Therefore, for a typical photonic crystal sample such as '500A' (from the plot in **figure 3.35**) (used for the repeatability measurement in **section 3.6**) with a t ½ of approx. 25 mins, the rate = 0.029/min x $3.17*10^{15}$ mol cm^{-2} and FQE = rate (mol cm^{-2} min^{-1})/$5.39x10^{16}$ photons cm^{-2} min^{-1}. FQE = = $1.29x10^{-3}$ molecules/photon (A. Mills reports 0.7-$10x10^{-5}$ for Activ M glass and 16-$20x10^{-4}$ for TiO_2 thick paste films).

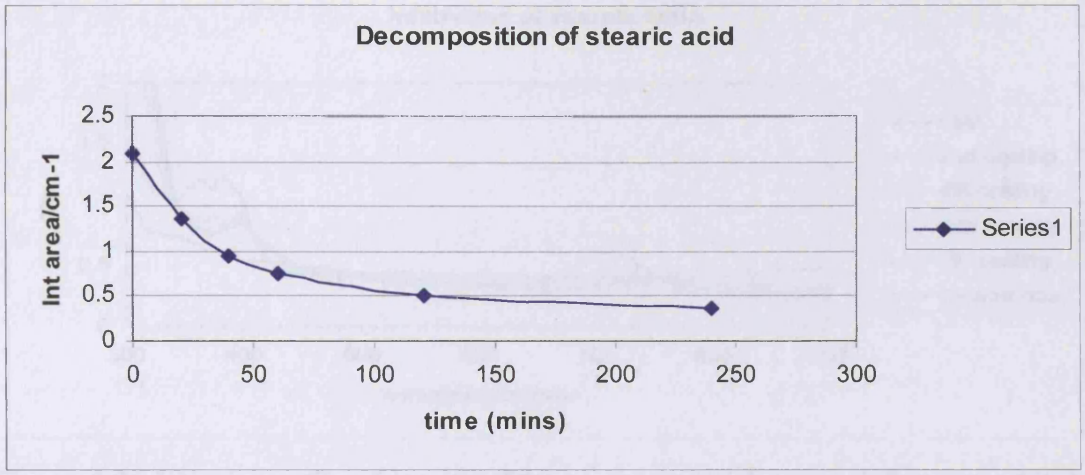

Figure 3.35 Profile for decomposition using sample '500A' from which the rate (mins) was extracted.

The calculation of the quantum yield involves obtaining a value for the fraction of light absorbed at 365 nm, from the sample's UV spectrum (**figure 3.36**), *f= (1-10^Abs (ε))* (ε = absorption of film at 365 nm). In this case *f* = 0.77 (ε = 0.65, for sample '500 A').

Quantum yield is calculated as follows:

$$\text{Quantum yield } (\phi) = \frac{\text{FQE}}{f} \qquad \textbf{(3.5)}$$

Stearic acid decomposition involves transfer of 104 electrons therefore maximum ϕ = 0.01 for any samples undergoing this process. For '5 A', $\phi = 0.16 \times 10^{-2}$. This matches the best yields reported by A. Mills *et al.* [85-86] obtained for thick paste titania films, but since the output of our lamp is lower it could be said to be a somewhat higher efficiency. The quantum yield value obtained for typical photonic crystal compares favourably with literature work on thick titania samples.

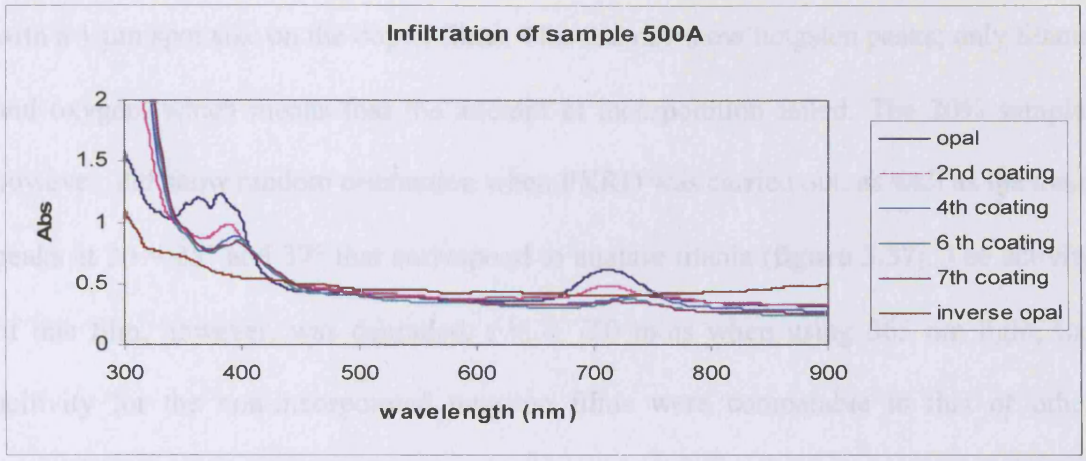

Figure 3.36 UV-vis profile of sample '500 A', from which value *f* (fraction of light absorbed at 365 nm) is extracted.

3.8 Doped Tungsten-titania Photonic Crystals

Do *et al.*[82, 83] show an improvement in the photo-oxidation of 1, 4-dichlorobenzene by adding tungsten dioxide to the surface of titania powder. As demonstrated in the literature survey in **chapter 1**, the opal template allows, once the precursor is varied, different types of photonic crystals to be made. Tungsten (V) ethoxide and titania tetraisopropoxide were mixed in varying amounts so that 2%, 6% and 20% (v/v) sol-gel solutions of tungsten doped titania sols were made. These were used to impregnate the opal structure as first described in **chapter 2**, by using a dip-coating device (6 cm/min). Tungsten trioxide inverse opal had its synthesis attempted by infilling with a sol made purely from tungsten ethoxide/ethanol. The effect on changing sols upon the infiltration is apparent by the fact that it takes >10 dips to infill the opal with a doped sol, as opposed to 7-8 when using a titania sol. To obtain fully crystalline samples as well as decomposing the opal, sample '29' were heated at 500 °C (3-4 hrs) under oxygen.

For the 2% and 6% WO_3 impregnated samples, there was no evidence of doping either from PXRD or Raman as the amounts were too small to readily detect. EDAX was carried out on these samples. The measurement consisted of using multiple spot analysis

with a 1 μm spot size on the doped films. This did not show tungsten peaks; only titania and oxygen, which means that the attempt at incorporation failed. The 20% sample, however, did show random orientation when PXRD was carried out, as well as the main peaks at 2θ = 25° and 37° that correspond to anatase titania (**figure 3.37**). The activity of this film, however, was degraded, t ½ ~ 750 mins when using 365 nm light; the acitivity for the non-incorporated tungsten films were comparable to that of other anatase titania films t ½ ~ 50-70 mins. Parkin *et al.* also found, when incorporating high (20%) amounts of tungsten onto titania films, a degradation in activity, though the 2% WO_3-TiO_2 films improved the activity of the titania, sol-gel derived, film.[82, 83]

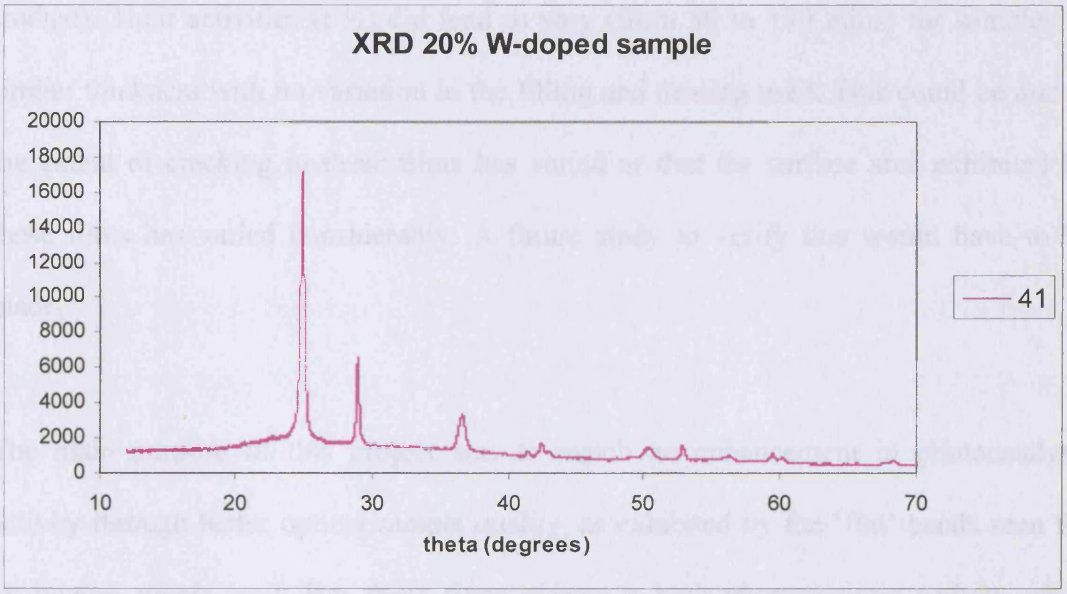

Figure 3.37 PXRD of 20% tungsten doped sample shows random orientation with the characteristic peaks for titania (anatase phase).

3.9 Conclusions

Photonic crystals of anatase titania, made from infiltration of voids of polystyrene film laid on glass via the Colvin method, as first seen in **chapter 2**, display very high photocatalytic activities. These crystals were heated at 450 °C- 500 °C, which yields the anatase phase; this was confirmed by running PXRD/Raman measurements. SEM showed a periodic array of air/titania pockets, an organised matrix network, whose thickness ranged from 1.5-4.0 μm.

The photocatalytic activity was quantified by the half-life (t ½) to decompose a stearic acid monolayer, which was ~20 mins for the best photonic crystal samples. These values were shown to be insensitive to degrees of filling of the PS opal. Titania/silica composite 4 shows, for example, that a small amount of titania can be deposited and still effect decomposition of stearic acid at an appreciable rate (t ½ = 50 mins). Sample '5B', whose profile for its filling is seen in **figure 3.1**, and whose SEM shows a highly cracked structure with a coating on top (**Figure 3.2**), suggesting an overfilling of the structure, shows a slightly longer (t ½) of 78 mins. The activities of these inverse opal titania photonic crystals are not correlated by thickness (albeit very thin films were not studied). Their activities (t ½) did tend to vary (from 50 to 150 mins) for samples of similar thickness with no variation in the filling and heating used. This could be due to the extent of cracking in these films has varied or that the surface area exhibited by these films has varied considerably. A future study to verify this would have to be made.

The main purpose of this project was to match an enhancement in photocatalytic activity through better optical sample quality, as exhibited by the 'flat' bands seen for an inverse titania opal. But these films display a high photocatalytic activity when displaying poor quality 'flat' bands, as seen in the UV-visible when compared to the PS opal bands that are infilled and inverted to yield these photonic crystals. The fine structure exhibited by the PS opals is washed away by inversion. Reflectance measurements that probe into the IR region do not yield any other optical properties. The optical absorption of these films did, however, extend into the visible range of the spectrum, unlike other types of titania such as films such as those produced by coating titania onto glass by APCVD, which does not decompose stearic acid at this range. Furthermore, the activities from the photonic crystal films are much higher than from

titania films as coated by sol-gel/screen printed standards (Degussa P25) onto glass. However, experiments with the Xenon lamp attached with appropriate filters that allow light that extends further into the visible through (over 400 nm) showed negligible activity.

The results obtained are repeatable and consistent as tested for groups of samples. The photonic crystal is a powerful catalyst; it does not need surface cleaning prior to photocatalysis.

There were no major differences in the optical quality of films derived from sol-gel and CVD. Therefore, after some usage of the latter technique, samples were made by infiltrating voids using a sol-gel solution.

Actinometry suggested that photoefficiencies, as given by the quantum yield for the best photonic crystal samples, were comparable to that of titania films described elsewhere in the literature (**Table 1**). The films themselves were not mechanically strong hence they are unlikely to act in applications such as self-cleaning window coatings.

Film Type	Rate ($x10^{13}$ molecules /cm^2/min)	FQE ($x\ 10^{-4}$)	*f* (fraction of light absorbed)	Quantum Yield ($x\ 10^{-2}$)
Paste (thick) TiO_2 *	69-105	16-22.9	1	0.16-023
Photonic Crystal of Titania	6.96	0.13	0.77	0.16

* A.Mills *et.al.*[85]

Table 1 Comparison of photoefficiencies between photonic crystal of titania and data by A. Mills *et al.*[85]

The films were super-hydrophilic with contact angles too low to measure and whose change upon irradiation could not be accurately measured; this tends to be the case for

highly porous films, which is seen by the SEM gathered from these structures. This porosity, and not a band extending toward the visible, could be these reason for the high photoactivity exhibited by these films. In **chapter 4**, the reasons for high photoactivity will be looked into by making controls where porous, and just as importantly, more disordered structures, are arrived at. These will be made by introducing a series of changes in the 3-step process that is used to make these structures outlined in **chapter 2**. Dye experiments will be used to see whether 'flat' band enhancement can be seen. Finally, further sets of photocatalysis experiments are presented.

Chapter 4 Further Photocatalysis and Discussion of Results

In **chapter 3**, an enhancement in photocatalytic activity for photonic crystals of titania compared to its other forms was noted in various tests, but the cause of this was not discussed. In the following chapter, numerous control experiments were carried out and the slow-photon band was looked at using dyes at various concentrations. Finally, photocatalysis using opal templates of different sizes was looked at. These experiments were undertaken to determine if the enhanced photocatalysis observed was due to a microstructure/surface area effect or whether the photonic crystal structure was responsible for enhanced light absorption through a "slow photon effect".

4.1 Control experiments

The thrust behind the following experiments was to make titania that had poor to no definition in the 'flat band' region, as shown by UV, as well as disordered structures, as shown by SEM. One way in which this was accomplished was to mix 220 nm and 290 nm latex spheres as the template for formation of these titania inverse opal. This was accomplished by evaporating a dilute solution of the mixed sized latex spheres in ethanol (18 ml) onto a glass slide as in the Colvin method (this was labelled as 'control 1'). SEM photographs were taken as an 'opal' structure - that is just the latex spheres, as well as in the inverse opal type structure- where its voids were infiltrated by titania and the latex removed by calcination. **Figure 4.1** shows the absence of any definition in the optical pattern as shown by UV measurement. Raman/PXRD patterns matched up to the anatase phase. **Figure 4.2** clearly shows quite a lot of microstructural disorder when compared with an inverse opal that was yielded from, say, 290 nm opals.

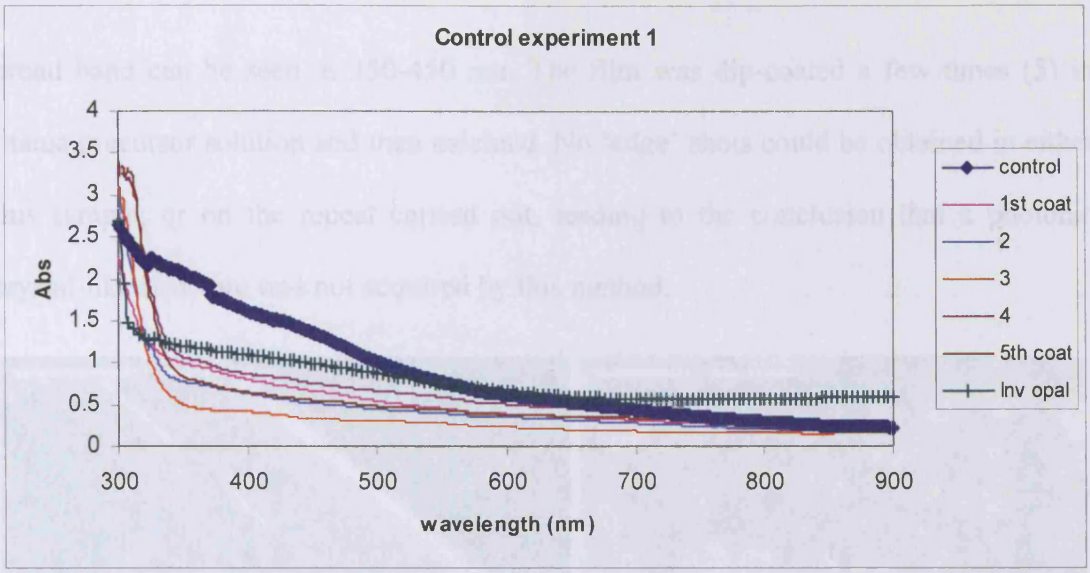

Figure 4.1 Infiltration profile of control sample (PS, 220 nm/300 nm mixture) assembled as described above. This was infiltrated by dip-coating into a titania precursor as seen previously in chapter 2 and 3. Since the 'stop' band could not be used as a guide for the number of coatings to be made it was decided that 5 (1st coat – 5 label in UV-vis profile, above) would be sufficient. Inv opal = profile of the structure obtained after removal of PS template by heating at 450 °C (3 h).

From **figure 4.1**, it can be seen that the structure has an optical absorption at 300-400 nm but the definition is not as good as that of a normal opal as seen in **chapters 2** and **3**. But, more importantly, once infiltrated and inverted, the structure has no definition in the 'flat' region, and no stop band. Also, SEM images displays what looks like a porous agglomeration of titania that appears to have a thickness of ~2μm, the same as some of the samples that showed good photocatalytic activity, as reported in **chapter 3**. Thus, a structure that is analogous to photonic crystals – has a comparable surface area with the same crystalline anatase titania phase- but one that does not have even a weak stop-band absorption is now obtained.

In another experiment: a mixture of 290 nm and 220 nm polystyrene spheres diluted in ethanol was dropped, by using a glass pipette, onto a piece of substrate when attached to a spin coating device. This procedure is akin to that of dropping stearic acid onto a film to test for photocatalysis. The film displayed no interference colours ('control 2'). **Figure 4.3** shows its infiltration. Both opal and inverse opal have a poorer definition; a

broad band can be seen at 350-450 nm. The film was dip-coated a few times (5) in titania precursor solution and then calcined. No 'edge' shots could be obtained in either this sample, or on the repeat carried out, leading to the conclusion that a photonic crystal-like structure was not acquired by this method.

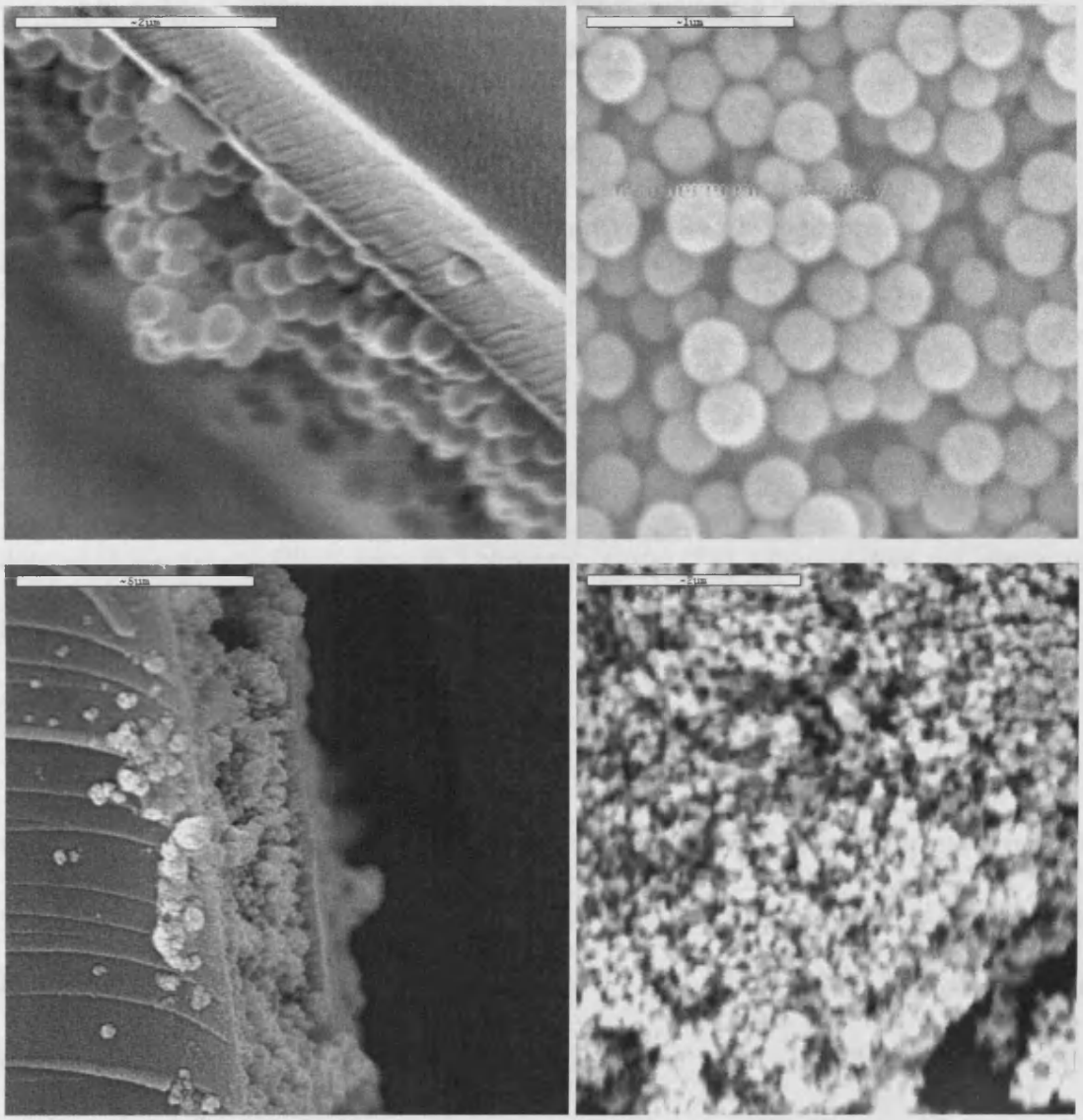

Figure 4.2 (clockwise from top left): Control sample '1' as opal (edge), control as opal (top), control as inverse opal (top), inv opal (edge).

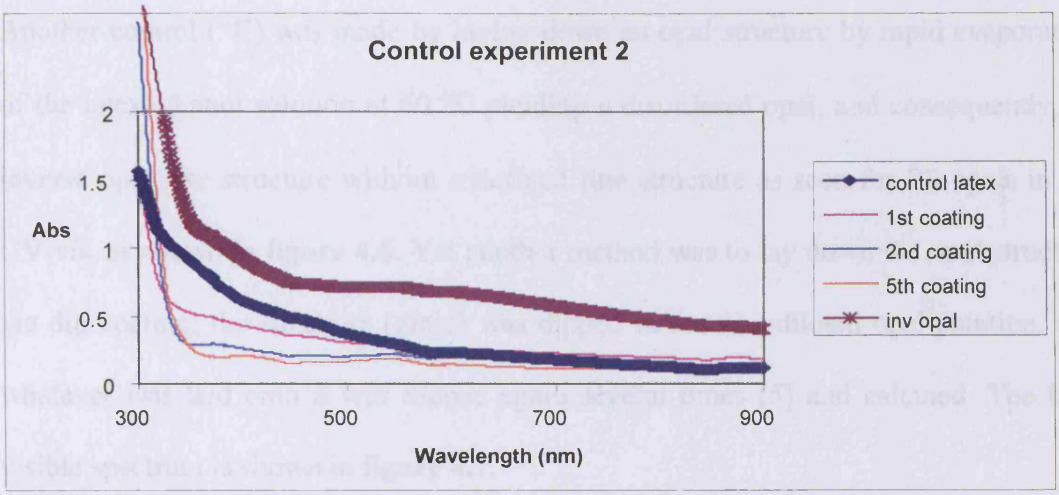

Figure 4.3 Infiltration and calcination of control film '2' made from a film made by dropping a polystyrene mixture (300/220 nm) onto a glass slide: labelled as 'control latex'. This was infiltrated by dip-coating with titania precursor: the 1st, 2nd and 5th coatings are shown. 'Inv opal' = the UV profile for the inv opal-like structure obtained after removal of latex by calcination at 450 °C (3 h).

The SEM seen in **figure 4.4** points to a structure that does have air pockets, further it does not have the continuity seen in a photonic crystal. The structure does not appear to have a regular sphere size, which would follow from being made with no template. The sample shows cracks but without an edge.

Other methods of making structures with UV spectra lacking in flat band definiton, and yet, ones that have a degree of likeness to a well ordered inverse opal structure (this was looked at using SEM photographs) were made for example by - part-infiltration of an opal. The samples were all calcined, the idea being that the structure would collapse to produce discontinuities in the air-titania matrix ('control 3'). **Figure 4.5** shows an inverse opal sample and the spectrum shifting to the red region after two coatings. These samples were calcined at 450 °C (3 hrs). The SEM pictures show well ordered parts, but here the glass substrate was seen as well as the cracks when looked at alongside an inverse opal structure as seen in **chapter 3**.

Another control ('4') was made by laying down an opal structure by rapid evaporation of the latex/ethanol solution at 60 °C yielding a disordered opal, and consequently, an inverse opal like structure without a defined fine structure as seen for PS opals in the UV-vis, as shown in **figure 4.6**. Yet another method was to lay down the opal structure via dip coating; the substrate (glass) was dipped in the non-diluted opal solution, and whatever was laid onto it was dipped again several times (5) and calcined. The UV-visible spectrum is shown in **figure 4.7**.

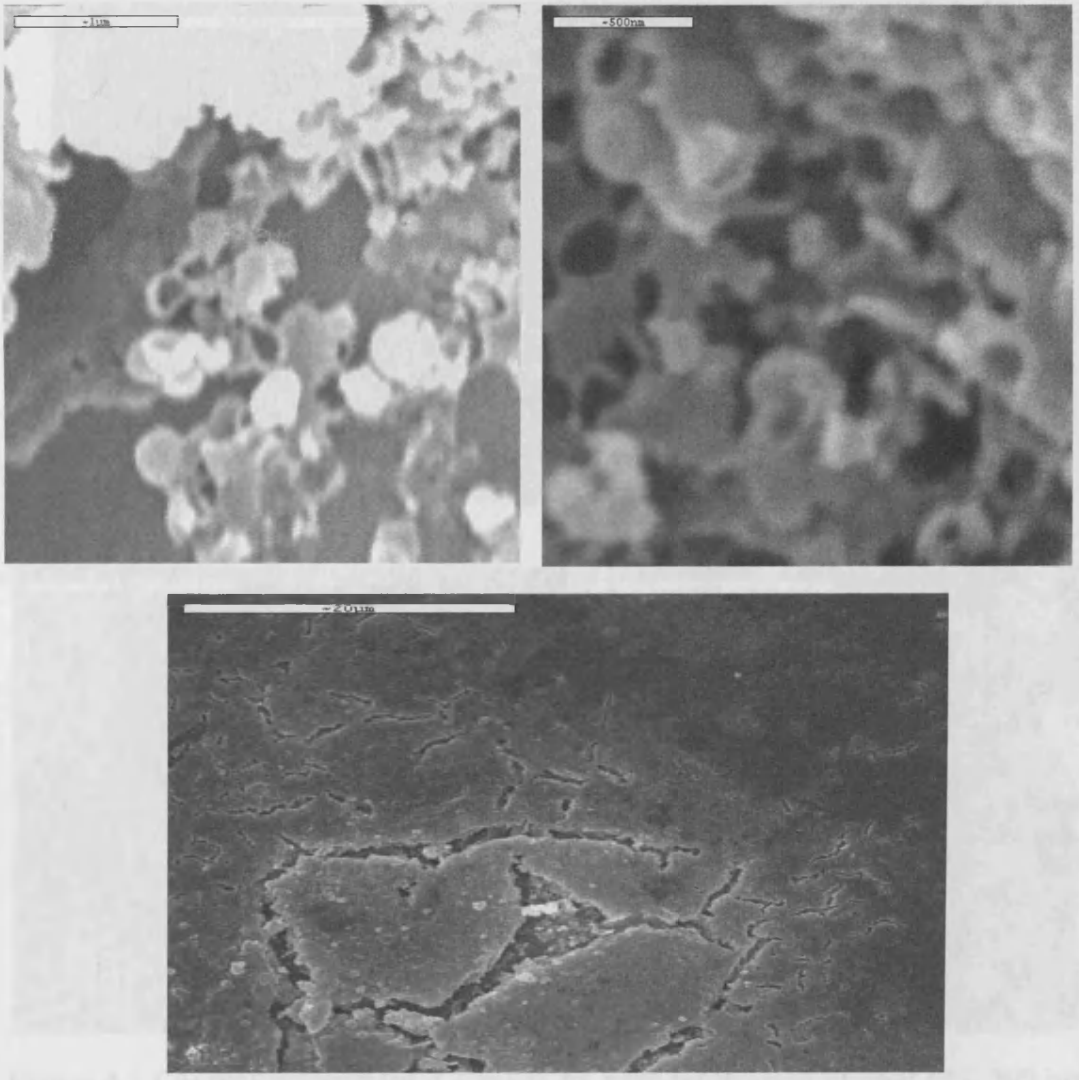

Figure 4.4 SEM micrographs showing structure of inverse opal made from 'dropped' spheres – control experiment 2.

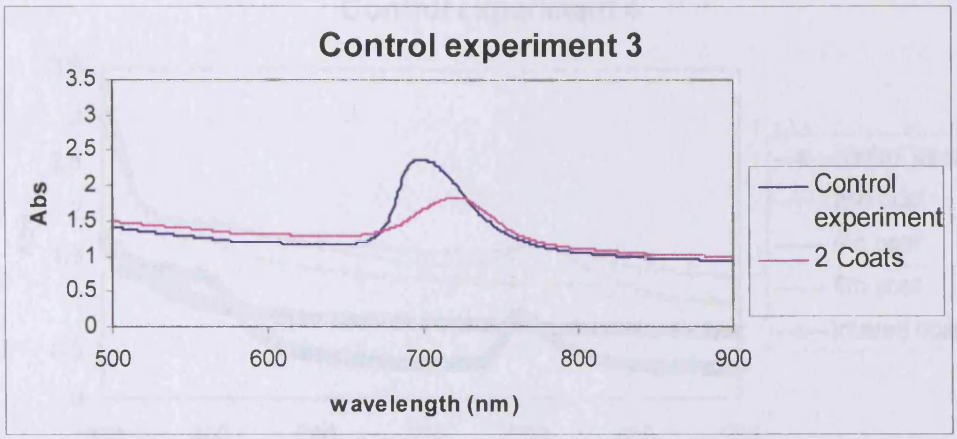

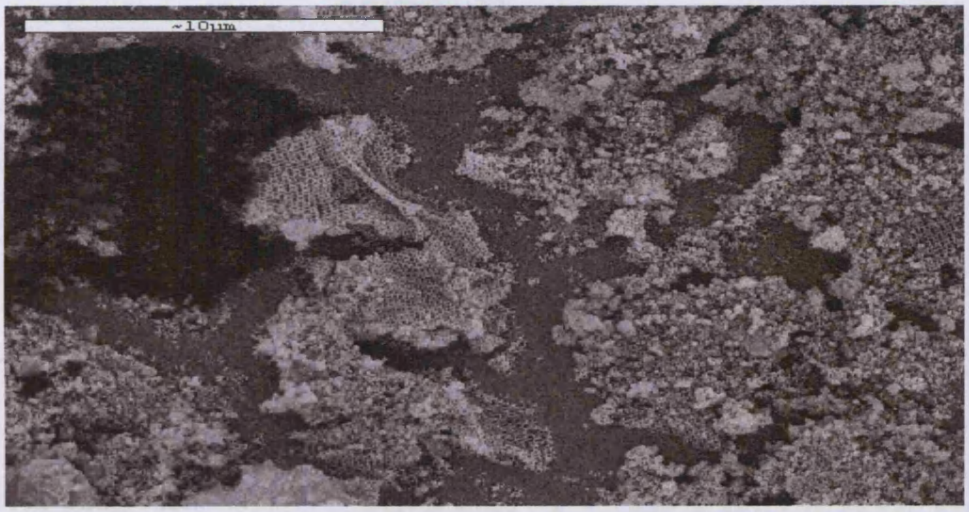

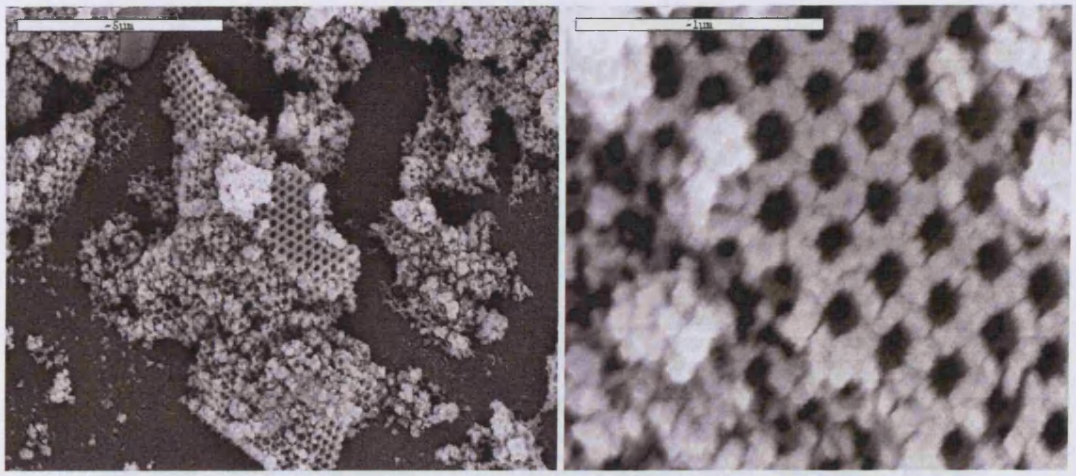

Figure 4.5 Control experiment 3 – made by part-infiltration of opal (PS, 300 nm). The UV profile shows the 'stop' band of the opal and the stop band once the structure was coated twice by dip-coating using titania precursor. The 'flat' band of the structure obtained, once calcined at 450 °C (3 h) shows no definition as with the two previous controls. The SEM micrographs shows top surface obtained for inverse opals made by using this method: a highly cracked structure is seen, as are discontinuities to the air/titania pockets.

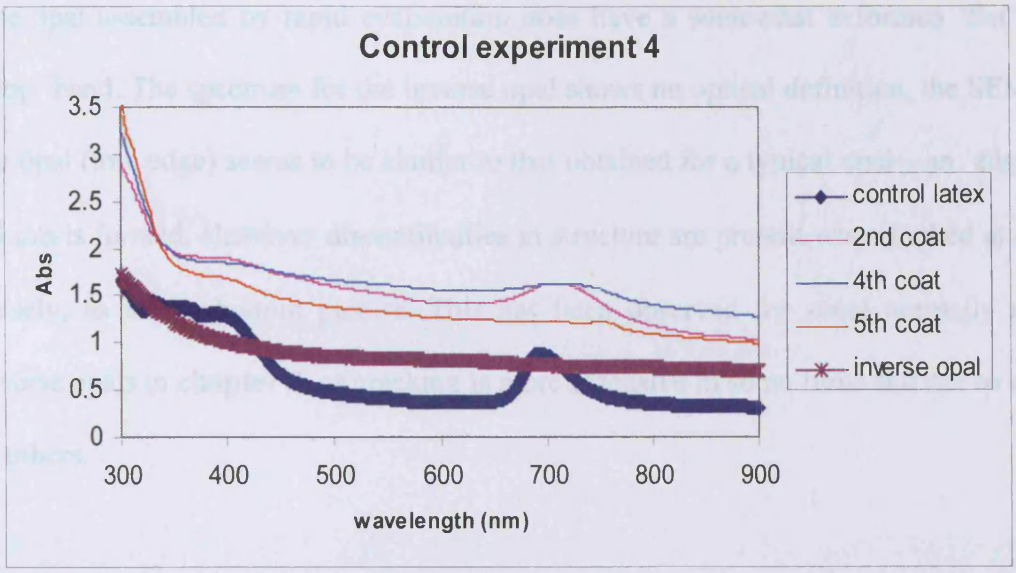

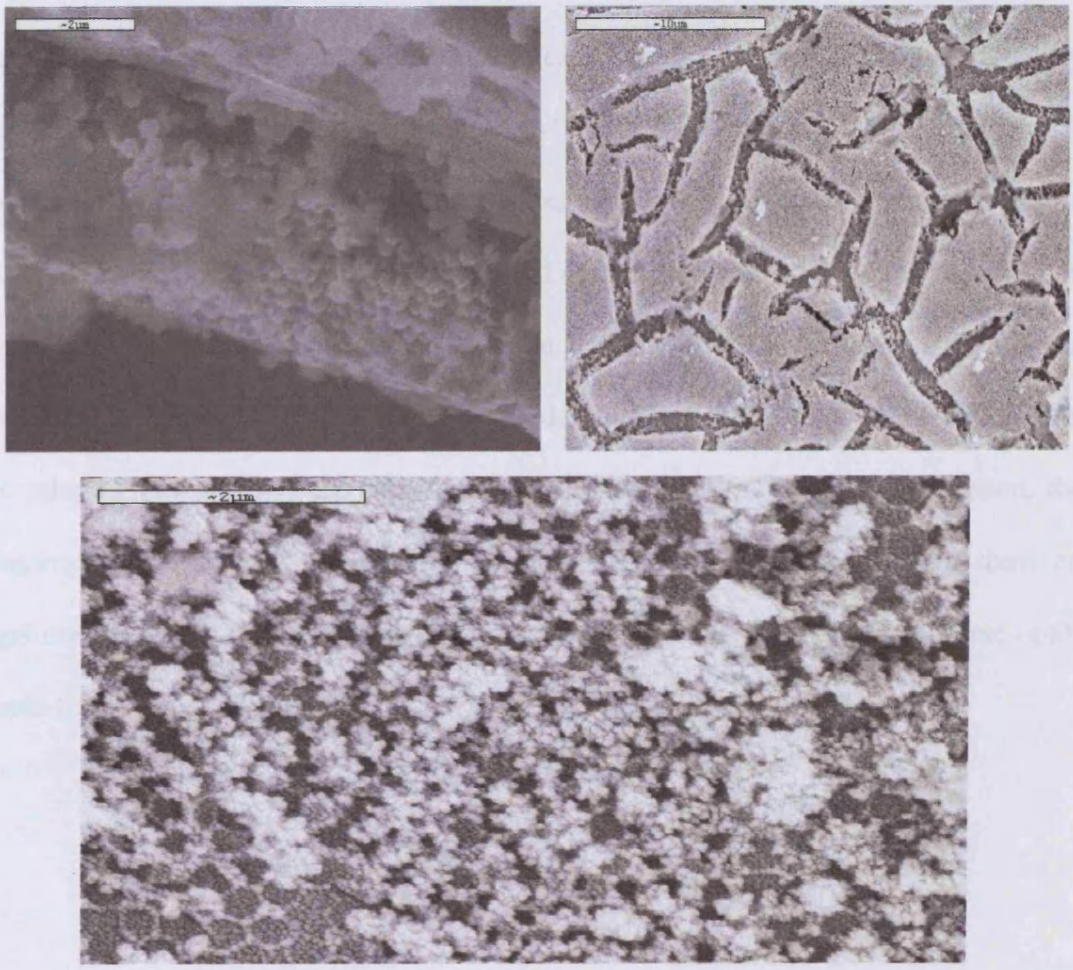

Figure 4.6 Control experiment 4 - Profile of UV infilling of opal (PS, 300 nm) assembled by rapid evaporation of latex/ethanol mixture. The UV-vis profile, top, also shows the effect of infiltration by dip-coating using titania precursor. Inverse opal = the profile shows the 'flat' band for the structure obtained, once calcined at 450 °C (3 h) with no definition as with the three previous controls. The SEM micrographs show (clockwise, from top left): edge of PS opal assembled by this method, top surface obtained for inv opals made by using this method, and another top surface micrograph.

The opal assembled by rapid evaporation does have a somewhat deformed 'flat' and 'stop' band. The spectrum for the inverse opal shows no optical definition, the SEM for the opal (top, edge) seems to be similar to that obtained for a typical opal – an 'edge' of ~3 μm is formed. However discontinuities in structure are present when looked at quite closely, as in the bottom picture. This has been observed for some normally made inverse opals in **chapter 3**, as cracking is more extensive in some films and not so much in others.

Figure 4.7 shows a type of inverse opal that was built when assembling an opal network by dip-coating substrate with a latex solution (290 nm) that is undiluted by ethanol. This was dipped onto a solution 5-10 times, with drying for 5-10 mins after each dilution. The thick blue line (for the assembled opal) does display a 'flat' and a 'stop' band region however this is not as well defined as those reported in chapter 3. On subsequent infiltration and calcination a flat line for this film is seen in the UV-vis spectrum- indicating a lack of long range order and loss of the stop-band ('control 5'). To reiterate this was not the case for inverse opals made in the previous section, the majority of which had a weak stop band in the UV-visible. The SEM's show an agglomeration of air/titania particles that do not look as tidily packed as inverse opals made from 'Colvin' opals.

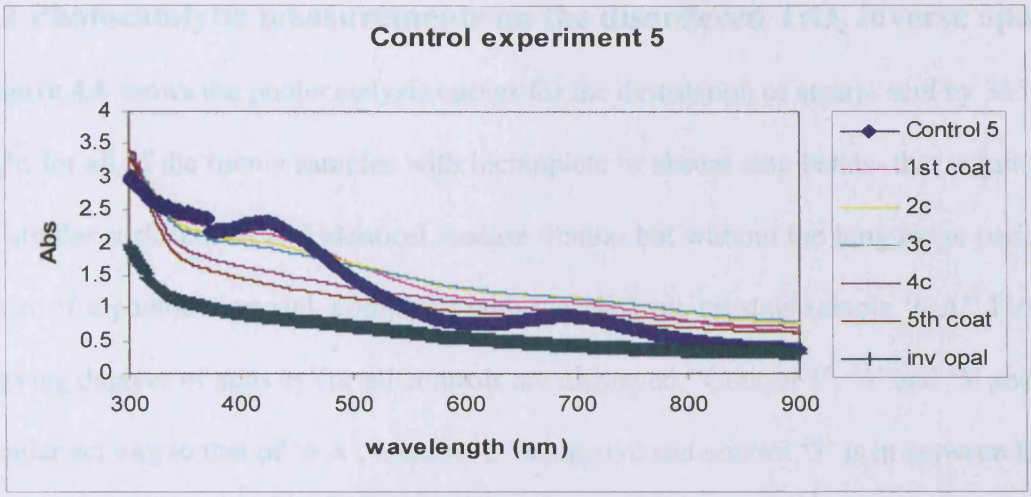

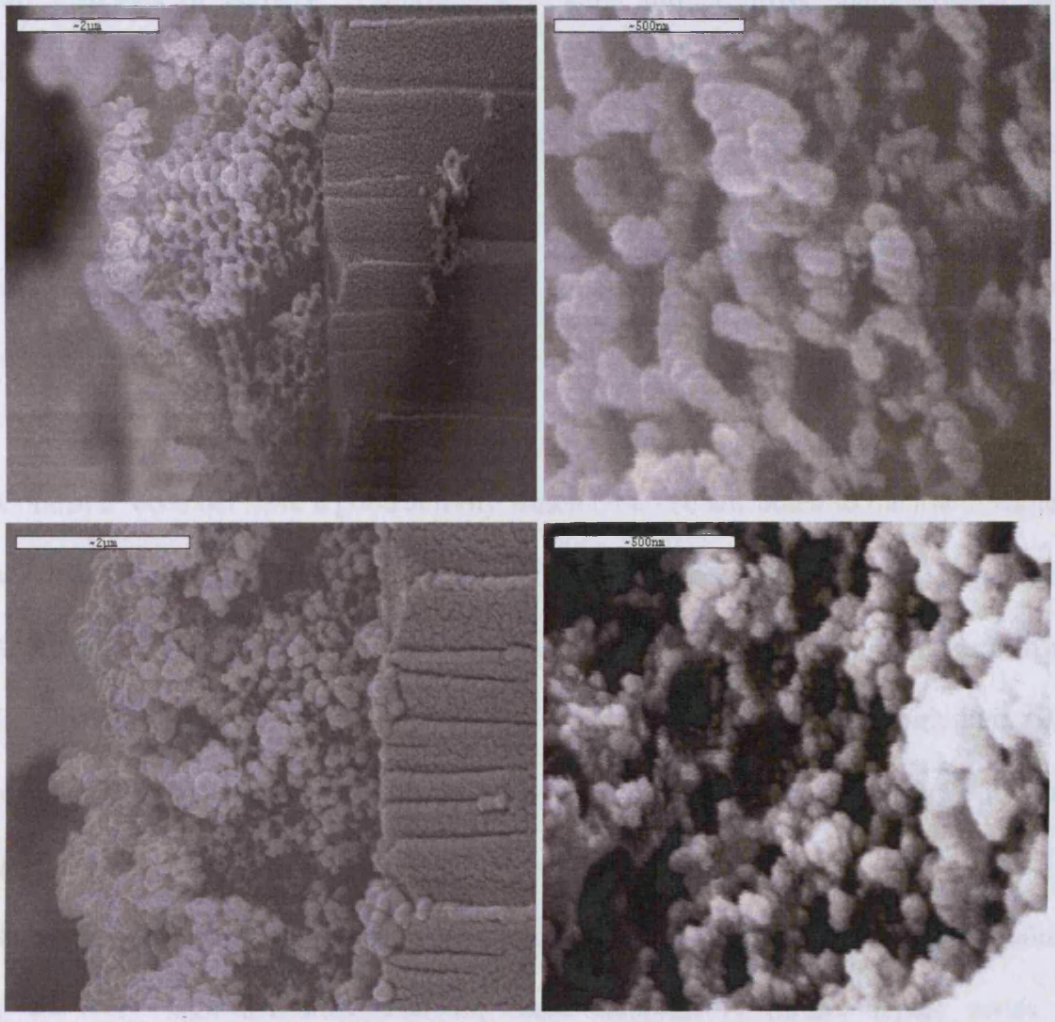

Figure 4.7 Control experiment 5 - Profile of UV infilling of opal (PS, 300 nm) assembled by coating an undiluted latex solution (PS, 300 nm, 7wt%) onto glass. The UV-vis profile, top, also shows the effect of infiltration by dip-coating using titania precursor. Inverse opal = the profile shows the 'flat' band for the structure obtained, once calcined at 450 °C (3 h) with no definition as with the three previous controls. The SEM micrographs show (clockwise, from top left): edge of PS opal assembled by this method, top surface obtained for inv opals made by using this method, and another top surface micrograph.

4.2 Photocatalytic measurements on the disordered TiO_2 inverse opal

Figure 4.8 shows the photocatalysis curves for the destruction of stearic acid by 365 nm light for all of the titania samples with incomplete or absent stop bands- that is samples of similar surface area and identical anatase titania- but without the long range periodic order of a photonic crystal, compared with the photonic crystals sample '6 A'. Firstly, varying degrees of activity for all controls are displayed. 'Control 1', '4' and '5' show a similar activity to that of '6 A', control '2' is inactive and control '3' is in between these two extremes of activity. 'Control 1/4/5' have similar gross characteristics when looking at the SEM, with small differences in the degree of ordering but more importantly all of these display a lack of fine structure in the 'flat' region of the UV whereas weak bands are present in '6 A' (both the controls and photonic crystals '6 A' have a lack of fine structure compared to a PS opal). What 'Control 1/4/5' have in common is their structure.

'Control 2' does not have a good activity which could be attributed to the low thickness, which is attributed to the fact that no 'edge' could be obtained when using SEM. 'Control 3' and its activity could be attributed to a collapsed structure as seen in the SEM but also a smaller amount of titania that is deposited as a result of only being dip-coated with precursor twice: the SEM top surface images show areas where only glass appears to be present. Though overall as controls '1/4/5' show, it is their structure as shown by SEM, and not its optical properties that is the most important factor resulting in the very high activities seen for these samples. A further repeat series of photocatalytic measurements was made - this showed excellent reproducibility in photocatalytic activity (as demonstrated by t ½ values) shown by all these controls.

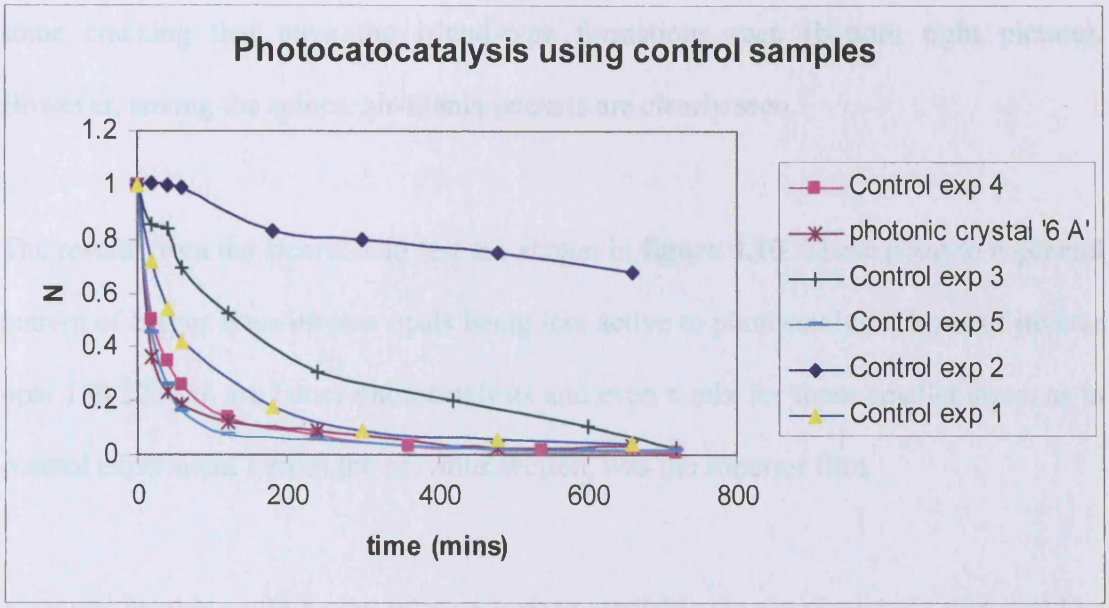

Figure 4.8 Photocatalysis run for the destruction of stearic acid overlayer using 365 nm irradiation for controls 1 – 5, and comparison of photocatalytic activity to that of one of our most active samples, photonic crystal '6 A': controls 1/3/4 show a similar t ½ to that of PC '6 A' indicating that only the increased surface area is responsible for the high activities obtained.

4.3 Photocatalysis and Size of Inverse Opals

Samples of 290 nm, 480 nm and 480/850 nm silica spheres were infiltrated by coating 5-8 times with titania precursor solution as before, using the experience acquired when infilling smaller sized silica/latex opals. The samples were heated at 450 °C to obtain the anatase form of titania (checked by Raman) and then placed in 20% sodium hydroxide solution for 3-4 days at 60 °C to remove the silica host matrix.

Samples prepared from 290 and 480 nm silica spheres produced colourful/white films that had 'spines' that could be seen along the top surface, when viewed using SEM, **figure 4.9**. The film made from 480/850 nm spheres did physically collapse from its substrate and SEM could not be obtained but photocatalysis was carried out with what remained of this film. The SEM photographs show discontinuities in the normally periodic structure, but, instead of these being due to cracking, as was the case for

samples made in **chapter 3** from calcination, these arose from the spines as well as some cracking that gave the island-type formations seen (bottom right picture). However, among the spines, air-titania pockets are clearly seen.

The results from the stearic acid test are shown in **figure 4.10**. These point to a general pattern of bigger sizes inverse opals being less active to photocatalysis. Sizes of inverse opal 150-220 nm are better photocatalysts and even a mix for these smaller sizes, as in control experiment 1 from the previous section, was the superior film.

A reason for this could be the relative surface available for photocatalysis that could be obtained when using these samples. Another reason could stem from the structural irregularities caused by the 'spines' so a repeat was carried out to verify this. This involved a slight variation of the 3-step process as described in chapter 2: placement in sodium hydroxide was decreased by two days (1-2 instead of 3-4). The effects were evident from the way the films looked. The 850 nm sample did not flake off as in the previous attempt and SEM photos were obtained and are shown, along with those of other sizes, in **figure 4.11**.

These structures were made by 7-8 infills with titania sol (90/10) (v/v). Survey of these structures by SEM (figure 4.11) shows a continuous assemblage of air-titania pockets. The cracks are not as evident as before. This shows that using titania with the sodium hydroxide treatment is beneficial from this perspective. The structures obtained are 3-6 μm thick which are thicker than the films obtained thus far (~4 μm). The UV-visible spectra for titania inverse opals made from 290, 480/850 nm silica opals are shown in figure 4.12. These display no optical bands in the any of the ranges at which the measurement was performed. That is not the case for the sample made from 480 nm

silica, which displays a stop band at ~900 nm with a broad band at 300-500 nm. In the 1st run with samples of these sizes, no optical properties were displayed by any of them. Shortened treatment with sodium hydroxide seems to make a slight difference here. Reflectance-transmission was carried out and no extra optical features were seen.

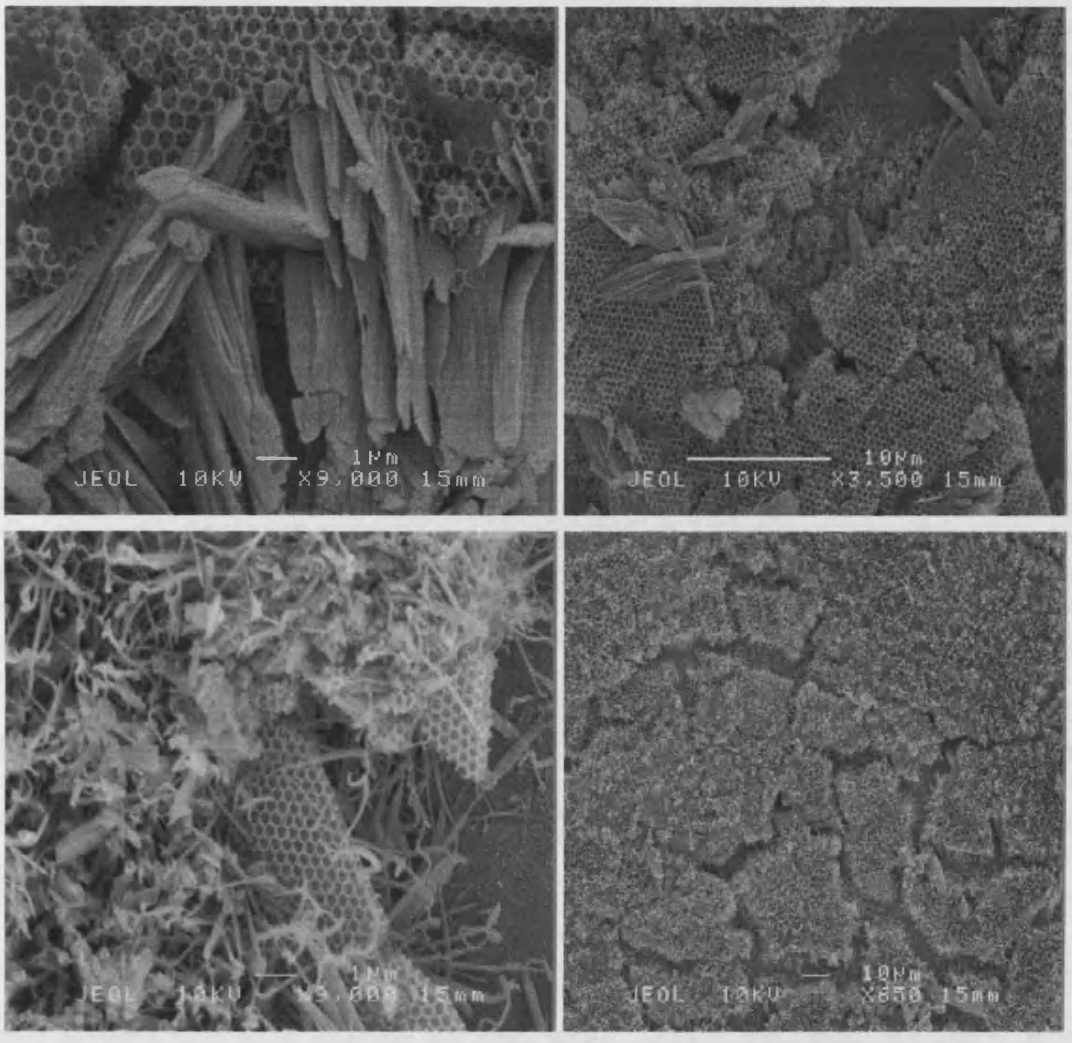

Figure 4.9 Inverse opals made from silica opal of the following sizes: 290 nm (top) and 480 nm (bottom).

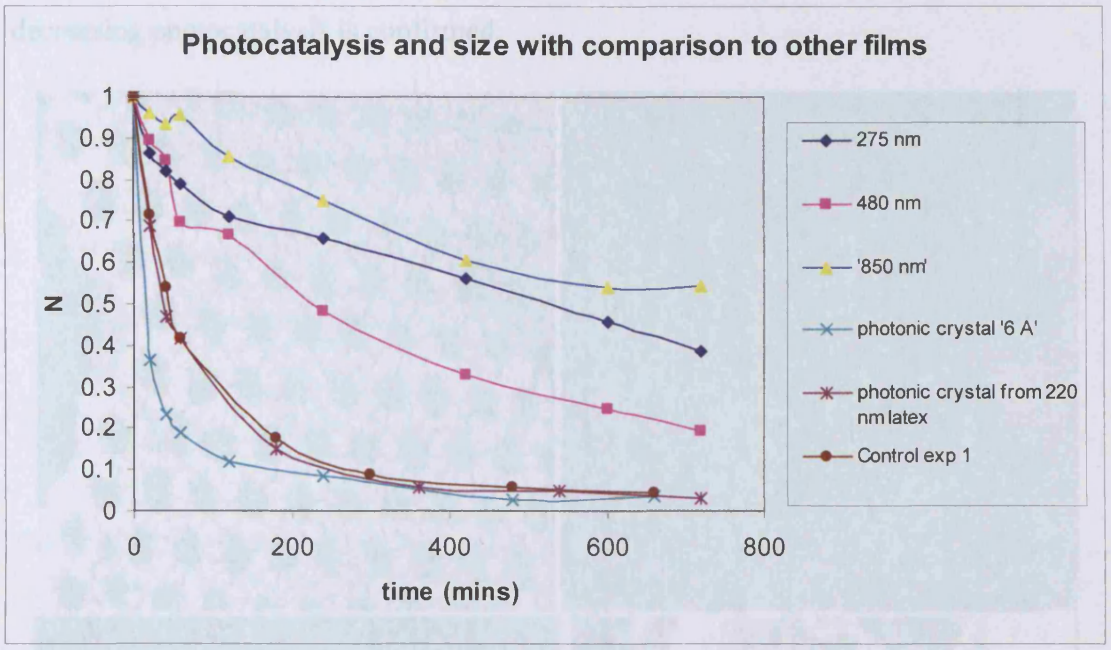

Figure 4.10 Photocatalysis run for the destruction of stearic acid overlayer using 365 nm irradiation - photocatalysis-size experiments: the size of spheres obtained from inversion of the silica opal into a titania inverse opal is shown. These inverse opals of the following sizes: 275, 480 and 480/850 nm are compared to photonic crystal '6 A', made from PS, 300 nm; PC made from PS, 220 nm and control experiment 1, which is one of the controls that have a comparable t ½ to photonic crystals.

The photocatalysis curves are shown in **figure 4.13**. The overall pattern remains, from run to run an increase in size of the silica template seems to correlate with a decrease in photocatalytic activity. The (t ½) values (see **Appendix** where the (t ½) for all the size experiments are listed) shows that, for samples prepared from 275 nm and 470-700 nm silica samples (shrinkage changes the opal sphere size) a significant increase (200 + mins) in half-lives was achieved for these samples. This is because of the change in treatment with sodium hydroxide solution (1-2 days instead of 3-4) yielding better structures as seem in the SEM. However, this was contradicted by the result obtained for 465 nm titania inverse opals where the reverse occurs. It was the only sample where an optical absorption feature of any sort was seen – but the 470-700 sample also displays a similar half-life with no optical absorption displayed. The lack or not of this optical feature does not seem to play a part in whether photoactivity will occur or not.

Overall, the general trend of increasing sizes (and, consequently, thickness) with decreasing photocatalysis is confirmed.

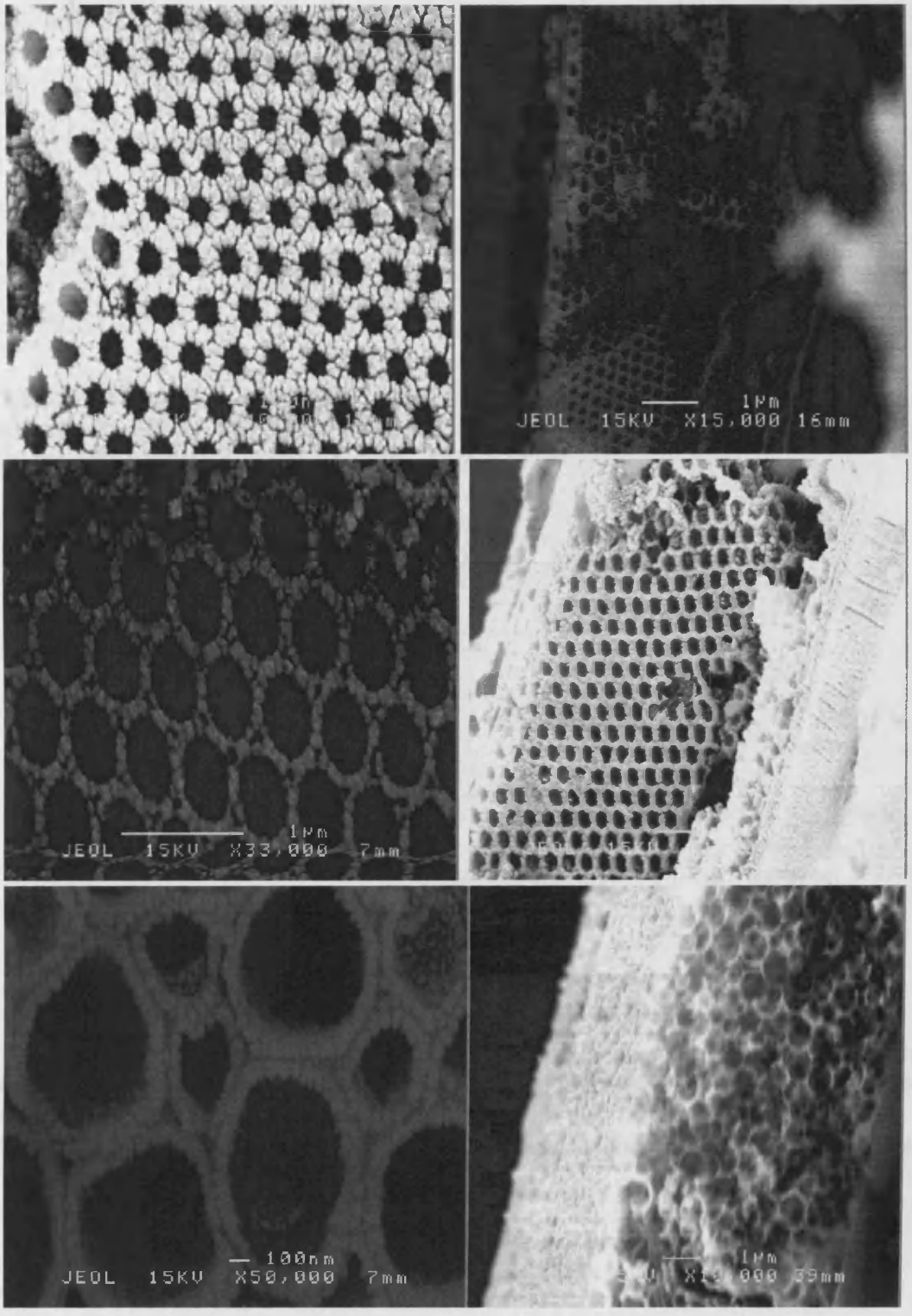

Figure 4.11 SEM for inverse opals made from different sizes: 275 nm (top), 465 nm (middle) and 470-700 nm (bottom) made by infiltrating silica opals, heating at 450 °C (3 h) then using a 20% sodium hydroxide solution at 60 °C to remove the template. Top images for each of these sized samples (left) and side-on (right).

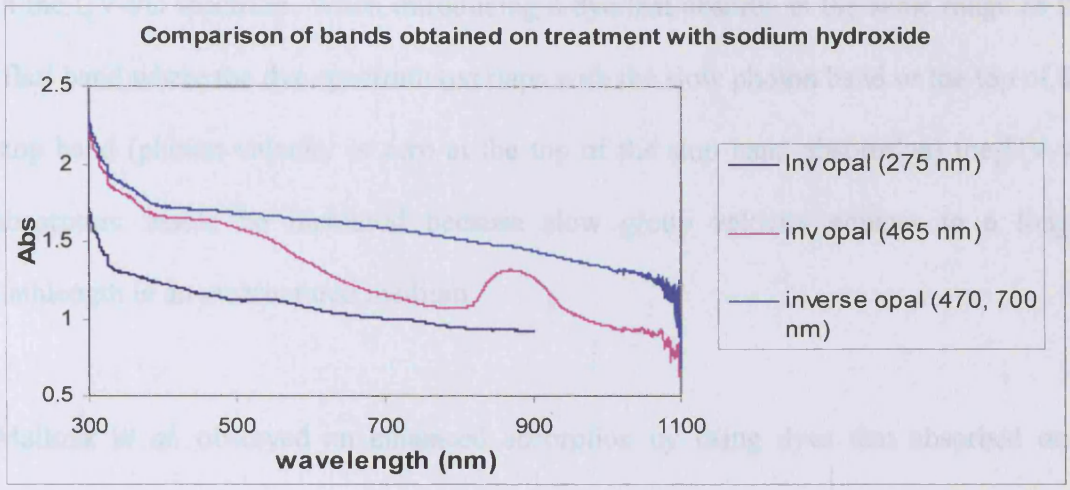

Figure 4.12 Comparison of bands obtained for inverse opals made from silica opals and whose activity was tested in a run (figure 4.13). None of these inverse opals display any definition in the 'flat' band part.

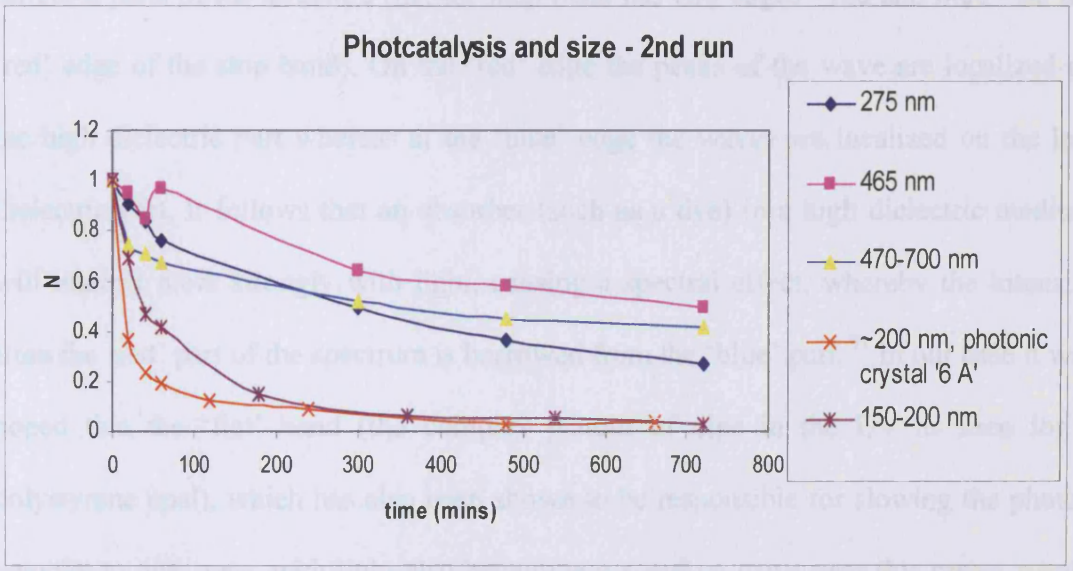

Figure 4.13 Photocatalysis run for the destruction of stearic acid overlayer using 365 nm irradiation - photocatalysis-size experiments: comparison between different sizes of titania. 275, 465 and 470-700 nm (made from silica opals of similar sizes) and inverse opals of size ~150-200 made from PS (as tested in chapter 3 and included here).

4.4 Dye experiments

The idea of this experiment was to observe, by looking at the UV-vis spectra, the enhancement that might be obtained via the slow photon effect when using these structures. The theory, as explained in **section 1.7** would translate as observable effects

in the UV-vis spectrum. When introducing a dye that absorbs in the same range as the 'flat' band where the dye spectrum overlaps with the slow photon band or the top of the stop band (photon velocity is zero at the top of the stop band absorption) the UV-vis absorption would be increased because slow group velocity equates to a longer pathlength in an unstructured medium.

Mallouk *et al.* observed an enhanced absorption by using dyes that absorbed on a similar range to the stop band for a titania inverse opal. Their hypothesis was that the group velocity of light is significantly reduced near the stop band: light effectively becomes a standing wave. The reasoning for this is that light waves are localized in different parts of the structure (i.e. the stop band has two edges - red and blue - on the 'red' edge of the stop band). On the 'red' edge the peaks of the wave are localized on the high dielectric part whereas at the 'blue' edge the waves are localized on the low dielectric part. It follows that an absorber (such as a dye) in a high dielectric medium will interact more strongly with light, causing a spectral effect, whereby the intensity from the 'red' part of the spectrum is borrowed from the 'blue' part.[91] In our case it was hoped that the 'flat' band (the complex pattern of dips in the UV as seen for a polystyrene opal), which has also been shown to be responsible for slowing the photon velocity to near zero, with light also becoming a standing wave near this range, would also display a similar effect. Thus the experiment involved soaking a polystyrene opal in a solution of the dye and measuring the UV before and after coating.

The expected result would involve an enhancement in absorption only at the 'flat' band region and not at the 'stop' band region as the dye does not cover such range. The dye chosen was HABA (2-(4-hydroxyphenylazo) benzoic acid). Its absorption maximum is at 348 nm. Several concentrations (10^{-3} to 10^{-5} mol dm^{-3}) were made with ethanol

resulting in a light orange solution. Crucially, enhancement would indicate that the greater absorption is making some contribution toward the observed photoactivity.

Using the dip-coating device at 5-6 cm/min, as before, a HABA/ethanol concentration of $\leq 10^{-3}$ mol was chosen as anything higher resulted in an orange powder covering the surface of the opal, interfering with the measurement on the films. Any subsequent washing to remove the excess might have left varying amounts of dye on the opal, making repeats unreliable. One of the opals used is shown in **figure 4.14**. Two others were used to check whether the effects observed were consistent. The photographs were taken after the experiments were completed.

Figure 4.15 shows the UV spectra before and after the polystyrene opal was immersed in a 10^{-4} mol dye solution for 30 minutes. The place in the opal film at which to measure the UV spectra was marked (using a marker pen) to ensure that any variability due to any structural defects was avoided. The absorption is increased for the 'flat' region but also for the 'stop' band region; enhancement is not localised to the 'flat' band region, as it should have been. A similar experiment was carried out at a lower concentration; the spectrum of the dye is superimposed onto that of the opal.

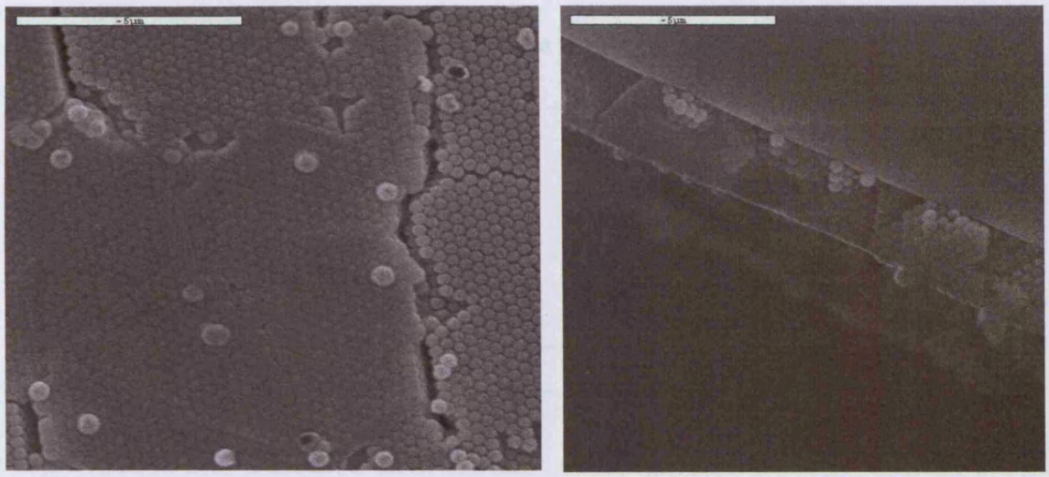

Figure 4.14 PS Opal (300 nm) used in dye experiments: top (left) and edge (right).

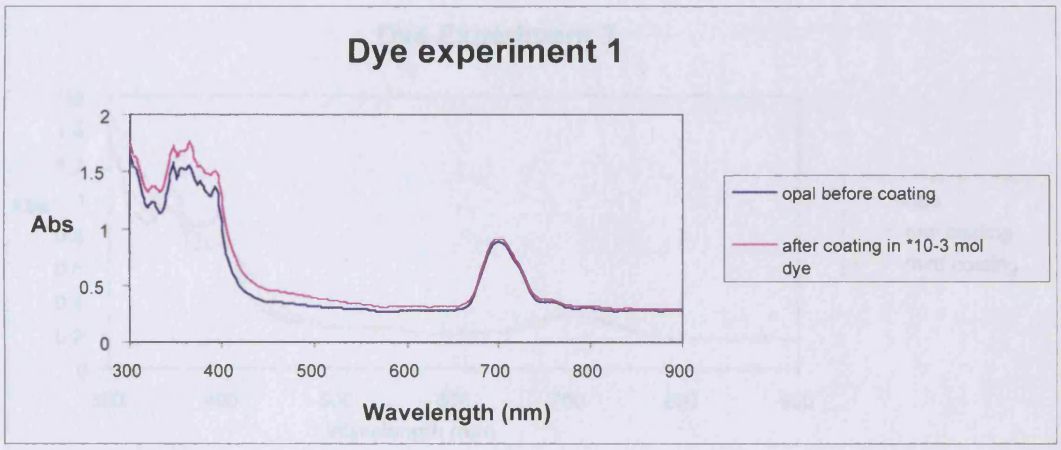

Figure 4.15 Dye experiment 1 on the PS opal (shown in figure 4.14): both 'flat' and 'stop' band absorptions seemed to be changed slightly after dip-coating with dye – no effect observed.

In further experiments, the scanning range of the UV-vis was widened to cover 190-900 nm instead of 300-900 nm but no effects were seen in the higher energy regions. The coatings would consist of immersing the opal into a dye solution for 30 minutes, then taking it out and measuring.

Figure 4.17 shows that, with further coatings, with supposedly higher amounts of dye being deposited that there is an effect upon absorption – the 'flat' band's absorption goes down, the 'stop' band's absorption is unchanged. However this is not a consistently repeatable effect. Another opal was used and the spectral effect (increase in absorption) was not observed.

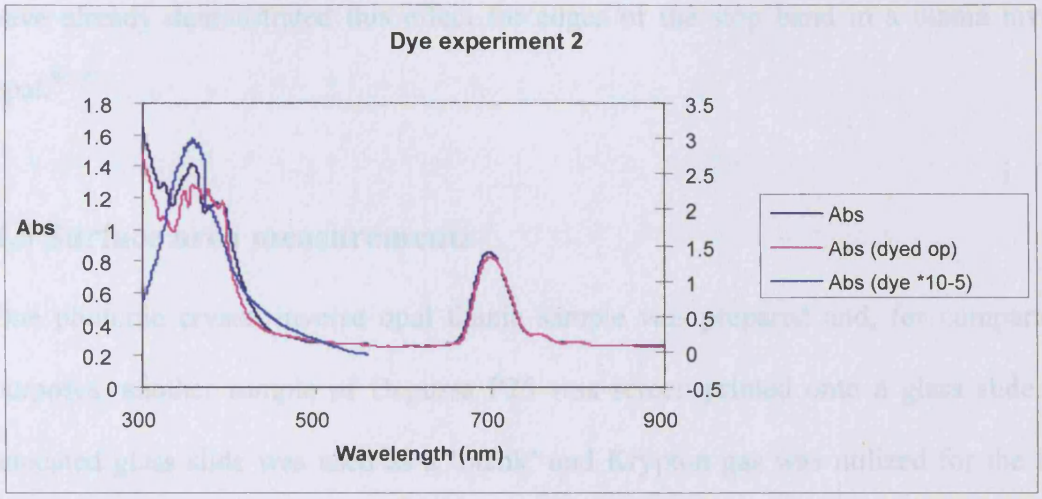

Figure 4.16 Dye experiment 2 on PS opal, as before.

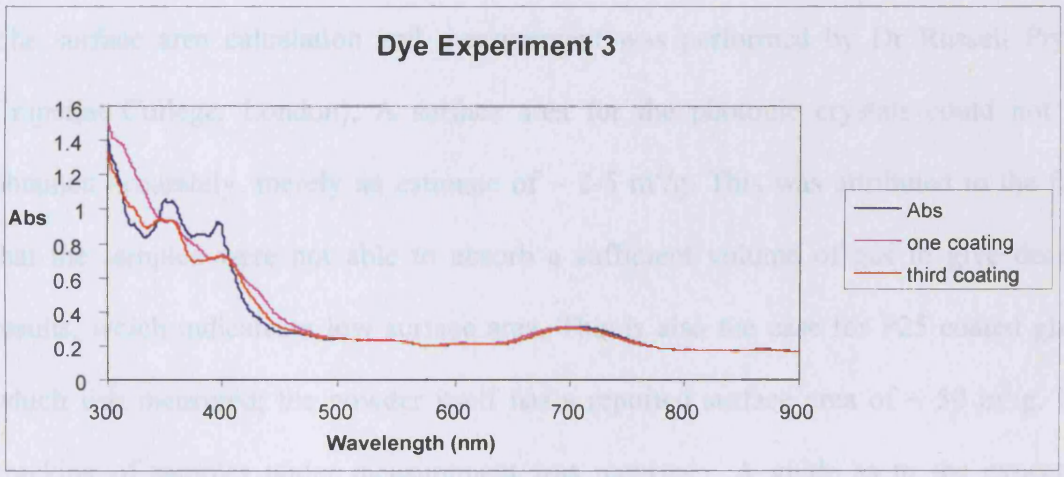

Figure 4.17 Dye experiment 3 on PS opal, as before.

Recently, these results have been contradicted by Ozin *et al.* [89] They show that the effects themselves are related to differences in thickness. Thicker films will depict different transmission dips than less thick ones. The measurements were performed in the IR region, by extracting a field transmission coefficient for the near-IR spectrum from light interferometry measurements and closer analysis of the band edges. However, variance was found when placed alongside values for theoretical calculations. It was concluded that perfect opals, whose quality is not yet achievable, are needed for slow photon enhancement of photonic properties.[89] Similar effects deriving from changes in thickness were seen by Lin *et al.* when measuring changes in band-edge from tungsten 3D photonic crystals made by a layer stacking method and Mallouk *et al.*

have already demonstrated this effect for edges of the stop band in a titania inverse opal.[90-91]

4.5 Surface area measurements

One photonic crystal inverse opal titania sample was prepared and, for comparative purposes, another sample of Degussa P25 was screen printed onto a glass slide. An uncoated glass slide was used as a 'blank' and Krypton gas was utilized for the BET measurements of surface area. The respective weights of the material were measured. The surface area calculation and measurement was performed by Dr Russell Pryce (Imperial College, London). A surface area for the photonic crystals could not be obtained accurately, merely an estimate of ~ 2-5 m^2/g. This was attributed to the fact that the samples were not able to absorb a sufficient volume of gas to give decent results, which indicates a low surface area. This is also the case for P25 coated glass which was measured; the powder itself has a reported surface area of ~ 50 m^2/g. No cracking of samples under measurement was reported. A guide as to the expected surface area is seen in a recent publication by Bu *et al.* where a manufactured porous titania film laid by using the sol-gel method and polyethylene glycol (PEG) as a template produced surface areas of 60-70 m^2/g, depending on the amount of PEG used.[92]

4.6 Conclusions

'Controls' were made by making use of several deviations from the 3-step process described in **chapter 2**. The good photocatalytic activity obtained suggests that the primary cause for this is the surface area obtained by making the structures and not the slow photon effect as evidenced by weak bands as seen in the UV-vis profile for a photonic crystal that is made as a result of the original 3-step process as detailed in

chapter 2. This is backed up by the measurements of inverse opals that were produced from templates of different sizes - the trend being that the larger the template size (smaller area for activity) the smaller the extent of photocatalysis - as well as the experiments with the HABA dye which do not show consistent enhancement or a slow photon effect.

Chapter 5 Sensors and Photonic Crystals

5.1 Introduction

Metal oxides exhibit gas-sensing properties if they are prepared in a porous form so that the surface electrical conductivity is dominant. It is desirable that when a sensor is prepared its microstructure can be controlled so that the sensitivity and discriminatory properties are increased. Control of microstructure is a significant problem for metal oxide sensors. Scott *et al.,* recently described one approach to control the latter and maximise the signal by adapting the preparation of an inverse opal photonic crystal to tin oxide. [93] Therefore, the overall objective was to determine whether one could improve the properties of metal oxide gas sensors (and in particular their reproducibility) by controlling the microstructure; this has been shown to be possible by using the 3-step to make inverse opals of titania as seen in **chapter 2**. Much of the cost, time and labour are spent in the calibration rather than the fabrication of devices. If a sensor could be made to be reproducible enough so that calibration was not necessary, this would reduce cost, so this is of interest from a commercial point of view. With an inverse opal, an extra amount of surface material could be made available, and this could increase the sensitivity of the material.

Ozone can be a difficult gas to work with, as it tends to decompose readily on sensor and its surroundings. Therefore, the ozone concentration is difficult to control, so it becomes difficult to determine the reproducibility of the sensors. Also, ozone experiments must be carried out manually, as the ozone generator is not computer controlled, so doing a large number of concentrations on multiple sensors would be labour intensive. Tungsten trioxide is very sensitive to ethanol, meaning that it is a good probe gas to use. It can also be used over large concentrations: from sub-ppm to percentage levels by using saturated ethanol vapour from a dreschel bottle. Since the

objective was to investigate the microstructural properties, any gas could in principle be used.

In this chapter the gas sensor behaviour of titania doped tungsten inverse opals are explored; this is chosen because tungsten trioxide is the material used for gas sensing, and an attempt to make these has been already made as seen in **section 3.8**. A three-resistor circuit model previously shown to represent well the microstructure effect on response was applied to represent microstructure effects on the gas response of a photonic crystal of tungsten doped titanium dioxide prepared via sol-gel procedure (see **section 2.2.1**). [93]

Work with titania substituted chromium oxide has shown that there is a correlation between the magnitude of gas (ethanol) response and the particle size and porosity. [94] Chromium titanium oxide (CTO) was chosen in the literature for this investigation because it has excellent stability and minimal response to humidity. This is an advantage over tin oxide, the other material that has been extensively used when dealing with the detection of reducing gases.

The purpose of this chapter is to show the results of a number of gas-sensing experiments with inverse opals, their response to ethanol, as well as applying the 3-resistor microstructure model to the unique microstructure generated in this thesis. It was hoped that these inverse opal structures infiltrated by the sol-gel procedure would offer improved reproducibility when compared with equivalent non-opal sensors.

5.2 Microstructure modelling

The gas response for a *p-type* material such as CTO is often modelled as: $R/R_o \propto C^{0.5}$, R = total film resistance under gas exposure, R_o is the baseline resistance and C = gas concentration. Experiments with CTO showed an obtainable gas response that shows a deviation from this law at high and low concentrations of reducing gas such as CO. [93-95]

A three-resistor model gives a qualitative understanding and forms the basis for a microstructural comparison between different films. The model has been used to compare single crystal CTO (fully dense, no grain boundaries) and APCVD prepared CTO (very dense, significant grain boundaries, extensive micro-cracking, thin films 500-1500 nm) (**figure 5.1**). [93] This model is formed by a set of assumptions; a surface limited, gas-sensitive region exists, which is of constant and uniform depth (denoted by R_s); that beneath this there exists a bulk region (R_b); and finally, a grain boundary region that is made of gas sensitive material may exist (R_{gb}) (see **figure 5.2)**.

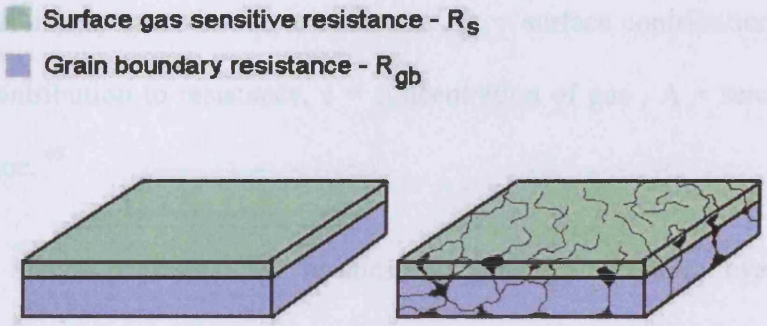

Figure 5.1 Microstructural comparison between Single crystals (left) and dense films (right) that can be gained from model. [93]

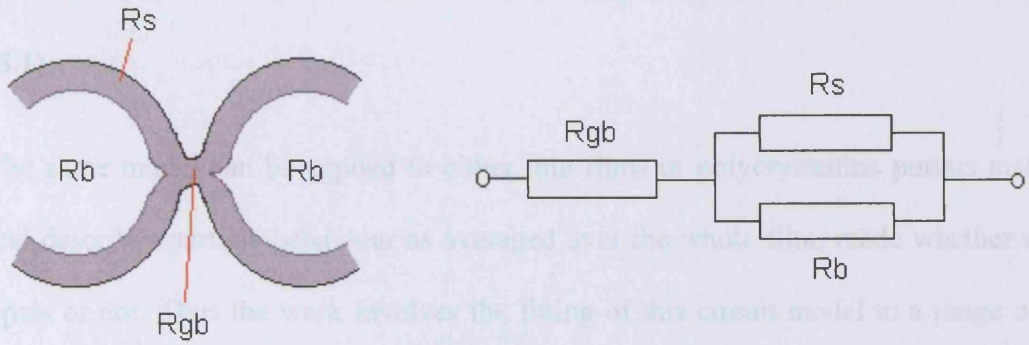

Figure 5.2 Film and its bulk, surface and 'grain boundary' shown (left) and equivalent circuit for conductance increase (n-type) response. [93]

The second major assumption is that the 'grain boundaries' are not thick enough to have a bulk-like, gas insensitive, contribution. A higher level of sintering increases the contribution from the bulk and therefore lowers the sensitivity. **Eqn. 5.1**, below is derived for a resistance decreasing response (n-type) from the assumption that the gas sensitivity of the surface and grain boundary is equivalent to one another and that a linear dependence of conductance on gas concentration applies:

$$R= \{R_{gb}/(1+Ac)\} + 1/(1/ \{R_s/(1+Ac)\} + 1/ R_b) \quad \textbf{(5.1)}$$

R_{gb} = grain boundary contribution to resistance, R_s = surface contribution to resistance, R_b = bulk contribution to resistance, c = concentration of gas , A = sensivity and R = total resistance. [95]

This model shows a power law response to gas concentration; even though the underlying response law is linear in gas concentration. Alternatively, **eqn. 5.2**, for a thin film, shows that if the R_b contribution can be ignored and that for (d) ≥ (l) then the conductance (R):

$$R = (R_{gb}/1+Ac) + (R_s/1+Ac) \quad \textbf{(5.2)}$$

Therefore $1/R \propto 1+Ac$, i.e. linear and shows a larger signal than that derived from **eqn (5.1)**.

The same model can be applied to either thin films or polycrystalline porous material and describes particle behaviour as averaged over the whole film, made whether using opals or not. Thus the work involves the fitting of this circuit model to a range of gas concentrations to inverse opals and thin films prepared in different ways aimed at changing the relative dimension of gas sensitive, and gas insensitive, 'grain boundary' regions. Sensor response has been measured for inverted opals of tin dioxide before but circuit fitting to the model was not applied. [96]

5.3 Results and Discussion

To make sets of sensors, five gas sensor substrates were attached onto a glass slide (see **experimental** section at the end of this chapter). To make 'thin film' materials the glass slide was then dipped into a sol gel solution of the precursor TiO_2/WO_3 mix, made from tungsten ethoxide and titanium tetraisopropoxide 80/20 (v/v). These substrates were labelled from A (top of slide) to E (bottom of slide) - see **figure 5.3 (left)**. To make 'inverse opal' materials the sapphire substrates were attached onto a glass slide as before but this time a set was first dipped onto a solution of latex spheres to create opal structures (300 nm sphere size) using the Colvin method. Interference colours were observed. These were then dipped in the same titania-tungsten solution, as before. After dip coating the gas sensors were then fired at 500 °C for 2h to remove the organic template. The gas sensitivity of the sensors was then measured.

A typical gas sensor response to ethanol for a typical sensor made from this method is shown below in **figure 5.3 (right)** where R = resistance for a range of concentration of target reducing gas (ethanol). The experiment is carried over several hours. These show

a response (i.e. resistance decreases for this *n-type* material), which increases with ethanol concentration (0.5-20 ppm).

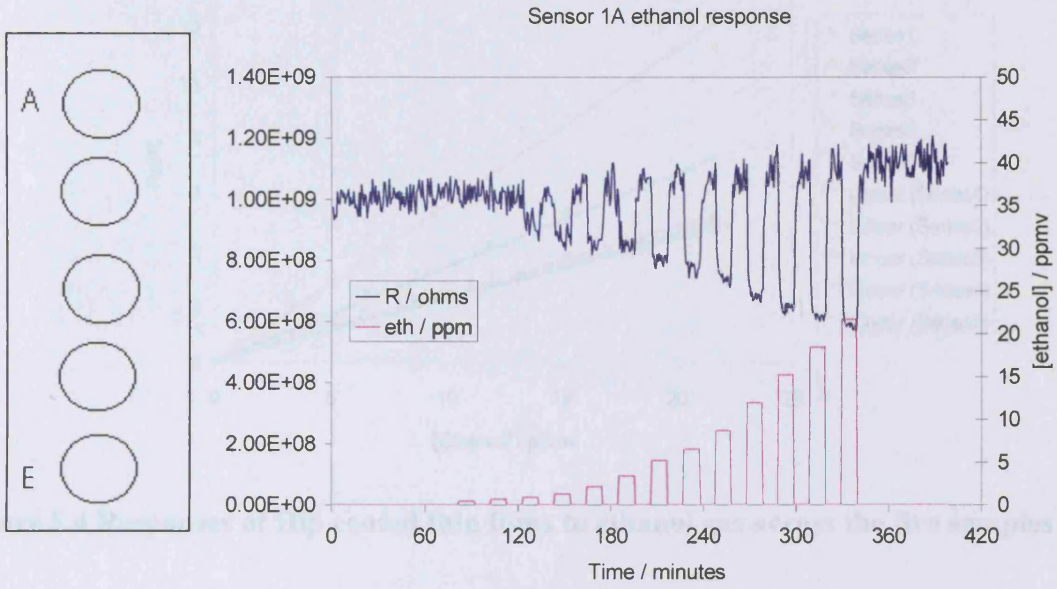

Figure 5.3 Gas response for sensor 1A (opal) to ethanol at a range of concentrations in dry air at 400°C (right) and diagram of method: glass slide attached to five, labelled - from A – E – sapphire substrates.

The microstructural model was applied to the resistance measurements (**figure 5.4 and figure 5.5**). The behaviour of the thin films can be approximated by a linear dependence of the conductance on concentration. The sensitivity seen in the plot for dip-coated (thin film) substrates can be interpreted as being dominated by a grain boundary/surface contribution. This is shown by the linear dependence of conductance on the concentration of ethanol gas (**eqn. 5.2**).

A similar behaviour was expected for the inverse opals made from tungsten oxide-titania composite, as its periodic structure, with interconnected pores, should facilitate gas access. Instead, a curved line response was found, implying that a gas insensitive 'bulk' region is present (**eqn. 5.1**). **Figure 5.5** illustrates this.

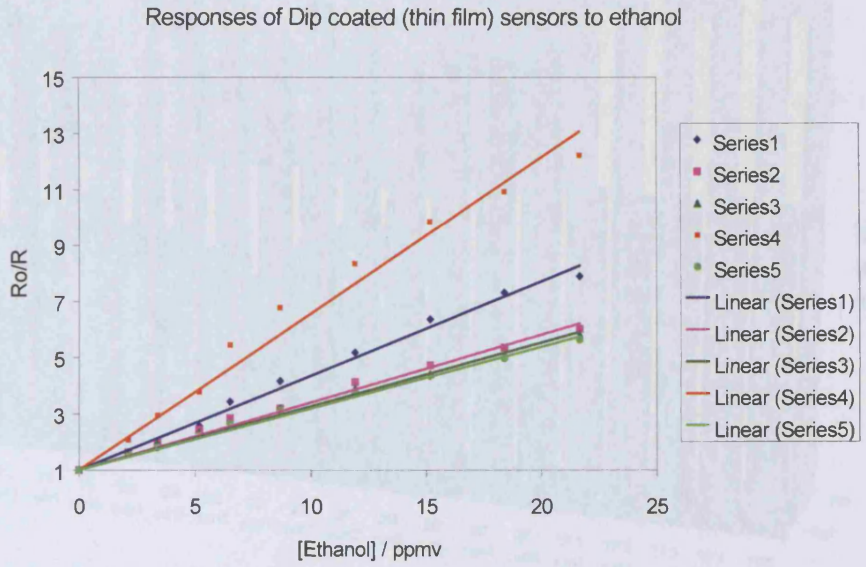

Figure 5.4 Responses of Dip coated thin films to ethanol gas across the five samples

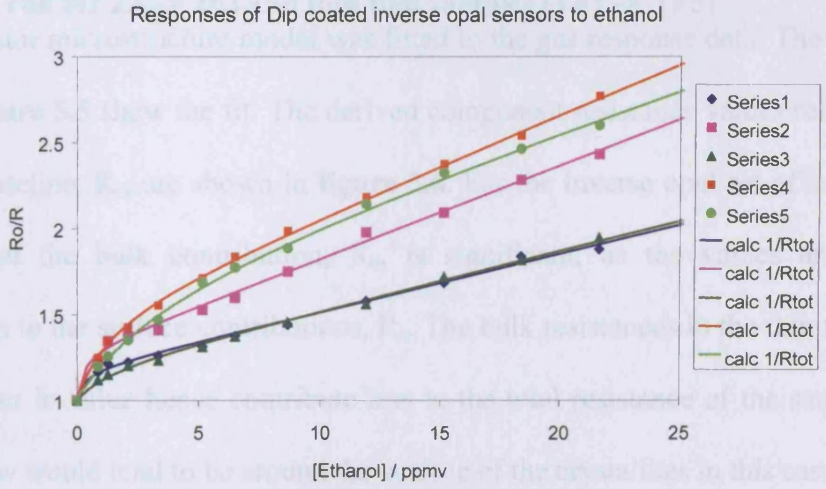

Figure 5.5 Responses of (top) inverse opals to ethanol

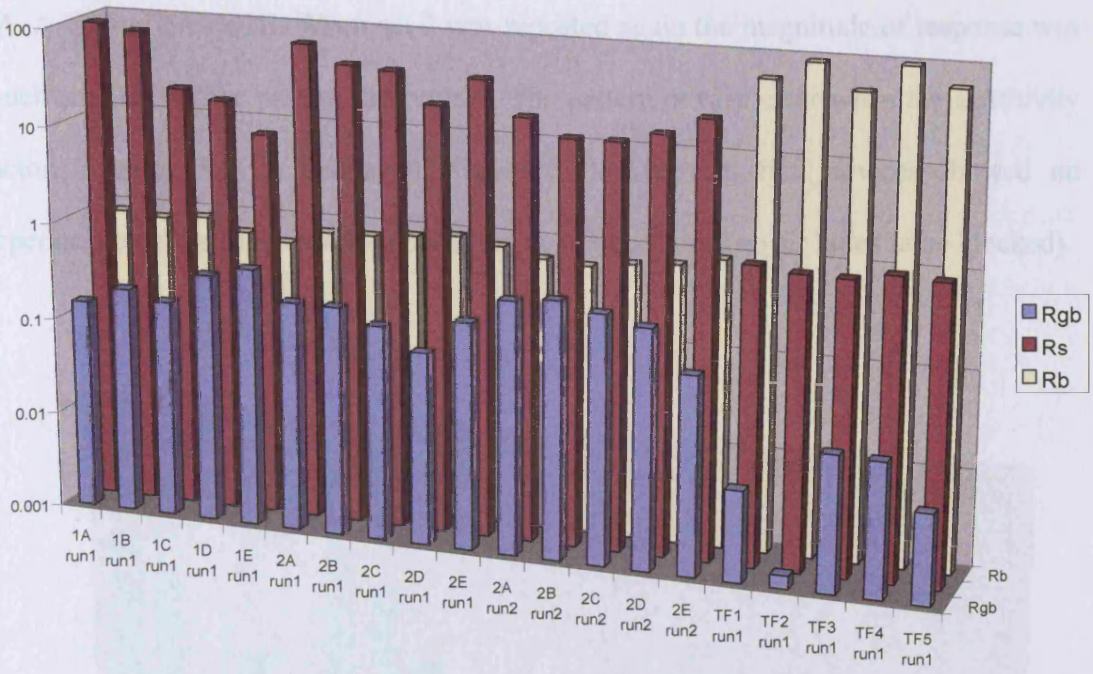

Figure 5.6 Plot showing the contributions toward resistivity from the bulk (Rb), surface (Rs) and grain boundary (Rgb) for each opal sample (1A -> 2E, with an additional run for 2A -> 2E) and thin film samples (TF1 -> TF5)

The 3-resistor microstructure model was fitted to the gas response data. The continuous lines in **figure 5.5** show the fit. The derived component resistance values relative to the gas-free baseline, R_o, are shown in **figure 5.6**. For the inverse opal set of samples it is evident that the bulk contribution, R_b, is significant, as the values are small in comparison to the surface contributions, R_s. The bulk resistances in the thin film set are much higher in value hence contribute less to the total resistance of the samples – the current flow would tend to be around the surface of the crystallites in this case.

A possible explanation for the behaviour is that overfilling by the precursor has covered the air holes thus hindering the access of the gas to the bulk of the structure and affecting the response. The data in **figure 5.7** shows that the higher the amount of filling (1E being at the bottom of the glass slide, which stays longer in the sol during infilling, see experimental section on details of the filling) the smaller the response that is obtained. This pattern is obtained for the two sets of infiltrated opals that were tested,

1A -> 1E and 2A -> 2E. When set 2 was repeated again the magnitude of response was much smaller but the pattern did remain. The pattern is very clear when the sensitivity factor, A (**eqn 5.1**) is displayed (**figure 5.7**). The thin film devices showed no dependence on the sensitivity factor during deposition time (no air holes to be blocked).

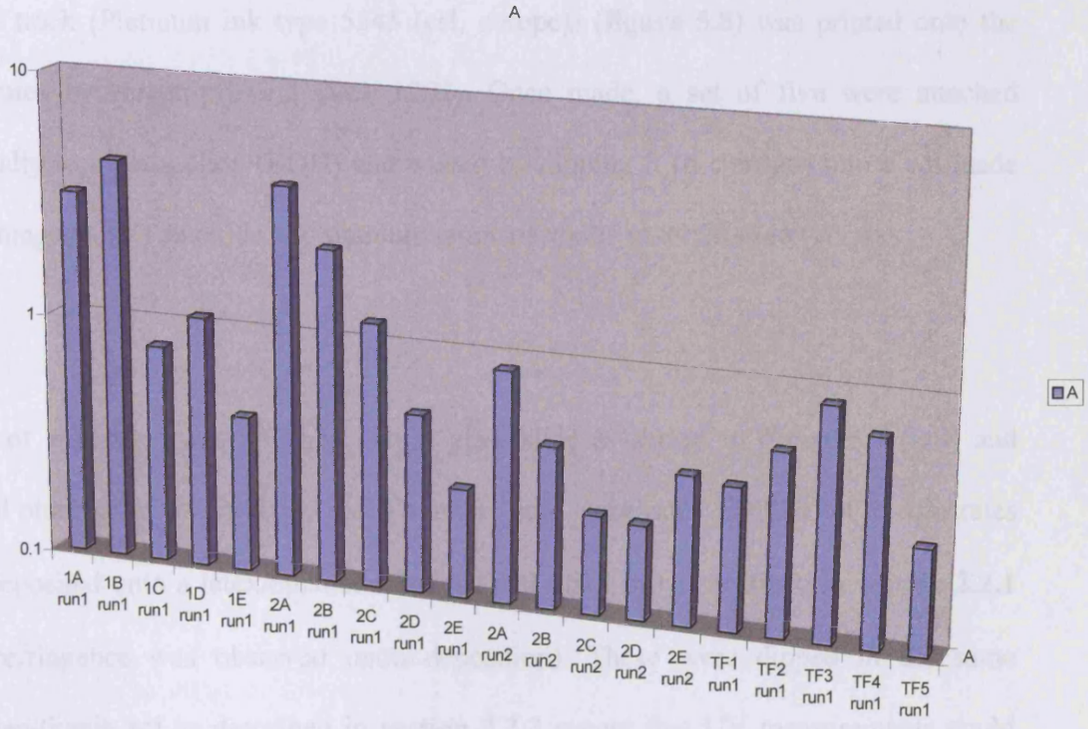

Figure 5.7 Sensitivity factor, A, across all sets of samples.

5.4 Conclusions

Several inverse opals were laid onto gold coated sapphire beads and these were made into sensors. It was hoped that the periodic arrangement of air/titania pockets would result in a consistent set of favourable responses. While a consistency is present from run to run, a bulk contribution is present, meaning that deformities in the structure undermine the effectiveness of the system. Further experiments would lead up to an optimisation of the system.

5.5 Experimental

The devices for study were prepared from sapphire substrates of random orientation (6mm d, 0.6 mm thick) (PI-KEM ltd). On the polished side a gold electrode pattern (organometallic thin film gold ink type 8081 (esl, europe)) and on the other a platinum heater track (Platinum ink type 5545 (esl, europe)) (**figure 5.8**) was printed onto the substrates by screen-printing (Dek 1202). Once made, a set of five were attached vertically to a glass slide (BDH) and coated by dipping it (6 cm/min) into a sol made from tungsten (V) ethoxide and titanium tetraisoproxide in 80:20 ratio (v/v).

A set of substrates was attached onto a glass slide as shown in **figure 5.3 (left)** and dipped onto the tungsten/titania sol. To make 'opal' substrates, another set of substrates was deposited onto a latex/ethanol solution (900 μl/18 ml) as outlined in **section 2.2.1** (a birefringence was observed upon deposition). These were dipped in the same tungsten/titania sol as described in **section 2.2.2** except that UV measurements could not be carried out. Instead, a latex opal film was used to estimate the number of infiltrations that were required. It was found that 12-15 infiltrations at 5-6 cm/min were needed, and the same amount of infills was used for 'thin' as well as 'opal' based substrates. The latex was removed from the slide and heated at 500°C for two hours and the same conditions were applied for dip coated thin films. A white coloration was seen on these substrates.

Raman was carried out as a pattern for tungsten trioxide/titania films has been obtained when spectra has been measured on inverted opal films on glass substrate but the gold/platinum background of the sensor substrates interfere with the measurement thus no spectra could be obtained.

Finally, these sensors were welded to metal pins sealed with glass into a base. An additional track was placed around the perimeter to 'screen' the electrode from the heater – i.e. so that any voltage applied to the heater does not affect the electrode. To study sensor responses the sensor are placed in a rig. The conditions of study are dry air and at 400°C. Details of the rig and of a typical study are to be found in the literature.[97] The measurements were carried out by K. Pratt (UCL).

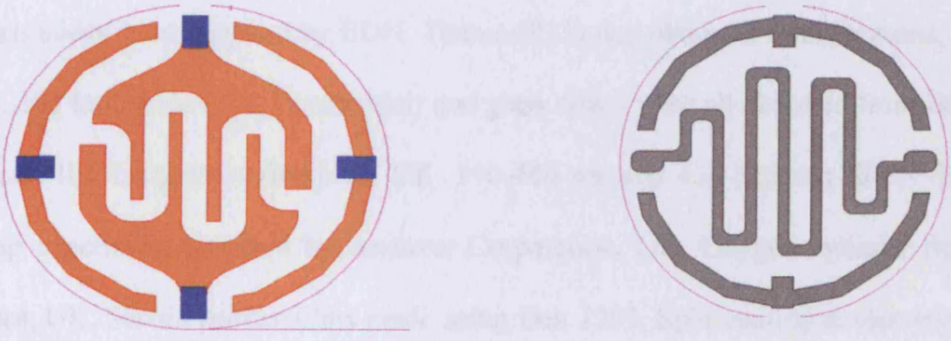

Figure 5.8 Scheme showing the heater (right) and electrodes (left) that was screen-printed onto the sapphire substrates

Chapter 6 Experimental

6.1 Sources of Chemicals, Materials, Analytical Techniques

Aldrich is the source of all chemicals for the CVD ans sol-gel experiments. All were 99% + pure, (the titanium precursors: isopropoxide, ethoxide, butoxide and tetrachloride) and the tungsten precursor (tungsten (V) ethoxide). Aldirch also supplied such as ethanol, isopropanol and also hydrochloric acid, sulphuric acid (0.05 M), iron (II) sulfate, 1, 10-phenanthroline, sodium acetate, sodium hydroxide pellets, stearic acid. Glass slides were supplied by BDH. Titania (P25) was obtained from Degussa, UK. 254 nm, 365 nm lamps (8W, Germicidal) and glass slides were all obtained from BDH, UK. Xenon IL1 lamp from Bentham, UK. 390-460 nm and 435-515 nm filters for Xenon lamp experiment supplied by Andover Corporation, UK. Oxygen cylinder from BOC gases, UK. Screen printer films made using Dek 1202. Spin-coating device supplied by Dek. Dip-coating device made by Dave Knapp, UCL. CVD rig maintained by Dave Knapp. Vladimir Kitaev supplied latex (all sizes) and silica opal solutions (all sizes). Potassium Ferrioxalate crystals and APCVD coated titania film were prepared and supplied by S.O'Neill. Vehicle is a mixture of volatile organic solvents whose proprietary composition is not known (ESL Ltd, UK). Distilled water was purified by the Milli-Q system.

Analytical techniques used (ranges at which these were used to cover materials under investigation in brackets): UV-visible spectra were carried out, in absorption mode, using a Helios double beam instrument (300-900 nm). The measurements covered the necessary range 300-800 nm range for the materials under investigation and could be widened from 190-1100 nm if needed. PXRD was carried out on a Siemens D5000 diffractometer using filtered radiation ($CuK_{\alpha 1}$ λ= 1.5406). The PXRD is equipped with

a Kevex detector (15 and 75 ^{0}) - this range covered all of the major peaks for the known phases of the compounds under investigation. Infrared spectroscopy measurements were carried out using a SHIMADZU FTIR-8700 (2850-2950 cm^{-1}). Raman Spectra was carried out on a Renishaw Raman system 1000 using a helium neon laser of wavelength 632.8 nm (100-1200 cm^{-1}). The Raman spectrum was calibrated against the emission spectrum of neon. The samples were imaged using Scanning Electron Microscopy (SEM), which was carried out on a Hitachi S570 filament scanning electron microscope (UCL/Toronto) and a JEOL 6301F (UCL). Magnification ranged from x 1000 to x 40.000. Reflectance measurements were carried out using a Zeiss minuature spectrometer: 200-1100 nm. Light reflected from the surface of the sample is collected far from the sample in a different direction to the incident beam.

6.2 Preparation of 'Colvin' films

6.2.1 Latex Solutions

Glass slides (7.5 cm x 1 cm) were cut in half, and these were cleaned by the following procedure. After wiping each piece using wet tissue they were placed in a clean beaker filled with toluene. This was then placed in an ultrasonic bath (10 min). The toluene was removed and replaced with ethanol, and sonicated (5-10 min). The procedure was repeated with water (10 min). Finally the beaker was filled with ethanol and the slides were sealed with aluminium foil until the pieces had to be used. An alternative cleaning procedure was to place the wiped glass pieces in a mixture of 3 parts sulphuric acid to one part hydrogen peroxide (overnight) and then to rinse these several times with distilled water and ethanol. They were finally placed under ethanol and the beaker sealed until further use.

Each glass piece was used in the following manner: The glass was dried by applying a stream of nitrogen gas (30 s). Two back clips were attached onto it and it was placed in a solution of latex microspheres (900 μl) (7 wt%) in ethanol (18 ml). This concentration is used for a sample of 220 nm latex microspheres. The sample vial was covered by a cylindrical dish raised off the support surface and then placed on an anti-vibration table in a draft free empty room. A sealed room was necessary, so as to not affect the rate of evaporation of the solvent, which took about three to five days (**figure 6.1**).

The glass slides ('Colvin Films') were characterised by UV spectroscopy and SEM.

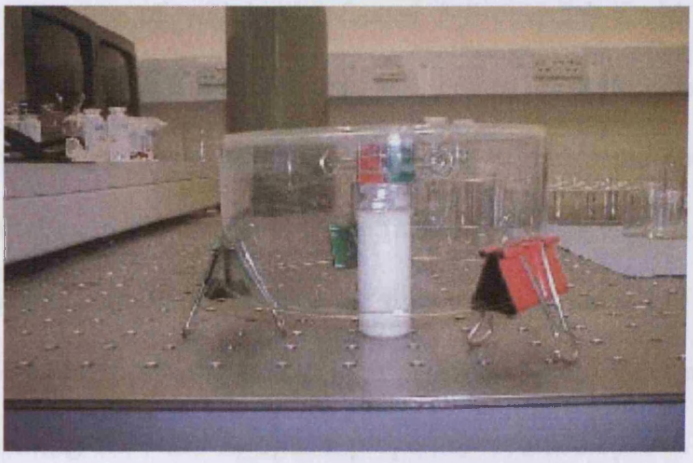

Figure 6.1 Colvin method set up.

The latex microsphere solutions (7 wt%) were supplied by Vladimir Kitaev. A surfactant-free polymerization process using ammonium persulfate as an initiator was used to make monodisperse PS particles.

6.2.2 Preparation of Latex films – Different Sizes and Thickness

The method above is adopted to produce films of different thickness by varying the concentrations of the latex/ethanol solutions. The initial solution was made as before: latex solution (sphere size ~250 nm) (900 μl) in ethanol (18 ml) but the amount of latex

is modified to 1200 μl, 1400 μl, 1600 μl, 1800 μl and 2000 μl in ethanol (18 ml). To deposit latex films with different size spheres different solutions were made and sent by Vladimir Kitaev. Solutions of different concentrations were made with ethanol (800 μl, 18 ml ethanol). Silica opal (290 nm sphere size), made by the Stober method, were coated onto glass films by diluting solutions of silica spheres (900 μl) in ethanol (18 ml).

6.3 Infiltration of Thin Film by Dip Coating

'Colvin Films' were dip-coated in titanium isopropoxide and titanium butoxide solution with ethanol as a solvent in a 5/95 (v/v) precursor/solvent ratio. A dip coater was used so that a constant rate of withdrawal (speed 5-6 cm/min) could be obtained. UV spectroscopy was used each time the opal was coated, to follow the infiltration. The sample was marked to ensure that it was placed at the same spot in the UV-vis spectrometer after each infiltration with the titania precursor was made. Once the stop band in the UV spectrum ceased shifting the slide was calcined at 450 ^{0}C for three hours to get rid of the latex microspheres, leaving the inverse opal. In **chapter 2** the structure was viewed by using SEM and its optical properties recorded by UV. Glass slides were dip coated by a dip-coating machine to give a uniform coating. The withdrawal rate was 6 cm/min for the titania as well for tungsten doped films. Normally films were calcined at 450 °C.

Any changes to the experimental procedure, such as a change in firing procedure (temperature or duration), precursor used or number of coatings were described in the relevant sections (such as **chapter 3.3**, which describes the making of opal-titania precursor composites).

All silica opals of the following sizes: 290 nm, 480 nm and a 480-850 nm, made via the Stober method, were infiltrated as described in **section 6.3** with titania sol (90/10) (v/v); the number of infills was 7-8 for each of these opals. The opal-titania composite was heated at (450 °C, 2-4 hrs) to yield the anatase form of titania.

To get rid of the silica template in silica-titania composite a treatment with a 20% sodium hydroxide solution is carried out by placing the glass slide in a sample vial with this solution (40-50°C, 1-2 days).

In chapters 3 and 4 all films were characterized by using UV-visible spectroscopy, PXRD, Raman and transmission/reflection measurements.

6.4 Preparations of Different Sol-gel Solutions

Transparent pure TiO_2 films: Titanium (IV) tetraisopropoxide (6 ml, 20 mmol) was added to propan-2-ol (50 ml). 2M HCl (0.2 ml) was added dropwise and the mixture was stirred (1 hr).

2%WO_3/TiO_2 mixed oxide films: Tungsten (V) ethoxide (0.164 g, 0.4 mmol) was added to titanium (IV) tetraisopropoxide (6 ml, 20 mmol). Isopropanol (50 ml) and a few drops of 2M HCl were added to the mixture and vigorously stirred (1 hr).

6%WO_3/TiO_2 mixed oxide films: Tungsten (V) ethoxide (0.489 g, 1.2 mmol) was added to titanium (IV) tetraisopropoxide (6 ml, 20 mmol). Isopropanol (50 ml) and a few drops of 2M HCl were added to the mixture and vigorously stirred (1 hr).

20%WO_3/TiO_2 mixed oxide films: Tungsten (V) ethoxide (1.637g, 4 mmol) was added to titanium (IV) tetraisopropoxide (6 ml, 20 mmol). Isopropanol (50 ml) and a few drops of 2M HCl were added to the mixture and vigorously stirred (1 hr).

Once made, all solutions were covered with a watch glass and left overnight before use.

These were used to infiltrate opals as described and also to make thin films. The latter were made by dipping glass slides, washed in water and isopropanol and dried under air, 1-3 times, in these doped titania solutions. After each dipping, the solvent was left to evaporate and the film left to dry (10 mins). These were calcined under oxygen at 500 °C (3-4 hrs).

6.5 Chemical Vapour Deposition

6.5.1 CVD rig

The CVD rig (**Figure 6.2**) was constructed by Nicolas Tetrault and Hernan Miguez (University of Toronto).

All nitrogen gas (99.999%) and oxygen was used as supplied by BOC. The film itself is placed in a small chamber in an upright position as shown in **figure 6.2**. When the latex film is placed inside, the glass chamber is sealed and filled with nitrogen to get rid of any air. To this chamber, a set of valves and two bubblers are connected; opening and closing these valves can control the flow of nitrogen, and to which bubbler the nitrogen flows.

Once the bubbler is opened, nitrogen flows into it to drive the gas out of it and to the chamber at the flow rate that is required (this is controlled by a flow meter). Once the gas passes through the chamber it goes through a KOH trap. All connectors were made of Teflon. Plastic screws were used to prevent leakage and were used to tighten the tubing. If the chamber was blocked during a run this was cleaned by immersing it in a 5% hydrogen fluoride bath for one hour. Then it was washed in water and dried in an oven for an hour at 100 ^{0}C.

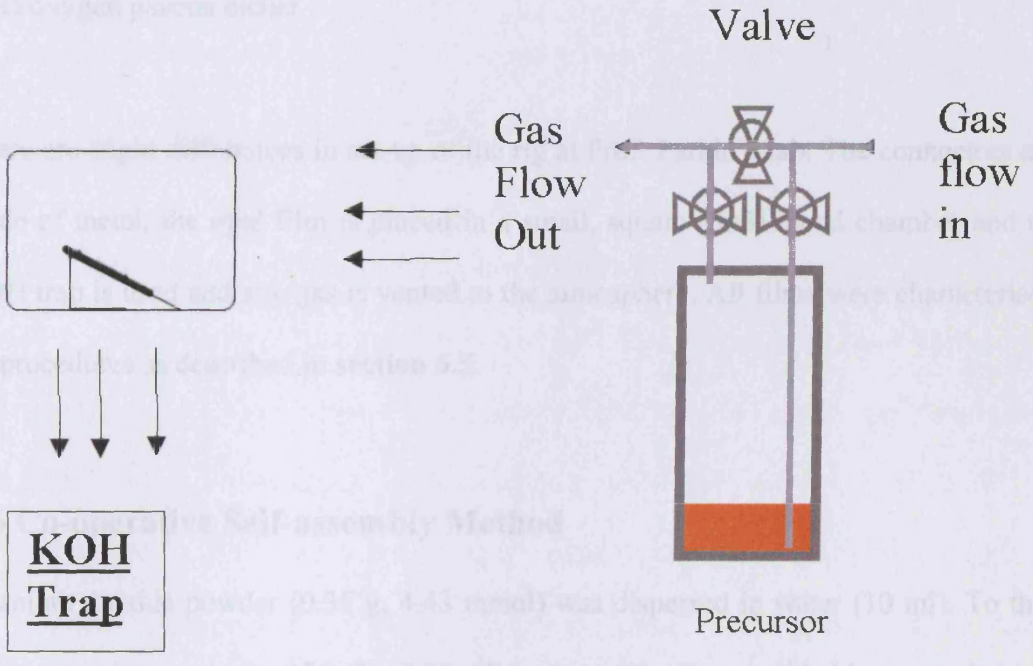

Figure 6.2 Bubbler in a CVD rig. The gas flows out to the compartment with the latex film sample and from there to the KOH trap.

6.5.2 Infiltration of 'Colvin' Films by Chemical Vapour Deposition

A glass slide with latex microspheres was placed inside the chemical vapour deposition apparatus (**Figure 2.15**). Once inside the rig was tightly sealed. The infiltration using titania CVD employed the following steps: 1) Purge with nitrogen at a flow rate of 100 ml/min (5 min), 2) fill system with water at 60 ml/min (5 min), 3) Purge with nitrogen at 35 ml/min (5 min), 4) Fill with titanium tetrachloride at 35 ml/min (10 min), 5) Purge with nitrogen at 100 ml/min (5 min). Each time this cycle is completed the thin film is characterised by UV spectroscopy. There were variations on the procedure: The

precursor was changed to titanium tetraethoxide. This was purged at 35 ml/min for 20 minutes as well as a further 10 minutes. The flow rate was also changed from 35 to 50 ml/min with this precursor. The water was also changed to 1M HCl. The preparation was as listed above and only used with titanium ethoxide precursor.

UV spectra were taken after each cycle was completed and once infiltrated the films were either calcined at ~450 °C for ~ 3-4 hrs or plasma etched by using a Harrick PDC-3XG oxygen plasma etcher

There are slight differences in set-up of the rig at Prof. Parkin's lab. The connectors are made of metal, the opal film is placed in a small, square (5x5) metal chamber and no KOH trap is used and any gas is vented to the atmosphere. All films were characterised by procedures as described in **section 6.5**.

6.6 Co-operative Self-assembly Method

Titanium dioxide powder (0.35 g, 4.43 mmol) was dispersed in water (10 ml). To this polystyrene latex solution (7 wt%, 0.32 ml) in water (8 ml) was added in a sample vial. A clean glass slide was placed inside as described earlier. This was placed in an empty room (3-5 days). The colloidal particles of titania that were used were prepared as follows: water (50 ml) was placed in a flask (250 ml) that was cooled in an ice bath (0-5 ^{0}C). Titanium (IV) tetrachloride (10.9 ml) was added dropwise under vigorous stirring. Water (200 ml) was added to decrease the concentration of titania. The resulting transparent solution was set-aside in a closed vessel for 5 days. The solution was then transferred to a round-bottomed flask and concentrated (rotary evaporator) and a white powder produced (4.95g, 62.7 mmol).

6.7.1 Photocatalytic Studies/ Hydrophilicity Measurement/ "Scotch" Tape Test

The photocatalytic activity of the films was measured by the photodegradation of stearic acid. The overall reaction corresponds to:

$$C_{17}H_{35}COOH + 26O_2 \xrightarrow[\text{Light} \geq E_{bg}]{\text{Semiconductor}} 18CO_2 + 18H_2O \qquad \textbf{(6.1)}$$

Stearic acid was chosen because it is easy to oxidise and it has good physical properties (low vapour pressure and stability). As the sample is irradiated with UV light, the C-H peaks in the IR spectrum decrease in intensity due to photodegradtion.

Photocatalytic activity of the films was studied by using the 'stearic acid' test. Stearic acid (7.5 μl) in a methanol solution (10^{-3} mol) was dropped onto the thin films using a syringe. These were dried using a spin coater at 3000 rpm (30 s). IR spectrum before and after deposition of stearic acid was recorded: 2850-2950 cm^{-1}, resolution 2 cm^{-1}, 8 scans. The peak at 2950 cm^{-1} is due to the asymmetric in plane C-H stretching mode of the CH_3 group; the peak at ~2850 cm^{-1}, due to the stretching mode of the CH_2 group. The thin film was irradiated using a 365 nm lamp (BDH, 8W) and taken out at certain periods (once every 20 mins for the first hour, then periods of 1-3 hrs until a profile consisting of measurements taken over a period of 10-12 hrs was obtained) for IR measurements. In some cases the experiment took place for 1-2 hours as all information regarding the particular experiment could be gathered in that time frame. The absorbance data was normalized - so that the integrated areas under the absorption peaks due to stearic acid C-H peaks (at time = 0 mins) would be equal to 1 - and a graph of normalized absorbance (N) vs. time (mins) decay profile was plotted. In every photocatalysis experiment, unless stated otherwise, the film was surface cleaned prior to

being laid onto by stearic acid using a 254 nm lamp (30 mins). All films were contained inside a cardboard box, and irradiated at the same distance from the lamp (10 cm).

Experiments to determine the hydrophilicity of the films were also performed by measuring the contact angle. A droplet of water (1 μl) was laid onto the surface of the film. The film was irradiated before and after measurement to see any changes. The contact angle was calculated using the relevant program. Values could not be obtained for photonic crystal films. The adhesiveness of the film was tested using the "Scotch" tape test. This involved attaching a piece of tape onto the surface of the film and pulling it.

6.7.2 Photocatalysis Using the Xenon Lamp

A Xenon lamp that emits light ranging from 200 nm – 2.5 μm (Bentham IL1) was used for some irradiation of photonic crystal films (**Figure 6.3**). This was attached with an extension to protect the optical filter. It allows light in the range of 435-515 nm to pass through. The whole set was enclosed in a metal box and the measurements were taken once a day with the experiments taking 3-5 days.

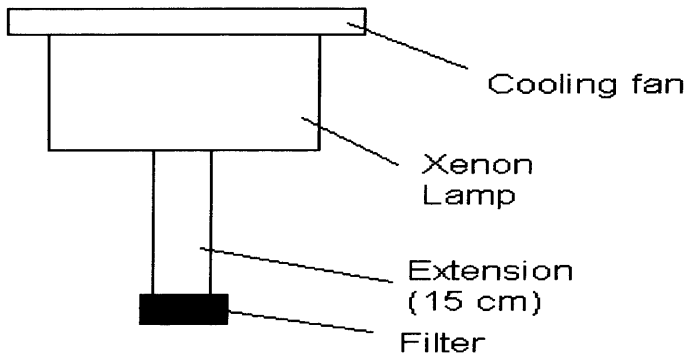

Figure 6.3 Diagram showing xenon lamp and its attachment placed to accommodate the filters.

6.8 Actinometry

A standard calibration graph was prepared by looking at the decomposition of a standard iron (II) solution, prepared from dilution of iron (II) sulphate (0.072 g) in water (100 ml) and concentrated sulphuric acid (5 ml), transferred to a volumetric flask (1000 ml), the mixture was diluted to the mark and mixed. Into five volumetric flasks (100 ml), 5, 10, 25 and 50 ml of standard iron solution were added, as well as sodium acetate buffer (10 ml), 1, 10-phenanthroline solution (10 ml) and hydroxylamine hydrochloride solution (1 ml). These were mixed and diluted to the mark. A 'blank' solution (no standard iron solution) was used as reference. The absorption was determined at 510 nm and a plot of absorption against concentration was obtained. The value for the molar absorption coefficient (ε) obtained is close (9908 mol^{-1} dm^3 cm^{-1}) to the value for a modern spectrometer (10000 mol^{-1} dm^3 cm^{-1}).

For the determination of the light intensity of the UV lamp all manipulations are carried out in the dark with a red searchlight. Potassium ferrioxalate solution (0.006 M) is prepared by mixing the pure green crystals (2.947 g) in water (800 ml) in a volumetric flask (1000 ml). Sulphuric acid (0.05 M, 100 ml) is mixed and the solution was diluted to the mark.

The ferrioxalate solution (~50 ml) was taken out and placed in a beaker under the UV lamp (BDH, 365 nm) and irradiated (30 s) so that ~ 5×10^{-8} moles of iron (II) (ml) was produced. An aliquot was taken (10 ml) and placed in a volumetric flask (25 ml) Phenanthroline (2 ml) and acetate buffer (5 ml, or about half of the amount of ferrioxalate taken) was added. This was mixed and diluted to the mark. A 'blank' solution (where the ferrioxalate solution is not irradiated) is prepared as above, with both solutions being stored (1 hr) before UV measurement. The amount of solution is

added to the UV cell by using different size pipettes and this is noted (4.31 ml). The 'blank' solution is used as a reference and the absorption is measured at 510 nm as before. The experiment was repeated twice more, with similar amounts in the UV cell, and the absorption measured as before.

6.9 Photocatalysis and Control Experiments

Control 1 was made by mixing polystyrene opal solutions of 290 nm/220 nm (1:1) and diluting this in ethanol (18 ml). The glass slide was cleaned as detailed in **chapter 2** and laid down as specified by the Colvin method. Control 2 involved using this mixture, but dropping it onto glass using a spin-coating device by using a pipette at 1000 rpm. Control 3 used a 290 nm opal as in **chapters 2 or 3** but this was partially filled as before. Control 4 involved modifying the Colvin procedure by rapidly evaporation an opal ethanol mixture (900μl/18 ml) by heating it in a furnace at 60 °C (2 days).

A slightly disordered film was laid onto glass and had its voids filled using dip-coating as described in **section 6.3**. Finally, control 5 was laid down by using the undiluted 290 nm opal solution and attaching the glass slide to the dip-coating and laying a covering and using it again once an opal-like surface was laid down to then fill any voids (~10 infiltrations at 5-6 cm/min). One side of the slide was covered using "Scotch" tape. All opal controls, once infiltrated, were subsequently calcined at 450 °C (2 hrs). All samples were checked for titania anatase by Raman/PXRD and photocatalysed as detailed in **section 6.7**.

6.10 Dye Experiments

Solutions were made from HABA/ethanol in concentrations that were varied from 10^{-3} - 10^{-5} M. An amount of these (15 ml) was used to fill a sample vial. An opal sample,

deposited via the colvin method, was immersed in this solution for varying lengths of time (at least 10 mins). Taken out, let out to dry (~ 10 mins). The UV spectrum was measured before and after deposition with dye solution. Permutations on this procedure included: 1) varying the length of immersion in solution (30 mins, 2 hrs) and the number of immersions (1-3). For re-usage, the opal was first washed by soaking in ethanol followed by measuring the UV spectrum as before.

6.11 Titania films for Surface Area Measurement

Titania (P25, degussa) was mixed with vehicle in a 1:4-5 (w/w) ratio using pestle and mortar. This was put through the mill to create an ink paste. The sample was screen printed onto a square piece of glass weighed before layering. The layer was dried under IR light (15 mins) and layered twice more with IR drying once any layering was completed. The film was heated at 450 ^{0}C (4 hrs) in a furnace. The piece of glass was weighed and the amount of titania deposited onto the glass was noted (0.0028 g).

A silica glass reference slide was weighed (0.5859 g) and was sent together with the P25 film as well as a typical photonic crystal film (0.0012g), whose weight was measured before being sent for BET analysis. BET analysis was carried out by Dr Russell Pryce at the materials chemistry department (Imperial Collge, London).

Chapter 7 Conclusions

The photocatalytic activity of titania, and of other metal oxides, has been investigated by a few research groups and via several means. Photonic crystals were first made and theorised in the late 80s, as a means of controlling the propagation of light, and therefore harnessing its energy for reactions; this has been the driving force behind the attempts at research into the making of these structures.

The aim of this project was to combine these two areas to see whether titania could be of use as a photocatalyst in a photonic crystal form. It was theorised that this could be achieved if, by making titania in this form, the photocatalytic efficiency of titania under the visible light could be increased via a 'slow photon' effect. Photocatalysis would be an ideal way to test for this.

Metal oxide photonic crystals have been synthesised by a variety of methods as reviewed in **chapter 1**. For the purposes of this project we went along with an approach that involved constructing an opal template from either polystyrene or silica opals, and, once this was laid onto glass, using sol-gel or chemical vapour deposition to infiltrate the voids quickly and effectively. The control of the infiltration involved using the shift in the stop band, which in turn signifies a shift in refractive index contrast, to indicate the point at which the voids were filled. The subsequent removal of template effectively inverts the opal structure hence the name 'inverse opal' of (in this case) titania to label the structure. The temperature of removal was regulated so that anatase titania, its most photocatalytically active form, was synthesised. Raman and PXRD were used to check for this.

Ultraviolet measurements reveal two weak bands at 300-400 nm. These are due to the flat band and the stop band. The latter has shifted from being at ~600-700 nm on an opal (of the 290-300 nm size; this will shift if the size of the template itself is different) to being now placed alongside the weak flat band in the spectra for the inverse opal. This is quite different to the spectra for other types of titania film, which show no absorption whatsoever at this range. However, upon the inversion process, this 'flat' band structure displayed by the UV spectrum for the opal is degraded (i.e. the fine structure, as seen for the opal is washed out) by the infiltration and inversion process, so that the inverse opal tends to display very weak bands at the 350-450 nm range. The photonic film's activity was tested for by looking at the decomposition of stearic acid under 365 nm UV light and, despite the poor optical properties, it showed the films to have t ½ ~20 mins at best, which are markedly superior to any other types of anatase titania that have been tested. The conclusion is that the structure generated by this process - titania/air pockets that are periodic throughout the film - is in fact responsible for the film's high activity.

But whatever the activity for a film, or a set of films sandwiched as shown in **figure 6.1**, this has been shown to be consistently repeatable; additionally, these can be re-used and will display high activity, whether cleaned prior to use (using a 254 nm lamp, as with other films in literature) or not (placed in the dark for a length of time instead). The activity of these films is much higher when compared to other titania films such as ones made via screen printing, or using sol-gel as before, as well as any films coated via APCVD. But activities do not extend further into the visible, as seen by experiments with the Xenon lamp (attached with appropriate filters). The photo-efficiency, quantified by extracting values for a quantum yield, is comparable to that of films surveyed in the literature.

The photonic crystals films are superhydrophilic. That is, they are 'water loving' films; such an effect goes hand-in-hand with a high photoactivity. However, this effect is not photoinduced, unlike so many other titania films and doped titania films to be found in the literature. It is likely that stearic acid molecules infiltrate the air pockets contained within the substance and are thus able to be decomposed more easily. Also, these films fail the Scotch-tape test, they are not physically strong enough hence they are ruled out when considering them for applications such as self-cleaning window coatings.

Other sets of experiments looked at the correlation between photocatalytic activity and variations in thicknesses – which were obtained by varying the latex/ethanol ratio through the Colvin method. There does not appear to be a correlation. In yet another experiment with silica, it was found that when this opal is coated lightly with titania, heated at 450 °C (temperature that effects conversion to anatase titania and would burn PS opals), creates a silica-opal/titania composite that is very photoactive. The structure must be heated to the appropriate temperature, and an anatase spectrum, as measured by Raman/PXRD, must be obtained as a prerequisite.

To understand the high photoactivity, despite the weak UV bands, controls were made which did not, for the most part, upon UV measurement, display the presence of the 'flat' band, or even the weak bands as seen before for photonic crystals, and yet its structure, as observed from SEM photographs has the similarities, i.e. air-titania pockets, and similar thickness with a degree of periodicity. These displayed similar amounts of activity, (t ½) were comparable to the best photonic structures. Coupled with the facts that increased size (presumably smaller surface area for activity) impedes upon photocatalysis, and that the dye measurements devised do not displayed an enhanced absorption as predicted for the 'flat' band region, tends to suggest that the

surface area, and not the slow-photon effect, is the main factor that is responsible for the high activities displayed throughout. BET measurements of krypton absorption in fact showed a small surface area in comparison to that of a screen-printed titania P25 (50 m^2/g). [65] If the surface area is indeed very small then it could be argued that the films are very good at making whatever area is available to photocatalyse the decomposition of an organic.

Chapter 5 shows results obtained from runs when the microstructure was applied to a gas sensing system. A reasonable response was displayed, as well as reproducibility from run to run but an unexpected bulk contribution, reasoned to be coming from a deformity in the photonic crystal's structure, undermines the work thus far. Optimisation of this system will lead to improvement in results.

Future work must also be carried out on looking at decomposition of other organics, as other researchers such as Douglas *et al.*[98] have done in the past for thin films of titania. Also, looking at obtaining better 'flat' band structured inverse opals and comparing photo-efficiencies between these as well as obtaining a measurement for the surface area of these films, would be another area for further work.

References:

[1]A. Mills and S. Le Hunte, *J.Photochem. Photbiol. A: Chem.,* 1997, **108**, 1 and references cited therein.

[2] A. Mills, S. Morris and R. Davies, *Chem. Soc. Rev.,* 1993, 417.

[3] C. Lettman, H. Hinrichs and W. Maier, *Angwen. Chem. Int. Ed.,* 2001, **40**, 3160.

[4] A. Pruden and D. Ollis, *J. Catal.,* 1983, **82**, 404.

[5] C. Hsiao, C. Lee and D. Ollis, *J. Catal.,* 1983, **82**, 418.

[6] H. Gerischer and A. Heller, *J. Phys. Chem.,* 1991, **95**, 5261.

[7] H. Gerischer and A. Heller, *J. Am. Chem. Soc.,* 1992, **114**, 5230.

[8] A. Fushijima and K. Honda, *Nature*, 1972, **37**, 238.

[9] W. Cross, *Chemical Vapour Deposition of Tungsten Oxide Thin Films from Single-source Precursors,* University of London, 2002.

[10] N. Serpone, G. Suave, R. Koch, H. Tahiri, P. Pichat, P. Piccinini, E. Pelizzetti and H. Hidaka, *J.Photochem. Photbiol. A: Chem.,* 1996, **94**, 191.

[11] J. D. Joannopoulous, Robert D. Meade and Joshua N. Winn, Photonic Crystals, Princeton, 1995.

[12] N. A. R. Bhat and J. E. Sipe, *Phys. Rev.* 2001, ***E*64**, 056604.

[13] G. Ozin, V. Kitaev and H. Miguez, *Appl. Phys. Lett.,* 2004, **84,** 1239.

[14] L. Heinch and J. K. West, *Chem. Rev.,* 1990, **90**, 33.

[15] R. M. Almeida and S. Potal, *Current opinion in solid state and materials science,* 2003, **7**, 151.

[16] S. Rabaste, J. Bellessa, A. Brioude, C. Bovier, J. C. Plenet, R. Brenier, O. Marty, J. Mugnier and J. Dumas, *Thin solid films,* 2002, **242**, 416.

[17] S. Rabaste, J. Bellessa, A. Brioude, C. Bovier, J. C. Plenet, R. Brenier, O. Marty, J. Mugnier and J. Dumas, *Appl. Phys. Lett.,* 2001, **79**, 2142.

[18] O. J. A. Schuller, G. M. Whitesides, J. Rogers, M. Meier and A. Dodabalapur, *Appl. Opt.,* 1999, **38**, 5799.

[19] S. Shimada, K. Miyazawa and M. Kuwabara, *Jpn. J. Appl. Phys.,* 2002, **41**, 291.

[20] R. T. Bise, R. S. Windeler, R. S. Kranz, C. Kerbage and B. J. Eggleton, *Optical Society of America,* 2001, 466.

[21] N. P. Johnson, D. W. McComb, A. Richel, B. M. Treble and R. M. De La Rue, *Synth. Metals.,* 2001, **116**, 469.

[22] R. Mayoral, J. Resquena, J. S. Moya, C. Lopez, A. Cintas, H. Miguez, F. Meseguer, L. Vasquez, M. Holgado and A. Blanco, *Adv. Mater.,* 1997, **9**, 257.

[23] J. S. Moya, C. Lopez, A. Misfud, H. Miguez, F. Meseguer and L. Vasquez, *Langmuir*, 1997, **13**, 6009.

[24] P. Jiang, K. S. Hwang, D. Mittleman, J. Bertone and V. L. Colvin, *J. Am. Chem. Soc.,* 1999, **121**, 11630.

[25] A. Imhof and D. J. Pine, *Nature*, 1997, **389**, 948.

[26] Gemstone opals, http://www.minerals.net

[27] D. Wang and F. Caruso, *Adv. Mater.,* 2003, **15**, 205.

[28] H. Miguez, N. Tetrault, S. M. Yang, V. Kitaev and G. A. Ozin, *Adv. Mater.,* 2003, **15**, 597.

[29] K. L. Choy, *Progress in Materials Science,* 2003, **48**, 57.

[30] H. M. Yates, M. Pemble, H. Miguez, A. Blanco, C. Lopez, F. Meseguer and L. Vasquez, *Journal of Crystal Growth*, 1998, **193**, 9.

[31] K. Busch and S. John, *Phys. Rev. E.,* 1998, **58**, 3896.

[32] H. S. Souzer, J. Haus and R. Inguva, *Phys. Rev. B.,* 1992, **45**, 13962.

[33] H. M. Yates, M. Pemble, H. Miguez, A. Blanco, C. Lopez and F. Meseguer, *Chem. Vap. Deposition*, 2000, **6**, 283.

[34] Y. Vlasov, X. Bo, J. Strurm and D. Norris, *Nature*, 2001, **414**, 289.

[35] A. A. Zakhidov, R. H. Baughman, Z. Iqbal, C. Cui, I. Kkhayrullin, J. Martin, S. O. Datas and V. G. Ralchenko, *Science*, 1998, **282**, 897.

[36] H. Miguez, E. Chomski, F. Garcia-Santamaria, M. Ibisate, S. John, C. Lopez, F. Meseguer, J. Mondia, G. A. Ozin, O. Toader and H. Driel, *Adv. Mater.*, 2001, **13**, 1634.

[37] G. Freymann, S. John, M. Schulz-Dobrick, E. Vekris, N. Tetrault, S. M. Yang, V. Kitaev and G. A. Ozin, *Appl. Phys. Lett.*, 2001, **84**, 224 and references cited therein.

[38] A. Rugge, J. S. Becker, R. G. Gordon and S. H. Tolbert, *Nano Letters*, 2003, **3**, 1293.

[39] A. Stein and R. C. Schroden, *Current opinion in Solid State and Materials Science,* 2001, **5**, 553 and references cited therein.

[40] S. Park and Y. Xia, *Chem. Mater.*, 1998, **10**, 1745

[41] B. Gates, Y. Yin and Y. Xia, *Chem. Mater.*, 1999, **11**, 2827.

[42] K. Yoshino, Y. Kawagishi, S. Tatsuhara, H. Kajii, S. Lee, A. Fujii, M. Ozaki, A. Zahkidov, M. Ishikawa and Z. Vardeny, *Microelectronic Eng.*, 1999, **47**, 49.

[43] T. Xu, Z. Cheng, Q. Zhang, R. Baughman, C. Cui, A. Zahkidov and J. Su, *J. Appl. Phys.*, 2000, **88**, 405.

[44] C. Blanford, H. Yan, R. C. Schroden, M. Al-Daous and M. Stein, *Adv. Mater.*, 2001, **13**, 401.

[45] G. Subramanian, V. Manoharan, J. Thorne and D. Pine, *Adv. Mater.*, 1999, **11**, 1261.

[46] G. Subramanian, K. Constant, R. Bisvas, M. Sigalas and K. M. Ho, *Adv. Mater.*, 2001, **13**, 443.

[47] O. Velev, P. Tessier, A. Lenhoff and E. Kaler, *Nature,* 1999, **401**, 548.

[48] P. Braun and P. Wiltzus, *Nature,* 1999, **402**, 603.

[49] P. Braun and P. Wiltzus, *Adv. Mater.*, 2001, **13**, 482.

[50] Wang and F. Caruso, *Adv. Mater.*, 2001, **13**, 350.

[51] D. Wang, R. Caruso and F. Caruso, *Chem. Mater.*, 2001, **13**, 364.

[52] K. Rhodes, S. Davis, F. Caruso, B. Zhang and S. Mann, *Chem. Mater.,* 2000, **12,** 2832.

[53] W. Zhou, L. Xu, M. Koslov, I. Khayrullin, I. Udod, A. Zakhidov, R. Baughman and J. Wiley, *J. Am. Chem. Soc.,* 2001, **123**, 763.

[54] P. Jiang, J. F. Bertone, K. S. Hwang and V. L. Colvin, *Chem. Mater.,* 1999, **11,** 2132 and references cited therein.

[55] R. Rengarajan, P. Jiang and V. L. Colvin, *Appl. Phys.lett.,* 2000, **77,** 3517.

[56] A. Nitrov and K. Nagayama, *Langmuir*, 1996, **12**, 1303.

[57] M. Yamaki, J. Higo and K. Nagayama, 1995, **11**, 2975.

[58] J. F. Bertone, P. Jiang, K. S. Hwang, D. M. Mittlemann and V. L. Colvin, *Phys. Rev. Lett.,* 1999, **83**, 300.

[59] J. Lopez, E. Lidon, E. Martinez and C. Lopez, *Phys. Rev. B,* 2003, **68**, 115109.

[60] H. Miguez, S. Yang and G. Ozin, *Langmuir*, 13, 3479.

[61] M. Turner, T. Trentler and V. L. Colvin, *Adv. Mater.,* 2001, **13**, 180.

[62] Q.B. Meng, C. H. Fu, Y. Einaga, Z. Z. Gu, A. Fujishima and O. Sato, *Chem. Mater.,* 2002, **14**, 83.

[63] Q.B. Meng, Y. Einaga, Z. Z. Gu, A. Fujishima and O. Sato, *Appl. Phys.lett.,* 2000, **77,** 4313.

[64] PXRD database

[65] Activ M glass, www.pilkington.com

[66] S. O'Neill, N. Elliott, R. H. Clark, A. Mills and I. P. Parkin, *J. Chem. Mater.,* 2003, **13**, 56.

[67] L. Burgio and R. H. Clark, *Spectrochim. Acta, Part A*, 2001, **57**, 1491.

[68] P. Sawunyama, A. Fujishima and K. Hashimoto, *Langmuir*, 15, 3551.

[69] P. Sawunyama, L. Jiang, A. Fujishima and K. Hashimoto, *J. Phys. Chem. B,* 1997, **101,** 11000.

[70] A. Heller, *Acc. Chem. Res.*, 1995, **28**, 503.

[71] H. Kominami, S. Murakami, J. Kato, Y. Kera and B. Ohtani, *J. Phys. Rev. B,* 2002, **106,** 10501 and references cited therein.

[72] V. Pore, A. Rahtu, M. Leskela, M. Ritala, T. Sajavaara and J. Keinonen, *Chem. Vap. Deposition,* 2004, **10**, 143.

[73] S. Jung, S. Kim, N. Imaishi and Y. Cho, *Appl. Cat. B: environmental,* 2005, **55,** 253.

[74] C. Gillard, D. Debayle, A. Gagnaire, H. Jaffrezic and Jean-Marie Herrmann, *Materials Research bulletin*, 2004, **39**, 1445.

[75] H. Taka and M. Tanaka, *Langmuir*, 1997, **13**, 360.

[76] G. Hill, N. Elliott, D. Fallis, J. Durrant and A. Mills and *Photochem. Photbiol. Sci.,* 2003, **2**, 591.

[77] K. Jung, S. Park and S. Kim, *Appl. Cat. A.,* 2002, **224**, 229.

[78] I. Arabatzis, S. Antonaraki, T. Stergiopolous, A. Hiskia, E. Papaconstantinou, M. Barnard and P. Falaras, *J.Photochem. Photbiol. A: Chem.,* 1997, **149**, 237.

[79] B. Sohn, T. Kim and K. Char, *Langmuir*, 2002, **18**, 7770.

[80] S. Kuai, S. Badilescu, G. Bader, R. Bruning, X. Hu and Vo-Van Troung, *Adv. Mater.,* 2003, **15**, 73.

[81] P25, http://www.degussa.com/en/home.html

[82] A. Rampaul, I. P. Parkin, S. O'Neill, J. Desouza, A. Mills and N. Elliott, *Polyhedron*, 2003, **22**, 35 and references cited therein.

[83] D. Tryk, A. Fujishima and K. Honda, *Electrochimica Acta,* 2000, **45**, 2363 and references cited therein.

[84] M. Miyauchi, A. Nakajima, T. Watanabe and K. Hashimoto, *Chem. Mater.,* 2002, **14**, 4714.

[85] A. Mills, G. Hill, S. Bhopal, I. Parkin and S. O'Neill, *J.Photochem. Photbiol. A: Chem.,* 2003, **160**, 185.

[86] A. Mills, A. Lepre, S. Bhopal, N. Elliott, I. Parkin and S. O'Neill, *J.Photochem. Photbiol. A: Chem.,* 2003, **160**, 213.

[87] J. Calvert and J. Pitts, Photochemistry, Wiley, New York, 1967, 783.

[88] Y. Paz, Z. Luo, L. Rabenberg and A. Heller, *J. Mater. Res.,* 1995, **10**, 2842.

[89] G. Von Freymann, S. John, S. Yang, V. Kitaev and G. Ozin, *not yet published.*

[90] S. Lim, J. Flaming, Z. Li, I. El-Kady, R. Biswas and K. Ho, *J. Opt. Soc. Am. B.*, 2003, **20**, 1538.

[91] S. Nishimura, N. Abrahams, B. Lewis, L. Halaoui, T. Mallouk, K. Benkstein, J. De Lagemaat and A. Frank, *J. Am. Chem. Soc.,* 2003, **125**, 6306.

[92] S. Bu, Z. Jin, X. Kiu, L. Yang and Z. Cheng, *Journal of the European Ceramic Society*, 2005, **25**, 673.

[93] G. A. Shaw, K. F. E. Pratt, I. P. Parkin and D. E. Williams, *Sensors and actuators B*, 2004

[94] G. Chabanis, I. P. Parkin and D. E. Williams, *Meas. Sci. Technol.*, **14**, 2003, 76.

[95] K. F. E. Pratt and D. E. Williams, *Sensors and actuators B*, **70**, 2000, 214.

[96] R. W. J. Scott, S. M. Yang, D. E. Williams and G. A Ozin, *Chem. Comm.,* 2003, 688.

[97] D. H. Dawson and D. E. Williams, *J. Mater. Chem.,* **6**, 409.

[98] R. Fretwell and P. Douglas, *J.Photochem. Photbiol. A: Chem.,* 2001, **143**, 229.

Appendix

All samples that have been tested are listed below with the method of their preparation, their activity and the conditions of testing. All samples were characterised by PXRD, Raman and SEM and EDAX when required. All samples gave peaks from Raman and XRD that correspond to the anatase titania phase and any that were not (e.g. doped samples) had its data discussed in the appropriate section.

Chapter and section	Sample number/name	Template, details of infiltration, Firing temperature	Photocatalytic Activity (t ½) (mins)
3.1	Inverse opal, '5B'	Polystyrene spheres (PS) 300 nm, CVD, 500°C (5h)	78
	Inverse opal, '21'	PS, 300 nm, sol-gel, 500 °C (5h)	16
	PS opal	PS opal, not infilled	-
3.2	Inverse opal, '2'	PS, 300 nm, sol-gel, 450 °C, (2-3 hrs)	~5800
3.3	Inverse opal, '6 A'	PS, 300 nm, sol-gel, 450 °C (1.5 hr)	25
	Titania-latex composite 1	PS, 300 nm, sol-gel (1 coat), no inversion	-
	Titania-latex composite 2	PS, 300 nm, sol-gel (several coatings), no inversion	-
	Titania-silica opal composite 3	Silica opal (300 nm), (1 coat), heating at 450°C (3hr), no inversion	~50
	APTiO2	Coated via APCVD	-
3.4	Inverse opal, (4.08) (thickness of sample)	PS, 300 nm, sol-gel, 450°C (3hr)	25
	Inverse opal, (3.95)	PS, 300 nm, sol-gel, 450°C (3hr)	160
	Inverse opal, (4.15)	PS, 300 nm, sol-gel, 450°C (3hr)	47
	Inverse opal, (3.5)	PS, 300 nm, sol-gel, 450°C (3hr)	135
3.5	Screen Printed Titania on glass	P25 titania, 450°C (3hr)	674
	Sol-gel coated Titania on glass	Titania sol, 450°C (3hr)	623
	Inverse opal made from silica opal	Silica opal (300 nm), sol-gel, 450°C (3hr), 20% NaOH (60°C, 1-2 days)	~280
	Inverse opal, '35'	PS, 220 nm, sol-gel,	40

		450°C (3hr)	
3.6	Inverse opal, '28400' A	PS, 300 nm, sol-gel, 450°C (3hr)	32
	Inverse opal, '28400' B	PS, 300 nm, sol-gel, 450°C (3hr)	32
	Inverse opal, '5 A'	PS, 300 nm, sol-gel, 450°C (3hr)	41 (repeat) (23)
	Inverse opal, '5 B'	PS, 300 nm, sol-gel, 450°C (3hr)	41 (20)
	Inverse opal, '12 A'	PS, 300 nm, sol-gel, 450°C (3hr)	30 (20)
	Inverse opal, '12 B'	PS, 300 nm, sol-gel, 450°C (3hr)	20 (20)
	Inverse opal, '14 A'	PS, 300 nm, sol-gel, 450°C (3hr)	192 (50)
	Inverse opal, '14 B'	PS, 300 nm, sol-gel, 450°C (3hr)	61 (39)
	Inverse opal, 3 days in 'dark'	PS, 300 nm, sol-gel, 450°C (3hr)	22
	Inverse opal, one week in 'dark'	PS, 300 nm, sol-gel, 450°C (3hr)	18
3.8	Inverse opal, '31'	PS, 300 nm, sol-gel, 6% doped tungsten titania sol, 500°C (3-4 hrs) under Oxygen	43
	Inverse opal, '41'	PS, 300 nm, sol-gel, 20% doped tungsten titania sol, 500°C (3-4 hrs) under Oxygen	~750
	Inverse opal, '29'	PS, 300 nm, sol-gel, 2% doped tungsten titania sol, 500°C (3-4 hrs) under Oxygen	75
4.1	Control experiment 1	PS opal mixture (290/220 nm), sol-gel, 450°C (3hr)	58
	Control experiment 2	PS opal mixture (290/220 nm), dropped onto glass, 450°C (3hr)	-
	Control experiment 3	PS opal (300 nm), sol-gel (2 coats), 450°C (3hr)	145
	Control experiment 4	PS opal (300 nm) assembled by rapid evaporation, sol-gel, 450°C (3hr)	36
	Control experiment 5	PS opal (300 nm), coated onto glass, sol-gel, 450°C (3hr)	54
4.3	290	silica opal, 290 nm, sol-gel, 450°C (3hr),	507

		20% NaOH (60°C, 3-4 days)	
	290-r	silica opal, 290 nm, sol-gel, 450°C (3hr), 20% NaOH (60°C, 1-2 days)	305
	480	silica opal, 480 nm, sol-gel, 450°C (3hr), 20% NaOH (60°C, 3-4 days)	221
	480-r	silica opal, 480 nm, sol-gel, 450°C (3hr), 20% NaOH (60°C, 1-2 days)	720
	480-850	silica opal, 480-850 nm, sol-gel, 450°C (3hr), 20% NaOH (60°C, 3-4 days)	>720
	480-850-r	silica opal, 480-850 nm, sol-gel, 450°C (3hr), 20% NaOH (60°C, 1-2 days)	368